

TRUCK/PAVEMENT/ECONOMIC MODELING AND IN-SITU FIELD TEST DATA ANALYSIS APPLICATIONS – VOLUME 4: EFFECTS OF SLAB SHAPE AND LOAD TRANSFER MECHANISMS ON PORTLAND CEMENT CONCRETE PAVEMENT



Shad Sargand and Jill Morrison

for the
New York State Department of Transportation

and the
Ohio Department of Transportation
Office of Research and Development

and the
United States Department of Transportation
Federal Highway Administration

State Job Number 147700 – SPR2(203)

September 2007



OHIO
UNIVERSITY

Ohio Research Institute for Transportation and the Environment



1. Report No. FHWA/OH-2006/3D	2. Government Accession No.	3. Recipient's Catalog No.	
4. Title and Subtitle Truck/Pavement/Economic Modeling and In-Situ Field Test Data Analysis Applications – Volume 4: Effects of Slab Shape and Load Transfer Mechanisms on Portland Cement Concrete Pavement		5. Report Date September 2007	
		6. Performing Organization Code	
7. Author(s) Shad Sargand and Jill Morrison		8. Performing Organization Report No.	
9. Performing Organization Name and Address Ohio Research Institute for Transportation and the Environment (ORITE) 141 Stocker Center Ohio University Athens OH 45701-2979		10. Work Unit No. (TRAIS)	
		11. Contract or Grant No. State Job No. 147700 – SPR2(203) Agreement No. 10212	
12. Sponsoring Agency Name and Address Ohio Department of Transportation Office of Research and Development 1980 West Broad St. Columbus OH 43223		13. Type of Report and Period Covered Technical Report	
		14. Sponsoring Agency Code	
15. Supplementary Notes Prepared in cooperation with the Ohio Department of Transportation (ODOT) and the U.S. Department of Transportation, Federal Highway Administration			
16. Abstract <p>A jointed concrete pavement on I-490 near Rochester, NY, was reconstructed using three different dowel bar spacings in eastbound test sections. Two sections in the westbound direction were instrumented to monitor environmental strain, deflections, and pavement temperatures. Monitoring of the westbound sections was conducted at the time of construction, after 28 days of curing, and at various intervals over the next two years. The instrumentation included deep and shallow linear variable differential transducers (LVDTs) to measure displacements in the center and the corners of the slabs, thermocouples at four depths near the center and at one corner of the slab, and vibrating wire strain gages with built-in thermistors in the center and the left wheel path. Air temperature data were also gathered during monitoring periods. Data were taken from the instruments at the time of construction, and at 37 days (after curing), 12 months, 16 months, and 28 months after construction. In addition to instrumentation readings taken over an approximately 24-hour period, each visit included slab shape measurements made with a Dipstick[®], and deflections measured with a falling weight deflectometer (FWD) on the westbound sections. The final data collection visit, in October 2004, also included FWD testing and profilometer measurements on the eastbound sections.</p> <p>In measuring the pavement response, the FWD and LVDT data both indicated some loss of support that varied in response to changing temperature conditions. Of the three dowel bar arrangements, the E2 arrangement that used bars with the smallest cross-section and the narrowest spacing had the best load transfer efficiency.</p>			
17. Key Words Portland Cement Concrete (PCC) pavement, falling weight deflectometer (FWD)		18. Distribution Statement No Restrictions. This document is available to the public through the National Technical Information Service, Springfield, Virginia 22161	
19. Security Classif. (of this report) Unclassified	20. Security Classif. (of this page) Unclassified	21. No. of Pages 106	22. Price

SI* (MODERN METRIC) CONVERSION FACTORS

APPROXIMATE CONVERSIONS TO SI UNITS

Symbol When You Know Multiply By To Find Symbol

LENGTH

in	inches	25.4	millimetres	mm
ft	feet	0.305	metres	m
yd	yards	0.914	metres	m
mi	miles	1.61	kilometres	km

AREA

in ²	square inches	645.2	millimetres squared	mm ²
ft ²	square feet	0.093	metres squared	m ²
yd ²	square yards	0.836	metres squared	m ²
ac	acres	0.405	hectares	ha
mi ²	square miles	2.59	kilometres squared	km ²

VOLUME

fl oz	fluid ounces	29.57	millilitres	mL
gal	gallons	3.785	litres	L
ft ³	cubic feet	0.028	metres cubed	m ³
yd ³	cubic yards	0.765	metres cubed	m ³

MASS

oz	ounces	28.35	grams	g
lb	pounds	0.454	kilograms	kg
T	short tons (2000 lb)	0.907	megagrams	Mg

TEMPERATURE (exact)

°F	Fahrenheit temperature	$5(F-32)/9$	Celsius temperature	°C
----	------------------------	-------------	---------------------	----

NOTE: Volumes greater than 1000 L shall be shown in m³.

APPROXIMATE CONVERSIONS FROM SI UNITS

Symbol When You Know Multiply By To Find Symbol

LENGTH

mm	millimetres	0.039	inches	in
m	metres	3.28	feet	ft
m	metres	1.09	yards	yd
km	kilometres	0.621	miles	mi

AREA

mm ²	millimetres squared	0.0016	square inches	in ²
m ²	metres squared	10.764	square feet	ft ²
ha	hectares	2.47	acres	ac
km ²	kilometres squared	0.386	square miles	mi ²

VOLUME

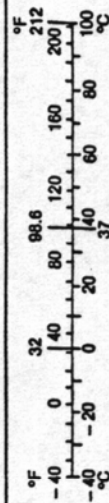
mL	millilitres	0.034	fluid ounces	fl oz
L	litres	0.264	gallons	gal
m ³	metres cubed	35.315	cubic feet	ft ³
m ³	metres cubed	1.308	cubic yards	yd ³

MASS

g	grams	0.035	ounces	oz
kg	kilograms	2.205	pounds	lb
Mg	megagrams	1.102	short tons (2000 lb)	T

TEMPERATURE (exact)

°C	Celsius temperature	$1.8C + 32$	Fahrenheit temperature	°F
----	---------------------	-------------	------------------------	----



* SI is the symbol for the International System of Measurement

Truck/Pavement/Economic Modeling and In-Situ Field Test Data Analysis Applications – Volume 4: Effects of Slab Shape and Load Transfer Mechanisms on Portland Cement Concrete Pavement

Prepared in cooperation with the
Ohio Department of Transportation
and the
U.S. Department of Transportation, Federal Highway Administration

Prepared by

Shad M. Sargand

Jill Morrison

Ohio Research Institute for Transportation and the Environment
Russ College of Engineering and Technology
Ohio University
Athens, Ohio 45701-2979

The contents of this report reflect the views of the authors who are responsible for the facts and the accuracy of the data presented herein. The contents do not necessarily reflect the official views or policies of the Ohio Department of Transportation or the Federal Highway Administration. This report does not constitute a standard, specification or regulation.

Final Report
September 2007

ACKNOWLEDGEMENTS

The authors would like to acknowledge the assistance and support of the pooled fund study members. The authors would like to acknowledge the contributions of the technical liaisons, particularly Dr. Julián Bendaña of the New York State Department of Transportation (NYSDOT), and project panel members to this project, including Roger Green, and the ODOT Office of Research and Development

The authors also acknowledge the contributions of ORITE Research Engineer Sam Khoury to this project.

TABLE OF CONTENTS

1	INTRODUCTION	1
1.1	General Problem Statement	1
1.2	Warping and Curling of Concrete Pavement	1
1.3	Load Transfer Across Joints	2
1.4	Literature Review	2
1.4.1	Slab shape deformation	3
1.4.2	Use of dowel bars.....	4
1.5	Objectives	5
1.6	Outline of Report.....	5
2	PROJECT DESCRIPTION AND INSTRUMENTATION	7
2.1	Project Location and Background.....	7
2.1.1	I-490 West, Rochester, New York	9
2.1.2	I-490 East, Rochester, New York.....	9
2.2	Instrumentation	10
2.2.1	LVDTs	10
2.2.2	Thermocouples.....	11
2.2.3	Vibrating Wire Strain Gages and Thermistors	12
2.2.4	Air Temperature	13
2.3	Instrumentation Layout	14
2.3.1	I-490 West Instrumentation.....	14
2.3.2	Linear Variable Differential Transducers (LVDTs).....	18
2.3.3	Thermocouples.....	21
2.3.4	Vibrating Wire Strain Gages and Thermistors	22
2.3.5	Instrumentation Wiring and Labeling	23
3	DATA ACQUISITION AND ANALYSIS	24
3.1	Introduction	24
3.2	Data Acquisition Equipment.....	24
3.2.1	Campbell Scientific CR7 Measurement and Control System.....	24
3.2.2	Campbell Scientific CR10 Datalogger	25
3.2.3	Dipstick®	25
3.2.4	Falling Weight Deflectometer	27
3.2.5	Profilometer.....	27
3.3	Data Acquisition Procedures.....	28
3.3.1	Deep LVDTs	28
3.3.2	Vibrating Wire Strain Gages and Thermistors	28
3.3.3	Thermocouples.....	29
3.3.4	Handheld LVDT.....	29
3.3.5	Air Temperature Thermistor	29
3.3.6	Dipstick®	29
3.3.7	Falling Weight Deflectometer	29
3.3.8	Profilometer.....	31

4	DATA PRESENTATION AND TESTING RESULTS	32
4.1	Introduction	32
4.2	I-490 West June 2002 Testing	32
4.2.1	Temperature Data	32
4.2.2	Deep LVDT	33
4.2.3	Dipstick®	34
4.3	I-490 West July 2002 24 Hour Monitoring Period	36
4.3.1	Temperature Data	36
4.3.2	Deep LVDT	37
4.3.3	Shallow LVDTs	38
4.3.4	Dipstick®	38
4.3.5	Falling Weight Deflectometer	40
4.3.6	Vibrating Wire	42
4.4	I-490 West June 2003 40 Hour Monitoring Period.....	44
4.4.1	Temperature Data	44
4.4.2	Deep LVDT	44
4.4.3	Dipstick®	44
4.4.4	Falling Weight Deflectometer	47
4.4.5	Vibrating Wire	49
4.5	I-490 West September 2003 24 Hour Monitoring Period.....	52
4.5.1	Temperature Data	52
4.5.2	Falling Weight Deflectometer	52
4.5.3	Vibrating Wire Strain Gages	54
4.6	I-490 West October 2004 Testing	55
4.6.1	Deep LVDTs	56
4.6.2	Shallow LVDTs	58
4.6.3	Dipstick®	58
4.7	I-490 East October 2004 Dowel Bar Testing	60
4.7.1	Slab Profiles	60
4.7.2	Falling Weight Deflectometer (FWD) Testing.....	63
5	CONCLUSIONS.....	70
5.1	PCC Pavement Response Conclusions	70
5.2	Dowel Bar Arrangement Conclusions.....	70
5.3	Implementation.....	71
6	REFERENCES.....	72
	Appendix A: I-490 West Data June 2002.....	74
	Appendix B: I-490 West Data July 2002	82
	Appendix C: I-490 West Data June 2003.....	86
	Appendix D: I-490 West Data October 2003.....	89
	Appendix E: I-490 West Data October 2004.....	96

List of Figures

Figure 1. Plan and Profile Views of Buildup of Pavement Structure on I-490.	8
Figure 2. Dowel Bar Overview	9
Figure 3. I-490 East Dowel Bar Detail.....	10
Figure 4. LVDT Picture.....	11
Figure 5. LVDT Cross Section	11
Figure 6. Geokon VCE-4200 Vibrating Wire Strain Gage.....	12
Figure 7. Vibrating Wire Strain Gage Cross Section	13
Figure 8. I-490 East and West Test Sections	15
Figure 9. I-490 West Instrumentation (25.4 mm = 1 in, 0.305 m = 1 ft).....	16
Figure 10. I-490 West Wiring Detail (2.54 cm = 1 in).....	17
Figure 11. I-490 West Slab Profile	18
Figure 12. Single Layer Deflectometer and reference rod diagram.....	19
Figure 13. Single Layer Deflectometer Detail	20
Figure 14. Thermocouple Stick (25.4 mm = 1 in).....	21
Figure 15. Installation of vibrating wire strain gage with steel box	22
Figure 16. Dipstick® Road Profilometer	26
Figure 17. Falling Weight Deflectometer attached to a van.....	27
Figure 18. ORITE Profilometer	28
Figure 19. Grid for Westbound FWD Test Drop Locations. Distances marked at edges in m (1 m=3.28 ft).	30
Figure 20. Temperature Gradients and Slab Temperature, June 11, 2002 (1C°/m = 0.046°F/in; air temperature scale range is from 32°F to 104°F).....	33
Figure 21. Deep reference LVDT data, June 11, 2002 (1mm = 39 mil; air temperature scale range is from 32°F to 95°F).....	34
Figure 22. Slab 1 profile at 3pm, June 12, 2002, referenced after joints were sawcut (1m=3.28 ft; 1 mm=39 mil)	35
Figure 23. Slab 1 profile at 9am, June 13, 2002, referenced after joints were sawcut (1m=3.28 ft; 1 mm=39 mil)	35
Figure 24. Temperature gradients and air temperature, July 17, 2002 (1C°/m = 0.046°F/in; air temperature scale range is from 32°F to 95°F).....	36
Figure 25. Deep reference LVDT data, July 17, 2002 (1mm = 39 mil; air temperature scale range is from 68°F to 93°F).....	37
Figure 26. Slab 1 profile difference between extreme gradients, July 17, 2002 (1m=3.28 ft; 1 mm=39 mil)	39
Figure 27. Slab 2 profile differences between extreme gradients, July 17, 2002 (1m=3.28 ft; 1 mm=39 mil)	39
Figure 28. Slab 1 deflection from FWD at 8am, July 17, 2002 (1m=3.28 ft; 1 mm=39 mil).....	40
Figure 29. Slab 1 deflection from FWD at 2pm, July 17, 2002 (1m=3.28 ft; 1 mm=39 mil).....	41
Figure 30. Slab 2 deflection from FWD at 8am, July 17, 2002 (1m=3.28 ft; 1 mm=39 mil).....	41
Figure 31. Slab 2 deflection from FWD at 2pm, July 17, 2002 (1m=3.28 ft; 1 mm=39 mil).....	42
Figure 32. Ideal thermal strain versus actual strain readings in left wheel path	43
Figure 33. Temperature gradients in slab as measured using thermistors in vibrating wire strain gauges, June 17, 2003 (1C°/m = 0.046°F/in)	45
Figure 34. Deep reference LVDT data, June 17, 2003 (1 mm = 39 mil; air temperature scale range is from 32°F to 113°F).....	45
Figure 35. Slab 1 profile difference between extreme gradients, June 18, 2003 (1m=3.28 ft; 1 mm=39 mil)	46
Figure 36. Slab 2 profile difference between extreme gradients, June 18, 2003 (1m=3.28 ft; 1 mm=39 mil)	46
Figure 37. Slab 1 deflection from FWD at 10am, June 17, 2003 (1m=3.28 ft; 1 mm=39 mil)	47

Figure 38. Slab 1 deflection from FWD at 2pm, June 17, 2003 (1m=3.28 ft; 1 mm=39 mil)	48
Figure 39. Slab 2 deflection from FWD at 10am, June 17, 2003 (1m=3.28 ft; 1 mm=39 mil)	48
Figure 40. Slab 2 deflection from FWD at 2pm, June 17, 2003 (1m=3.28 ft; 1 mm=39 mil)	49
Figure 41. Vibrating wire strain, center of slab, June 17, 2003 (1C°/m = 0.046°F/in)	50
Figure 42. Vibrating wire strain, left wheel path, June 17, 2003 (1C°/m = 0.046°F/in).....	50
Figure 43. Vibrating wire stress, center of slab, June 17, 2003 (1 MPa = 145 psi; 1C°/m = 0.046°F/in).....	51
Figure 44. Vibrating wire stress, left wheel path, June 17, 2003 (1 MPa = 145 psi; 1C°/m = 0.046°F/in).....	51
Figure 45. Thermistor gradients, September 30 - October 1, 2003 (1C°/m = 0.046°F/in).....	52
Figure 46. Slab 1 deflection from FWD at 10am, September 30, 2003 (1m=3.28 ft; 1 mm=39 mil)	53
Figure 47. Slab 1 deflection from FWD at 1pm, September 30, 2003 (1m=3.28 ft; 1 mm=39 mil)	53
Figure 48. Vibrating wire stress, center of slab, September 30 - October 1, 2003 (1 MPa = 145 psi; 1C°/m = 0.046°F/in).....	54
Figure 49. Vibrating wire stress, left wheel path, September 30 - October 1, 2003 (1 MPa = 145 psi; 1C°/m = 0.046°F/in).....	55
Figure 50. Temperature gradients in slab as measured using thermistors in vibrating wire strain gauges, October 27, 2004 (1C°/m = 0.046°F/in)	56
Figure 51. I490 West LVDT Deflection and Air Temperature Data October 29, 2004 (0.1mm = 3.9 mil; air temperature scale range is from 32°F to 68°F)	57
Figure 52. I490 West LVDT Deflection and Air Temperature Data October 30, 2004 (0.1mm = 3.9 mil; air temperature scale range is from 32°F to 77°F)	57
Figure 53. Shallow LVDT Readings, October 2004 (1m=3.28 ft; 1 mm=39 mil; Temperatures are: 7.2°C (45°F), 11.1°C (52°F), and 15.6°C (60°F))	58
Figure 54. Slab 2 profile at 10:30 am, referenced after joints sawcut (1m=3.28 ft; 1 mm=39 mil)	59
Figure 55. Slab 2 profile at 1:30 pm, referenced after joints sawcut (1m=3.28 ft; 1 mm=39 mil)	59
Figure 56. Slab 2 difference between 10:30 am and 1:30 pm profiles (1m=3.28 ft; 1 mm=39 mil)	60

List of Tables

Table 1. NYSDOT Class C Mix Design.....	7
Table 2. I-490 East Cross-Sectional Area of Steel in Joints	9
Table 3. I-490 East Dowel Bar Spacing	9
Table 4. Warping with Time at Varying Slab Locations	38
Table 5. I490 East Estimated Differences in Deflection Due to Environmental Factors for Individual Slabs (metric units)	61
Table 6. I490 East Estimated Differences in Deflection Due to Environmental Factors for Individual Slabs (English units)	62
Table 7. I-490 East 37.4 kN (8.41 kip) FWD, Slabs 1-25, October 26, 2004.....	64
Table 8. I-490 East 50.3 kN (11.3 kip) FWD, Slabs 1-25, October 26, 2004.....	65
Table 9. I-490 East 37.4 kN FWD, Slabs 26-55, October 26, 2004.....	66
Table 10. I-490 East 50.3 kN FWD, Slabs 26-55, October 26, 2004.....	67
Table 11. I-490 East 37.4 kN (8.41 kip) FWD, Slabs 56-84, October 26, 2004.....	68
Table 12. I-490 East 50.3 kN FWD, Slabs 56-84, October 26, 2004.....	69

1 Introduction

1.1 General Problem Statement

Environmental factors have a major impact on both the initial response and long term performance of Portland Cement Concrete (PCC) pavements. Past research has shown the significant influence environmental factors have on the longevity of PCC pavement [Hveem & Tremper, 1957]. However, additional research is needed to determine how to incorporate environmental factors into the PCC design process.

Additionally, the transfer of load from slab to slab by the use of dowel bars is critical for maintaining the quality of PCC pavement. The importance of this dynamic effect has long been recognized, but additional research is needed to determine the most effective dowel bar configuration.

The New York State Department of Transportation constructed test sections in Interstate 490 near Rochester, New York with the objective of evaluating the effects of environmental factors and dynamic loading on PCC pavements. This report describes the research methods used and the results obtained from this study of environmental and dynamic effects on the PCC pavement.

1.2 Warping and Curling of Concrete Pavement

Warping and curling of PCC pavements can result from heat of hydration and from environmental factors such as ambient temperature and humidity during curing. The pavement is influenced by these factors beginning at the time of curing and continuing throughout the service life of the pavement. Curling and warping both cause changes in slab shape; however, these changes are restrained by adjacent slabs, dowel bars, tie bars and friction with the subbase. Because the slab is restrained during deformation, stresses occur in the slab.

Warping is a change in pavement shape due to the moisture gradient. This predominantly occurs during the concrete curing phase when moisture is lost while the concrete is gaining strength. Since concrete is typically placed while the ambient temperature is high, the evaporation at the exposed surface is much higher than at the bottom of the slab. This loss causes an initial moisture gradient which is coupled with additional moisture losses from the long term curing process. These losses of water result in a decrease in volume, with a majority of the water being lost from the exposed surface of the slab. Therefore, it is believed by many researchers that soon after construction, slabs warp slightly upward resulting in a loss of support under the edges.

In addition to warping, concrete is also affected by a built-in temperature gradient during the curing process. While the concrete develops a positive built-in temperature gradient when placed in hot weather, the thermal stress on the concrete is insignificant during initial curing, before the joint cuts are sawn into the road; during this phase of the curing process the slab can be regarded as infinite in the longitudinal (travel) direction. Additionally, the slab undergoes stress relaxation because the concrete is a plastic material. As a result, the slab cures flat with a positive built-in temperature gradient. As the air temperature cools, the temperature gradient in the slab dissipates to zero. The slab reacts to this change in temperature gradient by the corners of the slab curling up; this behavior is typically associated with a negative temperature gradient

in the slab. Throughout the night the air continues to cool, inducing a negative temperature gradient in the slab. As the slab temperature gradient changes from zero to negative the slab corners curl up even more.

Both curling due to the built-in temperature gradient and warping due to moisture gradient affect the slab shape during the initial curing process. Because these processes happen simultaneously, the specific amounts of change in slab shape caused by each effect during this time cannot be directly determined. Additionally, the combined effect of curling and warping during initial curing may be so great that the slab never again regains the initial flat shape.

Curling is the change in slab shape due to a change in temperature gradient. If the slab were to undergo uniform temperature changes throughout the entire depth of the slab, it would expand and contract uniformly until restrained by external forces. However, this case of uniform deformations and stresses throughout the slab depth is not realistic; at most times a slab will have either a positive or negative temperature gradient. With a positive temperature gradient, the exposed side of the slab will be warmer than the bottom of the slab, resulting in the top expanding and the bottom contracting. In this case the slab will be concave down, but will be restricted by self weight, dowel bars, and tie bars. Therefore, the stresses in the slab will be compressive forces in the top of the slab and tensile forces in the bottom of the slab. When the slab experiences a negative temperature gradient, colder on the exposed side and warmer on the bottom, the bottom will expand and the top will contract resulting in a concave up shape. However, because the slab experiences restraints, the top of the slab will experience tensile forces while the bottom of the slab will be in compression.

1.3 Load Transfer Across Joints

Early shrinkage cracks result from stresses induced by changes in the pavement temperature gradient and moisture gradient. In order to control this cracking, it is necessary to construct joints in the PCC pavement. However, the joints themselves then present additional problems that must be considered in the PCC pavement design. If the joint is not properly designed, densification of the base can occur under the joint, which may lead to pavement faulting. This failure can be prevented when the joint properly transfers the load from the approach slab to the leave slab.

Load transfer across a joint is most typically accomplished through the use of dowel bars. The load transfer efficiency (LTE) of a joint is measured by the relative deflection of the approach and leave slabs as the load passes over the joint. By properly using dowel bars to control faulting and spalling, damage can be prevented and ride quality maintained. The design of dowel bar configurations for load transfer should take into consideration the slab deflection due to dynamic traffic loading and the slab deflection due to warping and curling from environmental changes. The current design practices for dowel bar size and spacing are determined primarily through theory and laboratory research; they have had little field research to validate them.

1.4 Literature Review

A PCC pavement consists of Portland cement concrete slabs erected on top of a prepared base that rests on compacted subgrade soil. A load transfer mechanism, principally steel dowel bars is used at the joints between slabs to help ensure a smooth road and transfer vehicle load from one slab to the next. In this project, the performance of the slab and the joints were the

subjects of study. In particular the deformation of the slab shape due to temperature and moisture issues after pouring, the load response of the slabs, and the effectiveness of the joints in transferring load and helping to preserve slab shape. The following is a review of the relevant research on these topics.

1.4.1 Slab shape deformation

Choubane and Tia [1986] used Falling Weight Deflectometer (FWD) test data and temperature information on slabs at different locations to verify analytically predicted stresses. The temperature distribution throughout the depth of a slab was found to approximately follow a quadratic equation. The authors thus determined that the temperature distribution throughout the depth of the slab is important when studying a PCC pavement, not just the temperature differential between the top and bottom of the slab.

Armaghani et al. [1986] studied the horizontal and vertical displacement of PCC slabs using LVDTs; pavement temperature was measured using thermocouples. This study found an approximately one hour time lag between the corresponding maxima in the ambient air temperature and the corresponding pavement temperatures; a similar relationship held for the temperature minima. It was also found that the displacement at undoweled joints was about 45% higher than the displacement in doweled joints. This finding indicates that while dowels resist slab movement, they also cause stresses in the pavement.

Rollings and Pittman [1992] determined that joint spacing and thickness of a PCC pavement slab influence the amount of differential shrinkage necessary to induce built-in curling. The study also found that stresses due to temperature can cause up to 60% of the total environmental and traffic loading stresses in PCC pavement; that is the thermal stresses can actually exceed the traffic load.

Two identical slabs were studied by Jeong and Zollinger [2004] to determine the moisture and creep effects on the warping and curling of jointed concrete pavement. Two different curing methods were used: one slab was membrane cured and the other was cured under an insulation mat. The membrane cured slab had larger built in curling and shrinkage while the slab cured under the insulation mat had a larger shift of tensile strain. The study also found that the dowel bars experienced bending moments corresponding to those of the joint displacements.

Sargand [2004] also compared membrane and traditional water curing on a concrete pavement installed on US Route 33 in Nelsonville, Ohio. For a standard Ohio Department of Transportation (ODOT) mix, the membrane cured concrete was found to have a greater amount of warping than the section cured in the traditional manner with wet burlap. The warping was measured using a profilometer after the curing period. For the other sections, which used an experimental blend with fly ash, similar results were observed with one mix and the opposite results seen with the other mix.

Three doweled and three undoweled slabs were studied in a temperature controlled environment by Sargand et al. [2003]. The temperature was held constant for the first 28 days of curing, and it was found that after the heat of hydration dissipated, the slab temperature gradient was nearly zero. It was found that the undoweled slabs had warped more than the doweled slabs. However, the forces were less than expected in the dowel bars because the stiffness of the bars caused an increase in the diameter of the dowel bar holes. It was determined that built-in curling can be reduced by inducing a positive temperature gradient, but a permanent loss of support at the base almost always occurs.

Sargand and Abdalla [2006] determined the lifetime of a concrete pavement as a function of joint spacing. They found that generally the expected lifetime increased as the spacing decreased, and the shortest spacing studied, 13 ft (3.96 m) had the longest lifetimes whether determined by the Huang, PCA, or Dominichi fatigue models.

1.4.2 Use of dowel bars

Concrete pavement slabs are rigid and must have a finite size to accommodate thermal expansion; in order to make a long and smooth road using concrete, a method of transferring load from one slab to the next must be used. The first use of dowel bars as a load transfer device in a concrete road was on a military road built in Newport News, Virginia, in 1917-1918 [Smith, 1922]. Following this first use of dowel bars, load transfer devices became widely used in concrete pavements. Other early alternative load-transfer mechanisms included T-sections, sliding key or bridge, rectangular tongue and groove, and rounded sockets and joints [Teller and Sutherland 1936]. However, the dowel bar has remained the most commonly used load transfer device.

Teller and Cashell [1958] conducted a laboratory study on the performance of dowel bars under repetitive loading. Slabs with dimensions of four feet by ten feet were constructed, with variations in the dowel bar diameter and length as well as the width of the joint opening. An analysis of the data obtained showed that there is an exponential relationship between the dowel bar diameter and load-transfer capability. It was found that the minimum dowel diameter to be used in a PCC pavement should be $\frac{1}{8}$ of the slab thickness. The required length of embedment for a $\frac{3}{4}$ in (19 mm) diameter dowel bar was found to be 8 dowel bar diameters (6 in or 152 mm) and the required length for larger dowel bars was found to be 6 dowel bar diameters (4.5 in or 114 mm).

The design of dowel bar installations on highways was initially determined by theoretical models [Timoshenko and Lessells 1925, Westergaard 1928, Bradbury 1933, Teller and Sutherland 1936, Friberg 1938]. More recently, the theoretical models have been updated using finite element methods, including programs such as ILLISlab and KenSlab. These programs divide the slabs into rectangular elements and then apply wheel loads and subgrade reactions as vertical forces concentrated at certain surface nodes. The dowel bars are assumed to act at certain other nodes, and are assigned a spring constant which is calculated based on the dowel diameter and spacing as well as the joint width. By analyzing a dowel bar configuration in a finite element program, it can be determined if the proposed configuration is adequate for the pavement design and loading conditions. [Tabatabaie and Barenberg, 1980]. Using finite element methods, Heinrichs [1989] reduced the distance of the point at which the maximum negative moment acts to 1.0*l* from 1.8*l* as used in earlier models. This decrease in distance between the maximum negative moment and the load thus increased the load carried by the most critical dowel.

Design practices presented in current text books and design manuals [e.g. Huang, 2004, Portland Cement Association, 1975] are still based primarily on the early theoretical models, particularly the solutions by Friberg [1938], and the dowel bar experiments of Teller and Cashell [1958]. If nothing else, the older solutions are analytic and familiar, at least to instructors.

In a study by Sargand and Cindar [1997], four types of dowel bars were instrumented with strain gages and installed in PCC pavement. These dowel bars were then subjected to environmental cycling of temperature and moisture, and were tested with FWD dynamic loading. It was found that the dowel bars function both as a load transfer mechanism and as a method of

reducing the magnitude of curling at the joints. It was also determined that the moments experienced by the dowel bars were significantly higher when subjected to environmental changes than when tested with FWD dynamic loading, indicating that the environmental changes were the primary contributor to the bending moments. Sargand [1998] studied the response of dowel bars in rigid pavements and found that the more rigid a load transfer system is, the better the system transfers load and the less curvature the slab experiences. However, the increased stiffness of the load transfer system transfers greater bending moments from the dowel bars to the concrete. When a less rigid load transfer system is used, the slab undergoes greater curvature due to environmental factors resulting in non-uniform support for the traffic loading. This will cause the slab to experience higher tensile stresses and the supporting layers to be subjected to greater maximum compressive stresses.

The performance of dowel bars in rigid pavement was studied by Sargand [2001]. Epoxy-coated steel dowel bars, fiberglass dowel bars, and stainless steel tubes filled with concrete were instrumented with strain gages and installed in high performance concrete pavement. The pavement was subjected to environmental moisture and temperature cycling as well as dynamic FWD loading near the joints. The study found that significant stresses were experienced by the dowel bars and in the surrounding concrete soon after the concrete was placed. Additionally, the temperature gradients in the slab subjected the dowel bars to high stresses during curing.

In a study for the Texas Department of Transportation, Owusu-Antwi et al. [1990] studied longitudinal joint tie-bar combinations of No. 4 and No. 5 bars (nominal diameters 12.7 mm ($\frac{1}{2}$ in) and 15.9 mm ($\frac{5}{8}$ in), respectively), 381 mm (15 in) or 635 mm (25 in) long, at 610 mm (24 in), 914 mm (36 in), or 1220 mm (48 in) spacing. It was determined that the spacings of 610 mm (24 in) and 914 mm (36 in) were more effective than 1220 mm (48 in). There was no statistical difference between the 610 mm (24 in) and 914 mm (36 in) spacings or between the two tie bar sizes. It was also found that if the pavement design and construction practices are the same, the 381 mm (15 in) and 635 mm (25 in) long tie bars are equally effective.

1.5 Objectives

In order to increase the research-based knowledge on the dynamic and environmental effects on PCC pavement and on dowel bar diameter and spacing, the objectives for this project were:

- Present descriptions of pavement instrumentation and data acquisition systems for measuring environmental and dynamic effects on PCC pavement sections.
- Evaluate the loss of support for PCC during the curing process and service.
- Investigate the effect of three variations of dowel bar diameter and spacing on load transfer efficiency (LTE) and pavement performance.
- Recommend layout design for dowel bars in transverse joints.
- Determine the environmental and dynamic effects on the pavement

1.6 Outline of Report

This report has five chapters:

Chapter 1 is this introductory chapter that includes the problem statement, literature review, and objectives.

Chapter 2 provides a description of project location, instrumentation, data acquisition systems, and test procedures. Details on instrumentation operation, selection, and positioning are presented.

Chapter 3 contains a description of the methods used to collect and analyze data.

Chapter 4 presents processed data and discusses the results of the environmental and dynamic testing.

Chapter 5 presents conclusions drawn from data and offers recommendations.

Additional data recorded but not featured in the report narrative are included in the appendices.

2 Project Description and Instrumentation

2.1 Project Location and Background

This research was conducted on concrete pavement located on I-490, approximately 16 km south-east of Rochester, New York as part of a two year reconstruction project of both the eastbound and westbound lanes. The pavement was placed two lanes at a time by a slip form paver. The jointed plain concrete pavement (JPCP) slab dimensions were 5 m long, 4.60 m wide, and 250 mm (9.8 in) thick, and the slabs were placed on a 75 mm (3.0 in) thick permeable concrete treated base on top of a 300 mm (11.8 in) thick aggregate base, as shown in Figure 1. The two 4.27 m (14.0 ft) wide traffic lanes were constructed first, with the 3.6 m (11.8 ft) wide exit ramp lane and 3.0 m (9.8 ft) wide concrete shoulders installed later. The typical dowel bar spacing was 305 mm (12 in) between centers, with a dowel bar diameter of 32 mm (1.25 in). The typical tie bar spacing was 714 mm (28.1 in) on center with a diameter of 19 mm (¾ in). The eastbound dowel bar diameters and spacings were varied as part of this study.

In the westbound driving lane two slabs were instrumented to study the environmental effects on the pavement. Additionally in the eastbound driving lane, nine sections of ten slabs each were studied to investigate the effect of transverse dowel bar spacing and diameter.

Both the eastbound and westbound test sections were paved with New York State Department of Transportation (NYSDOT) Class C mix as detailed in Table 1. The desired 28 day strength of this mix is 31.5 MPa (4.57 ksi). The concrete has a coefficient of thermal expansion of $12 \times 10^{-6}/C^{\circ}$ ($6.7 \times 10^{-6}/F^{\circ}$) and elastic modulus of 29,000 MPa (4200 ksi). The slabs are supported by a 100 mm (3.9 in) thick cement treated permeable base. This base was placed on a 150 mm (5.9 in) thick dense graded aggregate base.

Table 1. NYSDOT Class C Mix Design

Material	density		
	pcf	kg/m ³	
Water	9.9	158	
Cement	17.9	287	
Fly Ash	4.5	72	
Fine Aggregates	39.6	634	
Coarse Aggregates	(#1 Stone, 40% Split)	28.3	454
	(#2 Stone)	42.6	682
Water-Cement Ratio = 0.44			

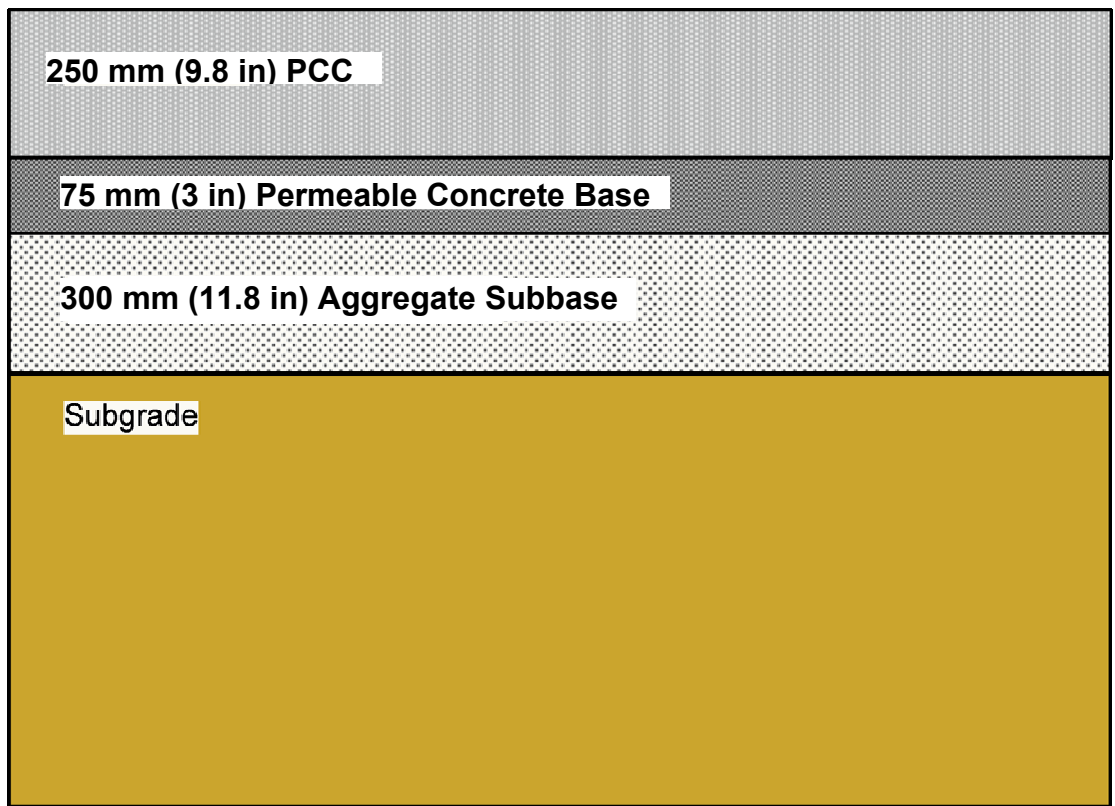
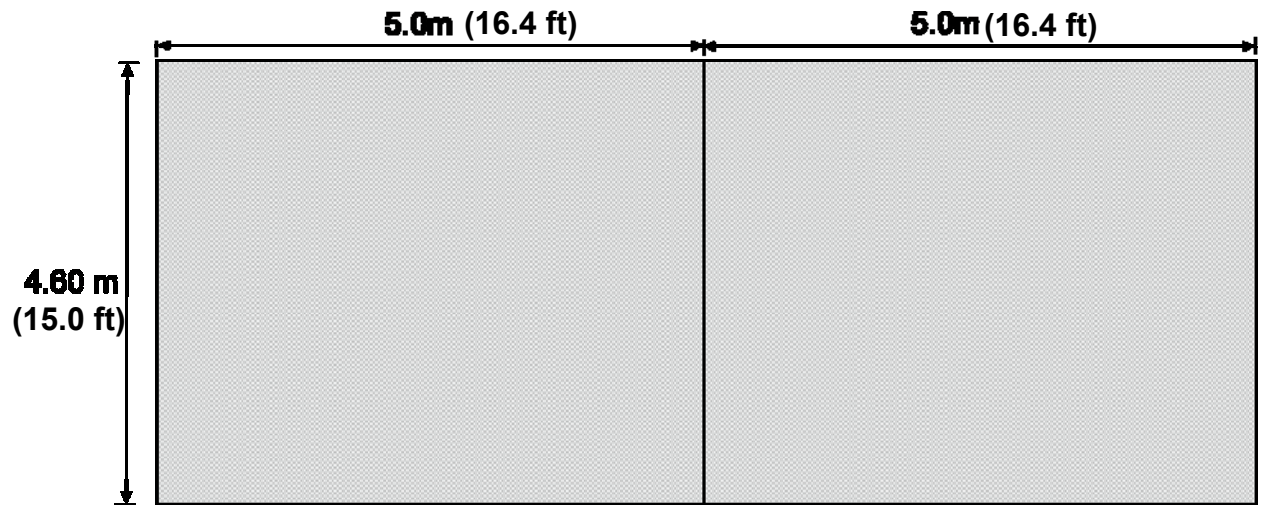


Figure 1. Plan and Profile Views of Buildup of Pavement Structure on I-490.

2.1.1 I-490 West, Rochester, New York

In the westbound driving lanes, two adjacent slabs were instrumented to monitor the environmental strain on the slabs as well the vertical deflection. The concrete strength, base type, base thickness, and drainage conditions were consistent for these two slabs. The slabs were monitored during construction so that the actual strains and deflections the slab experienced during the curing process could be recorded. Additional periods of monitoring occurred after the pavement cured.

2.1.2 I-490 East, Rochester, New York

The eastbound test section of I-490 included a series of slabs with three variations in transverse dowel bar diameters and spacing, designated as STD (“standard”), E1, and E2. The cross-sectional steel area of each configuration is indicated in Table 2. The test pavement included nine sections consisting of ten slabs each as shown in Figure 2. The dowel bar length was held constant at 450 mm (17.7 in) with the diameter and spacing as specified in Table 3 and depicted in Figure 3. All dowel bars were placed using baskets.

Table 2. I-490 East Cross-Sectional Area of Steel in Joints

Cross-Sectional Steel Area				
Section	Slab		1/3 Slab	
	mm ²	in ²	mm ²	in ²
STD	11,259	17.45	4,021	6.23
E1	10,468	16.23	3,695	5.73
E2	10,800	16.74	3,436	5.33

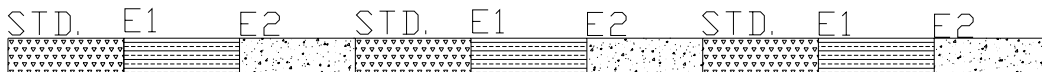


Figure 2. Dowel Bar Overview

Table 3. I-490 East Dowel Bar Spacing

Type	Diameter		Dowel Bar Spacing Dimensions							
			A		B		C		D	
	(mm)	(in)	(mm)	(in)	(mm)	(in)	(mm)	(in)	(mm)	(in)
STD	32	1.26	150	5.91	300	11.81	150	5.91	300	11.81
E1	28	1.10	180	7.09	240	9.45	120	4.72	240	9.45
E2	25	0.98	105	4.13	190	7.48	90	3.54	190	7.48

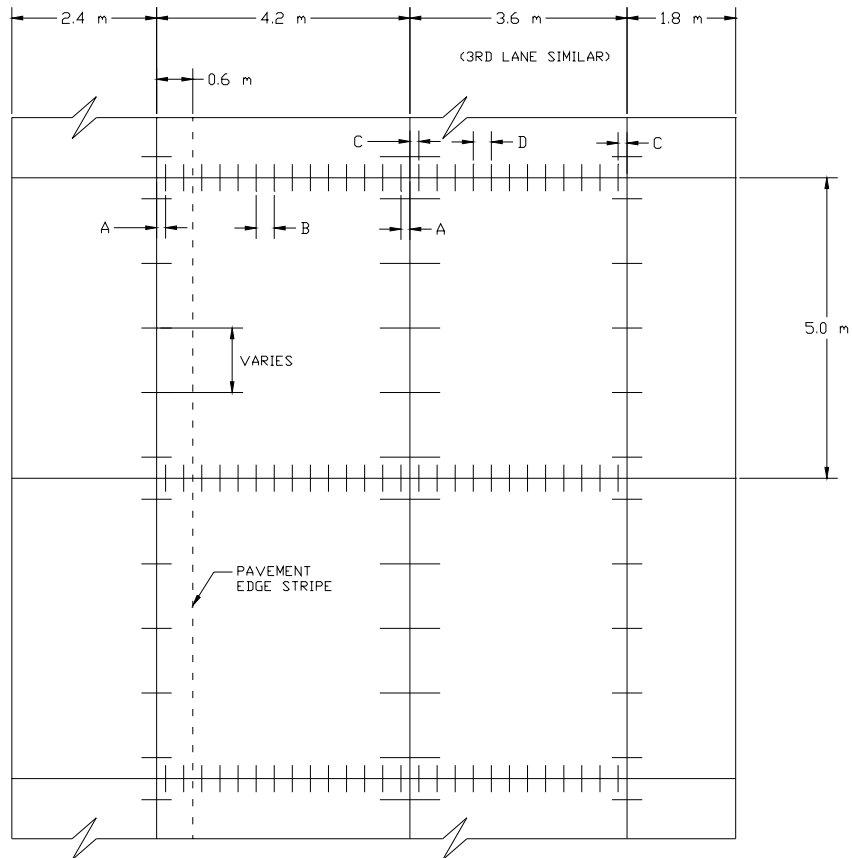


Figure 3. I-490 East Dowel Bar Detail

2.2 Instrumentation

2.2.1 LVDTs

The measurement of vertical slab deflection for this project was accomplished with the use of Direct Current (DC) Linear Variable Differential Transducers (LVDTs) manufactured by Macro Sensors. The LVDT model used for this project is the GHSD 750, which has a range of ± 12.7 mm (± 0.5 in). As depicted in Figure 4 and in the cross-section in Figure 5, the LVDT consists of a hollow cylindrical shaft containing a primary and two secondary coils, and a solid cylindrical core which slides through the shaft. The tip of the magnetic core is in contact with a reference rod, and the displacement of the reference rod initiates the movement of the magnetic core. A stiff spring is enclosed between the core and the end of the hollow shaft in order to recover this deflection and ensure constant contact between the LVDT and reference rod. The LVDT is made of stainless steel components in order to ensure the LVDT does not rust and maintains freedom for proper movement.



Figure 4. LVDT Picture

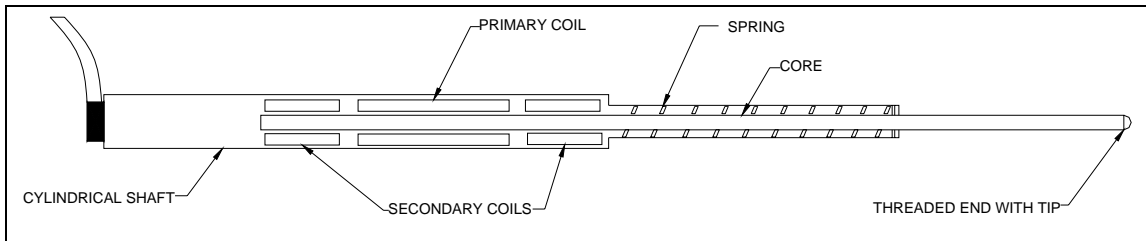


Figure 5. LVDT Cross Section

The electric output of the LVDT, measured in volts, is proportional to the position of the core in the shaft. By measuring the output voltage, one can determine the movement in the core as a result of the reference plate (slab) displacing the tip. The movement of the core changes the mutual inductance between the primary and secondary windings, causing the change in the output voltage; one secondary winding becomes more tightly coupled to the primary winding while the other secondary winding becomes more loosely coupled to the primary winding. Because the secondary coils are wired in opposition, the output voltage of the LVDT is the difference between the voltages developed in the secondary windings. This LVDT model requires an input voltage of ± 15 volts DC and has an output voltage range of ± 10 volts DC for the entire 12.7 mm ($\frac{1}{2}$ in) range. This corresponds to an output voltage of 0.79 volts per millimeter (20V/in) of displacement.

2.2.2 Thermocouples

Type T (copper-constantan) thermocouples from Omega were used in this project to determine the temperature gradient in the pavement. These thermocouples operate in the temperature range of -250°C (-418°F) to 350°C (662°F). The operating principle of the thermocouple is that when the junction of two wires made from different metals (in this case copper and constantan) is heated, the voltage of the circuit is a function of the temperature at the junction and the composition of the two metals. Additionally, the wires used to connect the thermocouple wire to the voltmeter introduce error, so the voltage read by the voltmeter is equivalent to:

$$V = \alpha(T_{J1} - T_{REF}) \quad \text{Equation 2.1}$$

Where:

V = Voltage reading from voltmeter

α = Seebeck coefficient, dependent on metal types and temperature

T_{J1} = Temperature at junction of metals

T_{REF} = Temperature at reference point

The temperature at the reference point is measured by a thermistor at the point where the thermocouple wire is connected to the voltmeter. This equation is then used to calculate the temperature at the connection point of the two metals.

The thermocouple data were collected, processed, and stored using a CR7 datalogger. The 723-T analog input card which the thermocouples were connected to included a platinum resistance thermistor (PRT) used as a temperature reference. The CR7 was programmed to take differential voltage readings of the thermocouples and calculate the pavement temperature referencing the PRT temperature. These pavement temperature data were stored in °C.

2.2.3 Vibrating Wire Strain Gages and Thermistors

Pavement strain was measured using Geokon vibrating wire strain gage model VCE-4200. A picture is shown in Figure 6 with the cross-section depicted in Figure 7. This strain gage operates on the vibrating wire principle. The gage is embedded directly in the concrete, and contains a steel wire which is tensioned between two end blocks. When the concrete is strained and deforms, the end blocks will move and change the tension of the wire. The wire is plucked by an electromagnetic coil, and the tension is proportional to the square of the measured resonant frequency of the vibrating wire. In turn, the wire tension is used to calculate the strain in the concrete. The readings are corrected for thermal variations due to temperature effects on the wire and also with a manufacturer-supplied “batch factor” (a 4.2% reduction in measured strain) to account for the shortening of the wire due to clamping the ends. The VCE-4200 has a strain range of $\pm 3000 \mu\epsilon$, with a sensitivity of $\pm 1.0 \mu\epsilon$. It is accurate over a temperature range of -20°C (-4°F) to $+80^{\circ}\text{C}$ (176°F). It has long term stability, high water resistance, and transmits accurately over long cable lengths. Components are constructed of stainless steel in order to prevent corrosion.



Figure 6. Geokon VCE-4200 Vibrating Wire Strain Gage

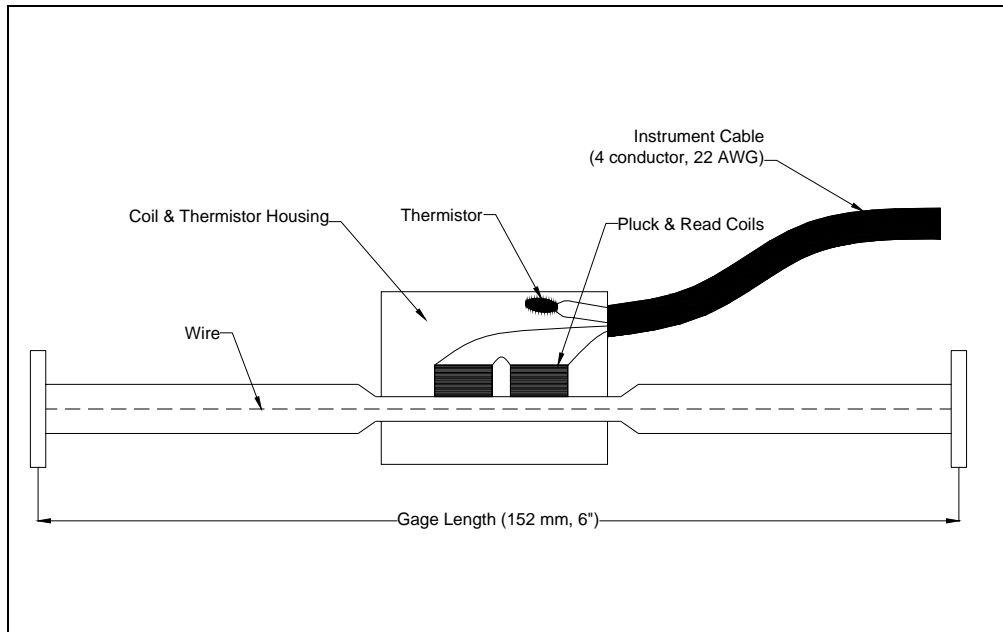


Figure 7. Vibrating Wire Strain Gage Cross Section

Additionally, the VCE-4200 includes a thermistor for internal pavement temperature measurement. The thermistor consists of a sensing element made of semiconductor material which was bonded by heating without melting. When a small temperature change occurs, a large resistance change in the sensing element is induced. The effect of the resistance of cable connecting the thermistor to the collection unit is insignificant, and the change in resistance can be translated into temperature by using the Steinhart-Hart Log Equation. This conversion was done by a program in the CR10 datalogger, which was used to collect the thermistor data and store the actual temperature value. The Steinhart-Hart Log Equation is:

$$T = \frac{1}{A + B(\ln R) + C(\ln R)^3} - 273.2 \quad \text{Equation 2.2}$$

Where:

T = pavement temperature in °C (converted from Kelvins (K) by subtracting 273.2)

$\ln R$ = natural log of thermistor resistance in ohms

$A = 1.4051 \times 10^{-3}$ (coefficients (in K^{-1}) calculated over the $-50^{\circ}C$ ($-58^{\circ}F$) to $+150^{\circ}C$ ($302^{\circ}F$) span)

$B = 2.369 \times 10^{-4}$

$C = 1.019 \times 10^{-7}$

The calculated temperatures are then used for the previously mentioned thermal corrections to the apparent strain readings.

2.2.4 Air Temperature

The air temperature was measured with a Campbell Scientific T108 Temperature Probe. The temperature probe has a thermistor encapsulated in an epoxy-filled aluminum housing. This thermistor can measure temperatures ranging from $-5^{\circ}C$ ($23^{\circ}F$) to $+95^{\circ}C$ (203°). The T108 Temperature Probe thermistor operates under the same principle previously described for the thermistor included with the vibrating wire strain gage. To protect the T108 Temperature Probe

from direct exposure to sunlight, the probe is enclosed in a radiation shield. The temperature probe was connected to the CR7 datalogger, which converted the measured resistance to temperature in °C.

2.3 Instrumentation Layout

In Figure 8 an overview is presented of the locations of instrumentation for the I-490 westbound and dowel bar variations in I-490 eastbound.

2.3.1 I-490 West Instrumentation

In this section the layout and installation procedure for the instrumentation of I490 West is presented. Detailed drawings of the instrumentation layout, wiring diagram, and the slab profile are presented in Figure 9, Figure 10, and Figure 11.

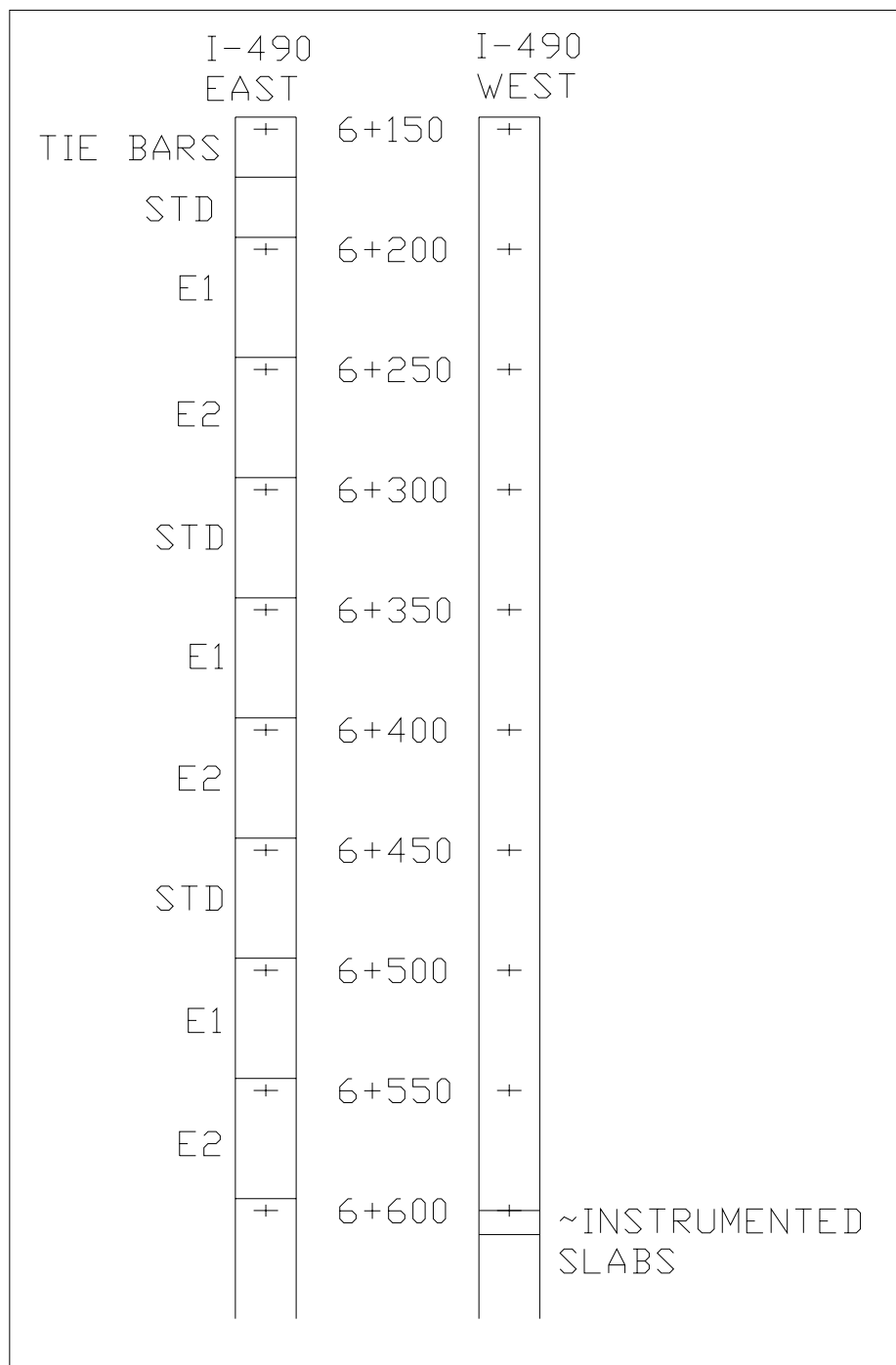


Figure 8. I-490 East and West Test Sections

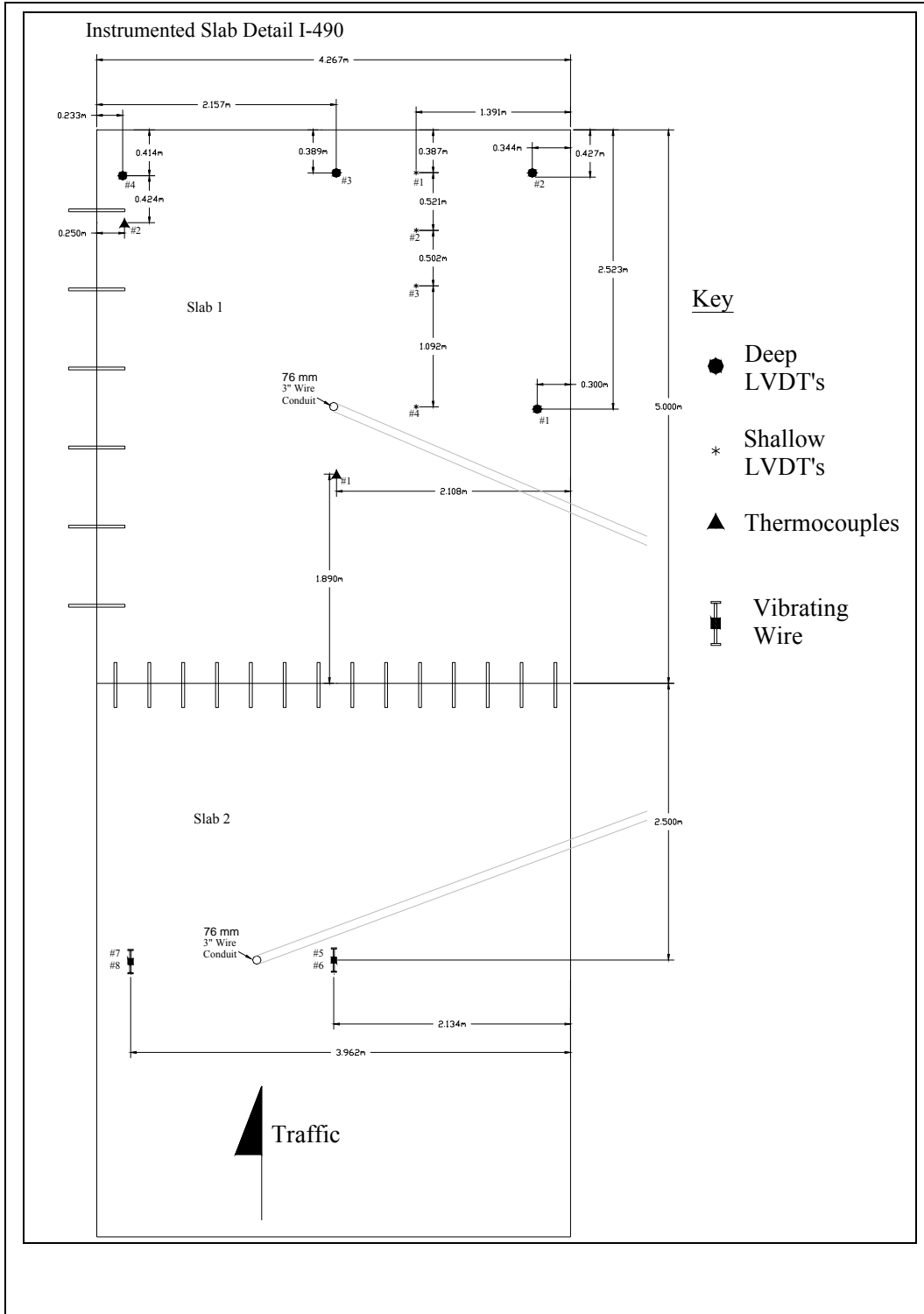


Figure 9. I-490 West Instrumentation (25.4 mm = 1 in, 0.305 m = 1 ft)

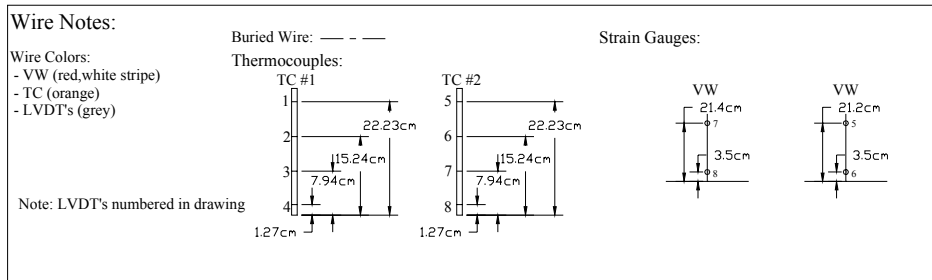
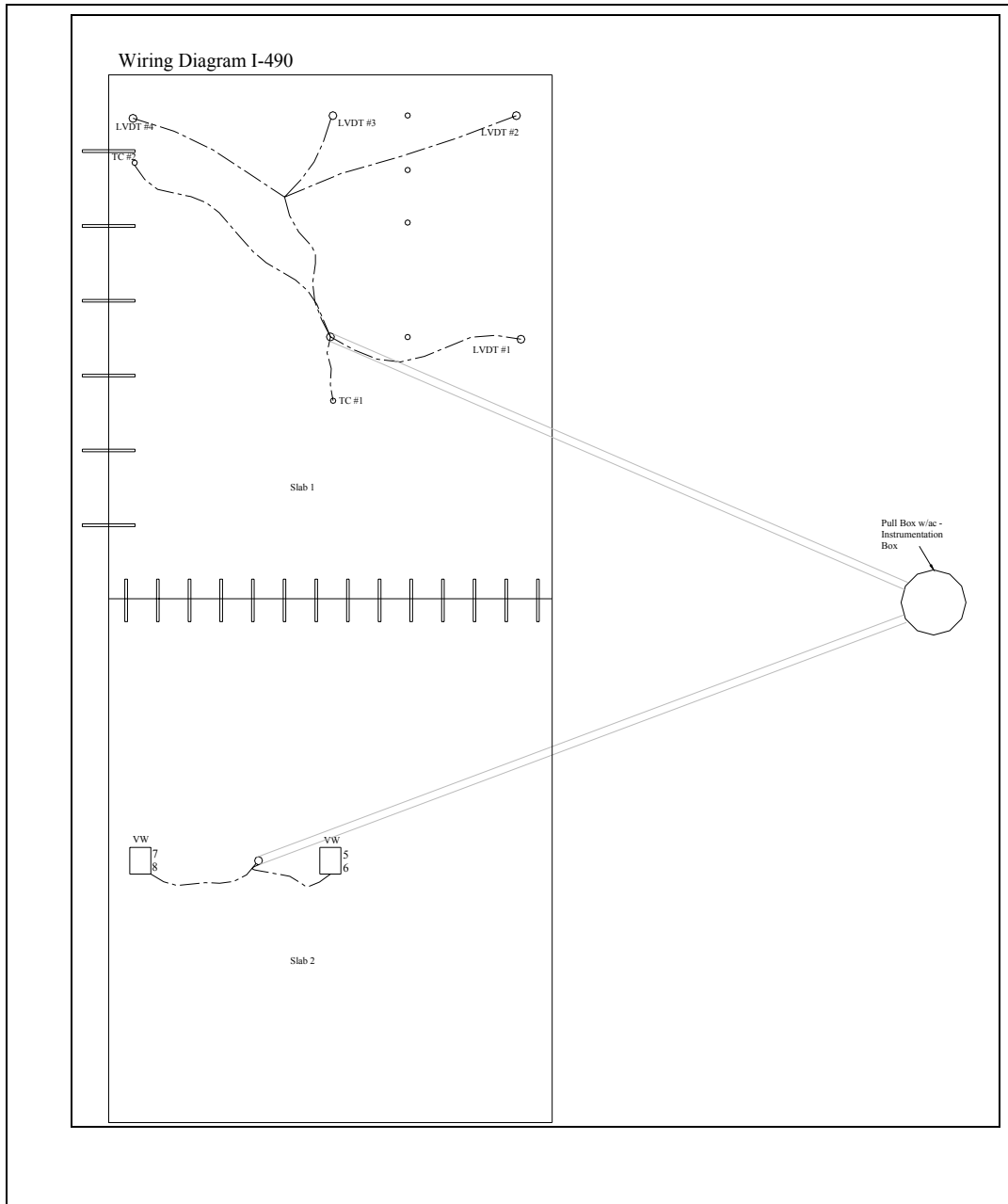


Figure 10. I-490 West Wiring Detail (2.54 cm = 1 in)

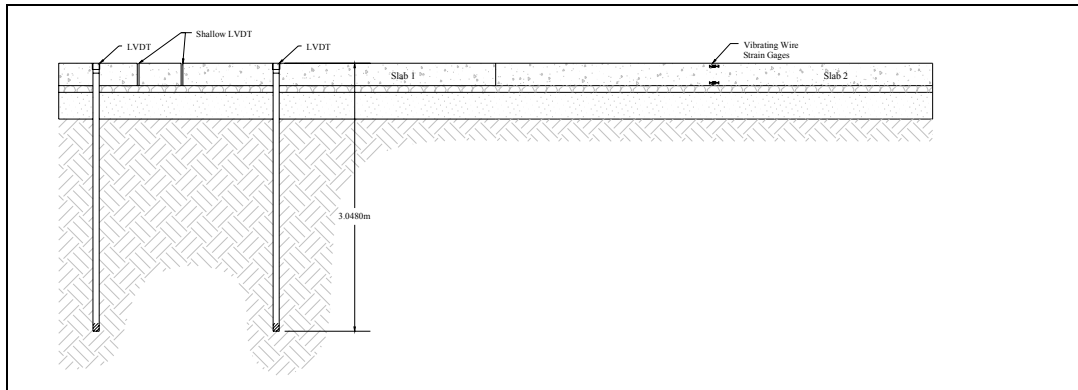


Figure 11. I-490 West Slab Profile

2.3.2 Linear Variable Differential Transducers (LVDTs)

A total of eight LVDT locations were installed in the westbound instrumented sections of I-490. Four deep LVDTs were installed before the placement of the pavement. Additionally, four shallow LVDT reference plates were installed prior to the pavement placement.

The first step in the installation of the deep reference LVDTs was the placement of the reference rods, as shown in Figure 12. A hole with a diameter of 63.5 mm (2.5 in) was augered to a depth of 3.35 m (11 ft) into the subgrade. A PVC pipe with a diameter of 50.8 mm (2 in) and a length of 3.05 m (10 ft) was then inserted into the augured hole in order to keep soil from caving into the hole. Any voids between the outer surface of the PVC pipe and the subgrade were then filled with sand. The steel reference rod with a diameter of 19 mm ($\frac{3}{4}$ in) and a length of 3.66 m (12 ft) was placed inside the PVC pipe and then driven approximately 0.3 m (1 ft) into the subgrade to the desired elevation. The bottom of the rod was then grouted with hydraulic cement.

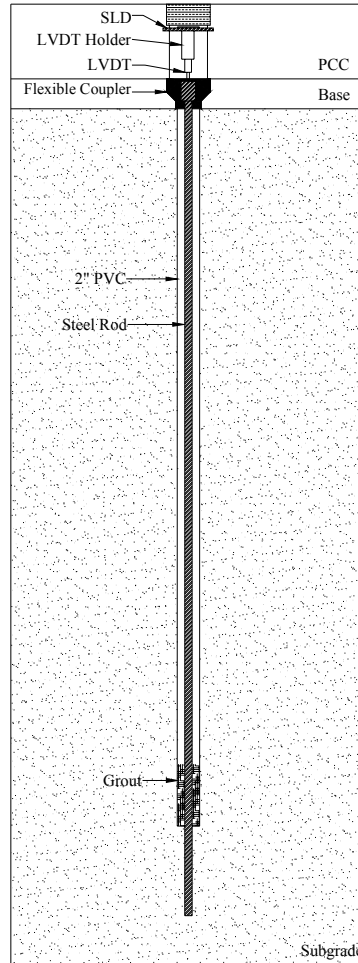


Figure 12. Single Layer Deflectometer and reference rod diagram

Next a Single Layer Deflectometer (SLD) was installed to develop a rigid connection between the pavement slab and the LVDT. The SLD, shown in Figure 13, was a specially designed steel unit which was embedded in the concrete slab directly above the reference rod during the paving process. The SLD was also connected to the PVC pipe by means of a flexible reducer. This reducer allowed the SLD to move vertically, yet was stiff enough to prevent moment in the horizontal direction. This kept the SLD from being pushed over by concrete when the paver and spreader passed.

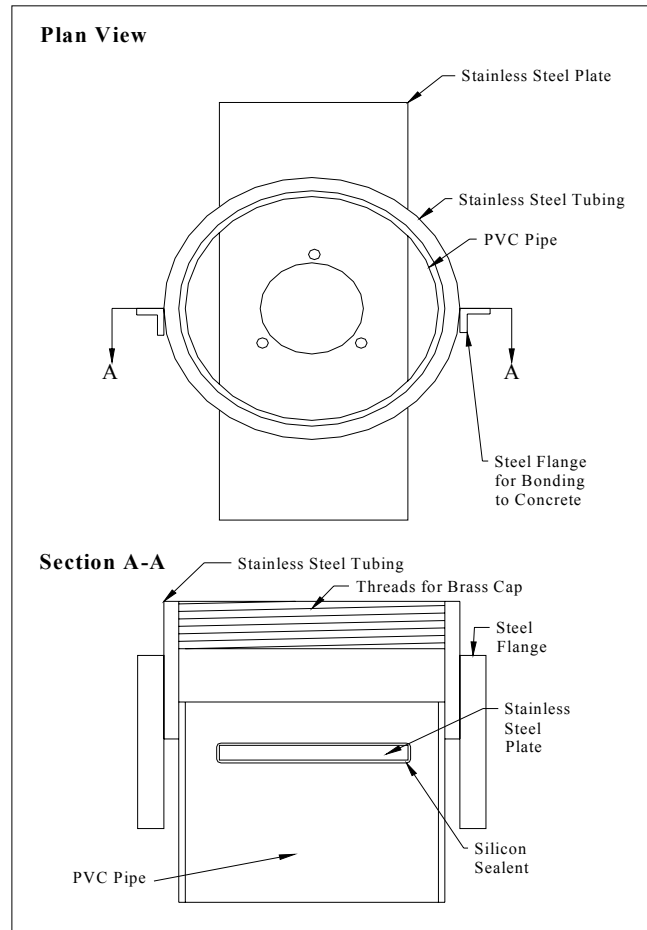


Figure 13. Single Layer Deflectometer Detail

The LVDT encased in a galvanized holder was then bolted to a stainless steel plate inside the SLD. This plate created a rigid connection between the concrete slab and the LVDT, allowing all vertical deflection to transfer to the LVDT. Deflection of the pavement was transferred through the stainless steel plate to the galvanized holder and then to the cylindrical shaft of the LVDT. The LVDT cylindrical shaft movements caused the magnetic core to move, and this displacement was measured using the stationary rod as a reference. Finally, a brass cap was screwed to the top of the SLD to prevent wet concrete from entering the LVDT set-up.

The deep reference LVDTs were arranged such that the deflection of the pavement at critical locations of the slab could be measured, as shown in Figure 9. Three of the deep LVDTs were located along the transverse joint: one at the midpoint and one at each of the corners. The fourth deep LVDT was located at the midpoint of the longitudinal joint next to the shoulder.

For the shallow reference LVDTs, four reference plates were placed in the right wheel path on top of the subbase with placement locations shown in Figure 8. After the base and concrete had been placed and the concrete had cured enough to walk on, holes were drilled down to the reference plates. The holes were large enough to set the LVDT in them to take a reading, and a small amount of grout was placed in the bottom to provide consistent readings. The same LVDT was used for deflection measurements in all four holes. As depicted in Figure 4, a metal

ring was permanently installed around the LVDT so that it would rest on the pavement surface when inserted into the holes.

The objective of installing the shallow reference LVDTs was to detect the warping and curling of the pavement. The center of the pavement will stay in contact with the base while the outer portions of the slab move up and down. Therefore, to most effectively study this phenomenon, the first shallow LVDT was installed at the center of the slab in the right wheel path. The other three shallow LVDTs were installed in the right wheel path at varying intervals toward the transverse joint.

2.3.3 Thermocouples

The thermocouples were used in this project to obtain a profile of the slab temperature throughout the depth of the slab. A total of eight thermocouples located at two positions were installed in the westbound instrumented slabs of I-490. As depicted in Figure 9, four thermocouples were installed at the center of the slab and four thermocouples were installed at the inside corner. As seen in Figure 14, at each location thermocouples were installed at depths from the top of pavement of 32 mm (1.26 in), 102 mm (4.0 in), 175 mm (6.9 in), and 241 mm (9.5 in). The thermocouples are inserted in and tied to a steel rod, which has holes drilled in it at the appropriate depths. The thermocouples were distanced from the steel rod by at least 25 mm (1 in) so that the heat properties of the steel would not affect the thermocouple readings. This rod was then driven into the base at the appropriate position before the start of paving.

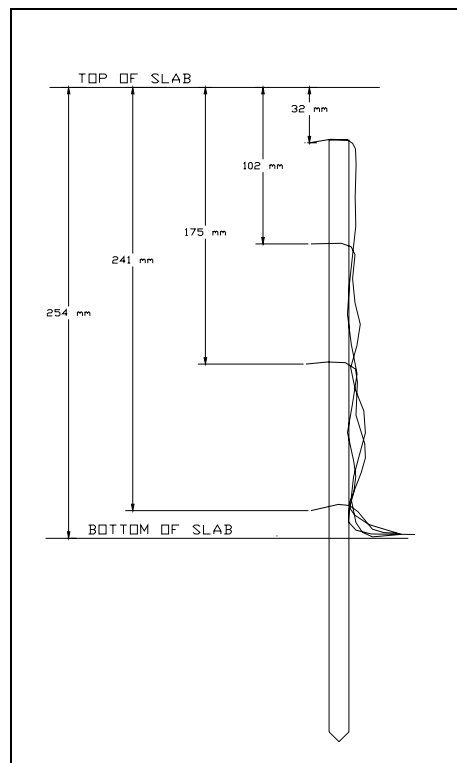


Figure 14. Thermocouple Stick (25.4 mm = 1 in)

2.3.4 Vibrating Wire Strain Gages and Thermistors

In this project a total of four VCE-4200 Vibrating Wire Strain Gages were installed to measure the effects of curling and warping. As shown in Figure 9, two gages were located at the center of the slab and two gages were located in the left wheel path. At both locations one gage was installed at 210 mm (8.3 in) and the other at 35 mm (1.38 in) from the bottom of the slab.

When installing the vibrating wire strain gages, it was necessary to provide full bonding between the gage and the concrete while maintaining the gage position specified in the plans. A procedure based on past experience was used in order to protect the gages from rotation, displacement, overstraining or destruction as the paver and spreader passed. In order to hold the gages at the correct elevation and position, the gages were tied to small steel chairs with plastic ties. The gages were then enclosed in a four sided sheet metal box with dimensions of 305 mm (12 in) by 152 mm (6.0 in) by 229 mm (9.0 in) in height. The height of the box was 12.7 mm (0.5 in) less than the pavement thickness in order to allow clearance for the paving and spreading machinery. Additionally, the boxes were stabilized by steel pins at each of the corners to prevent movement as the paver and spreader passed. This placement method is depicted in Figure 15. When the paving operation neared the strain gage location, concrete was placed by hand around and vibrated in the boxes. After the paving operation had passed, the box was removed and a small amount of concrete was added to fill in the volume the box occupied. Finally the paving crew finished the slab to provide a smooth driving surface.



Figure 15. Installation of vibrating wire strain gage with steel box

2.3.5 Instrumentation Wiring and Labeling

As shown in Figure 10, the wiring for all the instrumentation was routed to a concrete pull box on the side of the road. Prior to the pouring of the concrete, a metal pipe connected to the pull box was buried in the base at the center of each slab. All wiring was labeled with numbers and colors corresponding to the gage type and location.

3 Data Acquisition and Analysis

3.1 Introduction

The data acquisition equipment and procedures used for this project are described in this chapter. This includes a description of the systems which were used and how these systems were utilized to obtain measurements from installed instrumentation and collect data regarding the pavement structure and response.

3.2 Data Acquisition Equipment

Data were collected for this project by directly reading instrumentation and by recording data from external devices. The Campbell Scientific CR7 and CR10 data acquisition systems (dataloggers) were used to read and record data over extended periods of time from LVDTs, thermocouples, and vibrating wire strain gages. These fully programmable datalogger/controller systems are manufactured by Campbell Scientific, Inc. Programs were written so that the dataloggers could handle some of the initial data processing work, such as converting thermistor resistance into temperature units ($^{\circ}\text{C}$). The pavement warping and curling were determined by Dipstick[®] and profilometer surveys. Finally, pavement deflection and dynamic load transfer were measured using a Falling Weight Deflectometer (FWD). These systems and the components they are comprised of are described in this chapter.

3.2.1 Campbell Scientific CR7 Measurement and Control System

The CR7 datalogger was used to collect data from the LVDTs and thermocouples. It consists of a control module, input/output (I/O) module, and battery all enclosed in a durable fiberglass case.

The control module performs task initiation, measurement processing, and data storage. Additionally, it controls the keyboard and display interaction as well as communication with peripheral devices. The control module also contains a rechargeable battery and AC-charging circuitry.

The I/O module contains the processor card, precision analog interface card and seven card slots. The overall purpose of the I/O module is to perform all measurement and control functions. The processor card provides power for the analog and digital functions. In the precision analog interface card is a 16-bit analog/digital (A/D) converter and a precision voltage reference. For this project, the seven card slots were used to house 723 and 723T analog input cards, a 725 Excitation card, and two batteries. The 723 and 723T analog input cards contain 14 differential or 28 single ended inputs. The thermocouples are directly connected to these inputs on the 723T card. The 725 Excitation card consists of eight switched analog excitations, two continuous analog outputs and eight digital control outputs.

The CR7 communicates with a laptop computer through a SC32A RS232 interface device. Communication is facilitated through Windows based PC208W software. This software transfers a program to the CR7, monitors and displays real-time measurements, and collects CR7 data on demand.

3.2.2 Campbell Scientific CR10 Datalogger

The CR10 is a fully programmable datalogger and controller, which is sealed in a small rugged module. There is no integral terminal strip or keyboard and display as there was with the CR7. Additionally, the power supply is external to the module. In this study the CR10 was used to read temperature and strain from vibrating wire strain gages.

The CR10WP wiring panel takes the place of an integral terminal strip and is connected to the measurement and control module by two D-type connectors located at the end of the module. This detachable wiring panel consists of a 9-pin I/O port for datalogger communication and terminals for connecting sensor, control, and power leads to the CR10.

The CR10 does not have an integral keyboard and display, so it is necessary to connect it to an external display. For this study the CR10 was connected to a laptop computer via the SC32A optically isolated interface. This computer was equipped with PC208W software to facilitate communication between the computer and the datalogger. Through this connection the CR10 is programmed from a group of instructions entered into a program table. In this program table an execution interval is specified, which determines how frequently the program table is run. For this study the interval was typically set at 15 minutes. Each time the program table is executed, the instructions are run from beginning to end, then the CR10 waits through the remainder of the time period before re-executing the program table. In effect, the CR10 was used to collect data every 15 minutes from the temperature and strain gages during the site visits by the research team. In addition to data collection, the program table also contains instructions for the number of loops to perform, datalogger channels utilized, locations for final data storage, and some data manipulation. In addition, some temperature data were collected between site visits and were downloaded and archived by NYSDOT personnel.

There is no built in power supply for the CR10, and there are a variety of options to provide power to the system. For this study, power was supplied by the Campbell Scientific PS12 power supply which transforms incoming AC power into 12-volt DC power. This DC power is then supplied to the CR10 through a 12-volt terminal and ground terminal, with an on-off switch provided to control power flow. The incoming AC power also is regulated by the PS12 to charge a 12-volt, 7.0 amp-hour lead acid battery through a temperature compensated charging circuit. This charged battery serves as temporary back-up power for the CR10 in the event that the AC power supply is interrupted.

Since multiple vibrating wire strain gages are utilized in this project, an AM416 multiplexer is used to connect the strain gages to the CR10. The vibrating wire strain gages are connected directly to the multiplexer, and the multiplexer is connected to the CR10 via an AVW vibrating wire interface. The multiplexer allows multiple vibrating wire strain gages to be monitored as one CR10 datalogger channel signals the multiplexer to switch between sixteen channels in four lines. Additionally, the multiplexer makes it possible for one bridge completion circuit or voltage dividing circuit to be used for several sensors. Without the multiplexer it would be necessary to complete the bridge for each vibrating wire gage, thus increasing the number of precision resistors needed as well as the time required to assemble the circuits.

3.2.3 Dipstick[®]

The Dipstick[®], pictured in Figure 16, is a road profilometer used in this study to determine relative differences in elevation of concrete slabs. The Dipstick[®] unit contains an inclinometer positioned such that it is coplanar with the two feet. This inclinometer is capable of measuring the elevation difference between the two feet to two-hundredths of a millimeter (0.8

mil) at 305 mm (12 inch) intervals. Additionally, the Dipstick[®] unit displays the elevation difference on two digital screens. The Dipstick[®] is connected to an A22-T computer, which stores the collected data on a removable flash memory card. A handle assembly is used to guide the Dipstick[®] as well as to signal the Dipstick[®] to measure and record elevation.



Figure 16. Dipstick[®] Road Profilometer

The data stored by the Dipstick[®] on the USB Flash Memory card can easily be transferred to a personal computer through the use of a USB cable. This data can then be processed and manipulated using the RoadFace software developed by the FACE[®] company. A data set is opened in RoadFace, and the data points can then be unboxed. These box and diagonal points were then processed in RoadFace to calculate the average elevations for each slab at each collection time. The averaged data were then imported to Excel and zeroed relative to the first reading of the Dipstick[®] run. The zeroed data were then saved as a text file and imported into Matlab. In Matlab, the data were then plotted in a three dimensional graph depicting the slab deformation relative to the slab shape after initial curing in June 2002.

3.2.4 Falling Weight Deflectometer

The Falling Weight Deflectometer (FWD), the trailer pictured in Figure 17, is a non-destructive testing device which measures the vertical deflection of a pavement under a known applied load. This dynamic load is similar in magnitude and duration to that of a single heavy moving wheel load. The vertical deflection resulting from the dynamic loading is then recorded by a series of seismometers, also called geophones. The recorded deflections are then used to calculate the load transfer efficiency, in-situ resilient modulus, and approximate slab support.



Figure 17. Falling Weight Deflectometer attached to a van

3.2.5 Profilometer

The ORITE Profilometer, pictured in Figure 18, was used to measure pavement elevation relative to the device's integral guide rail. The profilometer records a measurement every 13 mm (0.51 in) over a distance of 2.84 m (9.3 ft). These measurements are stored in an ASCII file. The profilometer is mounted on an eleven foot frame along with a notebook computer for controlling the instrument and collecting data. A 12-volt gel electrolyte battery and a 12 VDC/115 VAC inverter provide power for the profilometer. The profilometer is transported between measurement locations by retractable wheels.



Figure 18. ORITE Profilometer

3.3 Data Acquisition Procedures

3.3.1 Deep LVDTs

The output voltage from the LVDTs is in the range of ± 10 volts. However, the voltage input to the CR7 is limited to 2.5 volts. Therefore, a voltage divider circuit using two precision resistors is used to reduce the LVDT output voltage by a factor of four to keep the input voltage within the required range of the CR7. The CR7 reads the differential voltage measurements between ports H1 and L1 on each channel of the multiplexer, then reads ports H2 and L2 on each channel of the multiplexer. The other LVDTs in this project did not require a reduction in the voltage output.

3.3.2 Vibrating Wire Strain Gages and Thermistors

The VCE 4200 strain gages measure temperature with an internal thermistor, and strain by measuring the resonant frequency of a built-in vibrating wire. The strain is proportional to the square of the resonant frequency, and adjustments are also made to account for the effects of temperature and to account for the shortening of the wire due to the nature of the construction of the device (the “batch factor correction”). The strain gages are connected to the multiplexer; the CR10 datalogger first reads the thermistor measurement and then the strain measurement on each of the sixteen multiplexer channels. This process is repeated every fifteen minutes.

3.3.3 Thermocouples

The eight thermocouples used in this project were wired directly to the 723-T card in the CR7 datalogger. This card includes a platinum resistance thermistor (PRT) as a reference. The copper lead wire of the thermocouple was connected to the H1 input and the constantan lead was connected to the L1 input of a differential channel on the 723-T card.

3.3.4 Handheld LVDT

Handheld LVDT measurements were made by inserting a GHSD 750 LVDT into each of four holes drilled in the pavement. A reference plate was placed at each handheld LVDT location prior to paving the road. The differential voltage at each hole was read directly from the readout box and recorded by hand. The readout box consists of a digital voltmeter and power supply.

3.3.5 Air Temperature Thermistor

The air temperature readings were collected with a Campbell Scientific T108 temperature probe connected directly to the CR7 datalogger. The T108 is capable of measuring air temperature in the range of -5°C (23°F) to $+95^{\circ}\text{C}$ (203°F).

3.3.6 Dipstick[®]

The Dipstick[®] data were collected by “walking” the Dipstick[®] unit around a predetermined path on the concrete slab. This path consists of a box around the perimeter of the slab and a diagonal from the outside to the inside of the lane; data readings were collected every 30.5 cm (12 inches) along the path. Both the box and the diagonal are covered twice at each data collection in order to verify the data. Prior to data collection the Dipstick[®] is zeroed on a flat surface. One corner of the slab was taken as a zero point or reference relative to which all the other dimensions were recorded. Data points are collected by pushing a switch on the Dipstick[®] handle which indicates to the Dipstick[®] unit that a data point is to be collected. An audible signal and a visual signal indicate when the data collection at a point is complete. These data points are then stored in the memory card and transferred to a desktop computer for ease of processing.

3.3.7 Falling Weight Deflectometer

For the evaluation of support under the westbound slabs, FWD data were collected in the precise grid pattern shown in Figure 19. This collection pattern allows comparison between testing times of data from the exact same locations. At each point on this grid pattern a load of approximately 71 kN (16 kip) was dropped at times when the slab experienced maximum positive and maximum negative temperature gradients. For the eastbound slabs, loads of approximately 517 kPa (75 psi) and 724 kPa (105 psi) were dropped at each transverse joint. The resulting deflections from all loads were recorded for further processing.

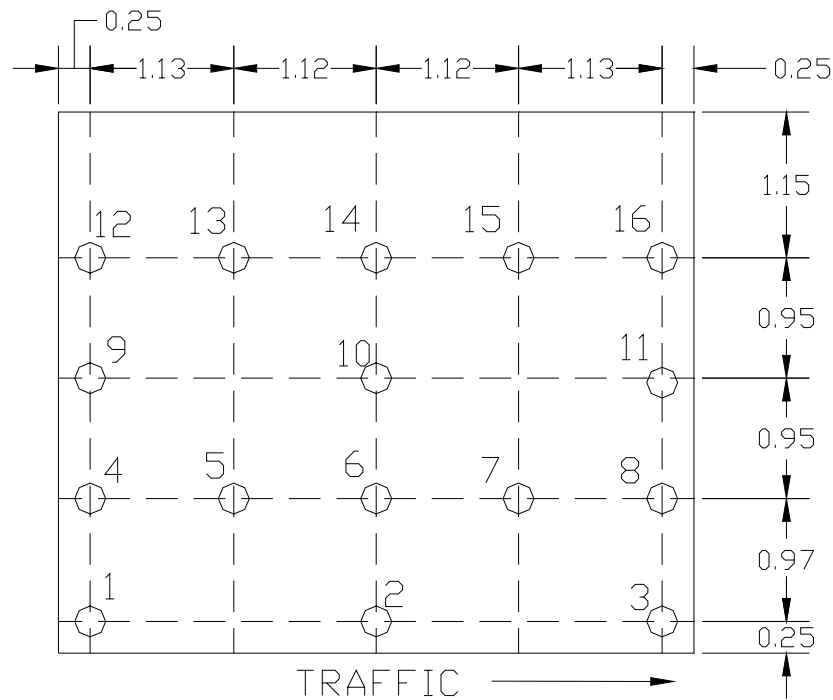


Figure 19. Grid for Westbound FWD Test Drop Locations. Distances marked at edges in m (1 m=3.28 ft).

The eastbound FWD data were used to calculate the load transfer efficiency across the dowel transverse joints. The geophones were arranged such that the deflection on both the approach and leave slab was recorded. The approach load transfer efficiency (LTE) is calculated with the following equation:

$$\text{approach LTE} = \frac{D_2}{D_0} \cdot 100 \quad \text{Equation 3.23}$$

Where:

D_2 = deflection behind the plate

D_0 = deflection at the load cell

The leave LTE is calculated by the following equation:

$$\text{leave LTE} = \frac{D_1}{D_0} \cdot 100 \quad \text{Equation 3.24}$$

Where:

D_1 = deflection 305 mm (12 in) in front of the plate

D_0 = deflection at the load cell

Additionally, the Joint Support Ratio (JSR) is calculated by dividing the deflection at the load cell after the joint by the deflection at the load cell before the joint.

3.3.8 Profilometer

The profilometer was set up at the initial test location, as close to the edge of the pavement as possible. The collection sequence was then initiated and the 51 mm (2.0 in) diameter 14 mm (0.55 in) wide ball bearing follower measured the pavement elevation over the 2.84 m (9.32 ft) profilometer test length. This bearing is attached to an arm which is connected to an incremental optical rotary encoder. Each increment records the change in elevation of the bearing to a precision of 0.13 mm (5 mil). Additionally, the angle of the profilometer guide rail is measured with respect to horizontal using a servo inclinometer reading with a precision of 0.001°. After the first run is recorded, the profilometer is moved to the end of the first run, and the subsequent run is initiated.

Because the inclinometer records the angle to the profilometer guide rail with a precision of 0.001°, sequential profilometer runs can be nearly seamlessly concatenated together. The initial profilometer run is first rotated about the first elevation reading to the angle of the inclinometer beam reading. The subsequent profile is then translated vertically by adding a constant to all 210 profilometer readings in that profile to adjust the elevation readings to a reference at the final elevation reading of the previous run. Since the last reading of the previous run is the same as the first reading of the current run, one of these data points is then discarded. The subsequent profile run is then rotated to the angle of the inclinometer beam reading. This process is then repeated for each subsequent profile until all continuous profilometer runs have been concatenated.

4 Data Presentation and Testing Results

4.1 Introduction

Data were collected from both the westbound and eastbound test sections during the time span of the project. The gages installed in the westbound test section were performing properly after the construction of the two test slabs. Data were collected over a 24 hour period from the westbound test section in June 2002, just after the concrete for the westbound slabs was placed, to observe shrinkage, curling, and warping. Subsequent 24 hour test periods occurred in July 2002, June 2003, October 2003, and October 2004. The temperature, strain, stress, and deflection readings are plotted versus time. Additionally, 3D plots of the slab deflection from FWD testing and slab shape from Dipstick[®] surveys are presented. The Eastbound test section was monitored in October 2004 to determine curling and warping as well as slab response to dynamic loading. For the dowel bar test sections, FWD results of load transfer and joint support are presented as well as curling data from the slab profiles, which are presented in Appendix E.

4.2 I-490 West June 2002 Testing

Data collection began on June 11, 2002 at 9:00 am, one hour prior to the placement of the pavement. Joints were cut at 6:00 pm, 9 hours after the start of the test, which will be referred to as 9 hours “test time”. Data were collected every fifteen minutes. The thermocouples and deep LVDTs were monitored continuously for 48 hours from the start of construction. Strain data were recorded from a Geokon readout box and are presented in Appendix A. Additionally, Dipstick[®] surveys were taken at times of extreme pavement temperature gradient.

4.2.1 Temperature Data

The air temperature as well as the temperature gradient at the center and corner of the instrumented slab for the first 48 hours following pavement placement are depicted in Figure 20. The pavement was placed in June 2002, and the maximum air temperature reached during the monitoring period was 35° C (95°F) at five hours after slab placement (6.5 hours “test time”). The highest internal slab temperatures occurred at the top of the slab on the day of placement and were due to the heat of hydration as well as solar radiation. The slab temperature gradient is the difference between the temperature at the thermocouple nearest the top of the slab (32 mm (1.26 in) below the surface) and the thermocouple nearest the bottom of the slab (13mm (0.51 in) above the bottom surface) divided by the thickness of concrete between the thermocouples (0.209 m (8.23 in)), and reached a maximum of 27C°/m (1.2°F/in) at the center of the slab and 22C°/m (1.0°F/in) at the edge at a test time of 6.75 hours.

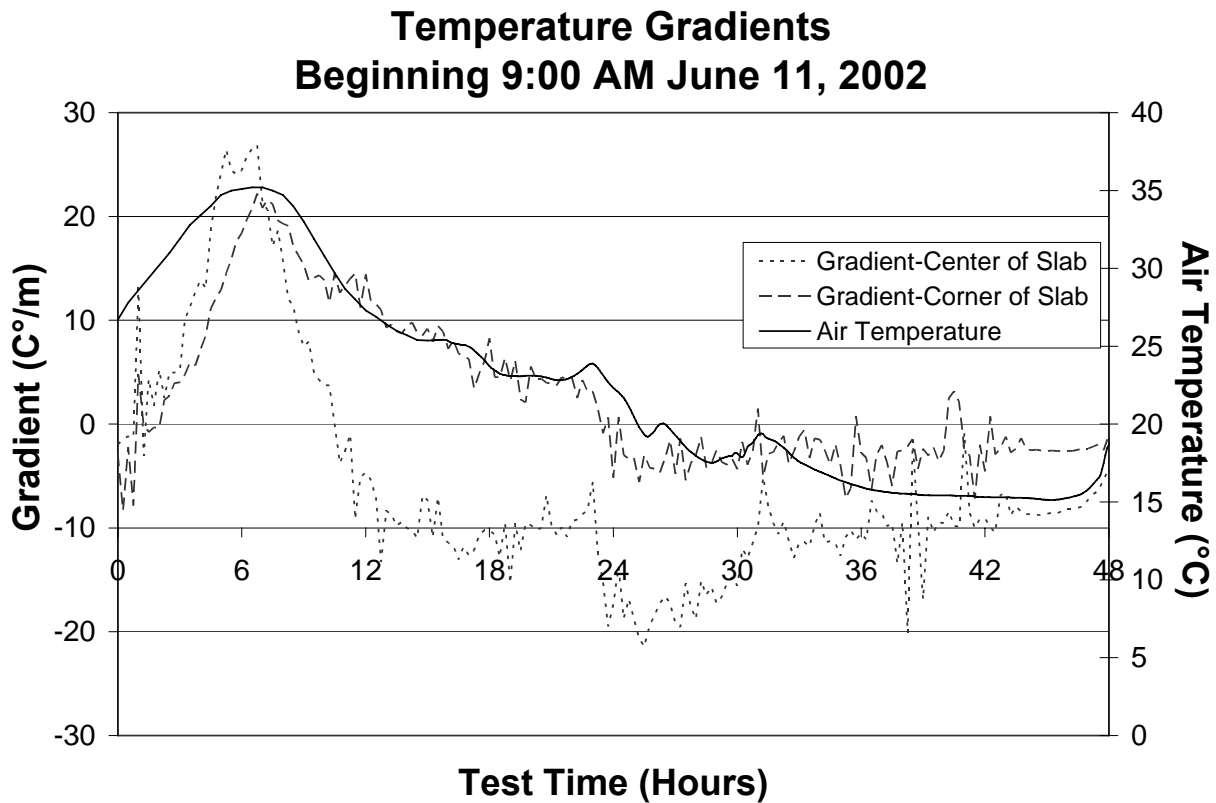


Figure 20. Temperature Gradients and Slab Temperature, June 11, 2002 (1C°/m = 0.046°F/in; air temperature scale range is from 32°F to 104°F)

This high temperature gradient during the cooling process along with the high initial heat build up resulted in the transverse joints cracking shortly after they were cut. The air temperature decreased starting around the test time of 9 hours and at a test time of 24 hours a thunderstorm passed through the area lowering the air temperature below 20°C (68°F). This decrease in air temperature combined with the continued heat of hydration resulted in a negative slab temperature gradient from approximately hour 12 to the end of the test period.

4.2.2 Deep LVDT

One hour after cutting the joints, the deep LVDTs were set to zero. It is assumed that no deformation occurred in the slabs prior to this time. As shown in Figure 21, the corners of the slab rose during the next 34 hours of the curing process.

Deep Reference LVDTs Beginning 9:00 June 11, 2002

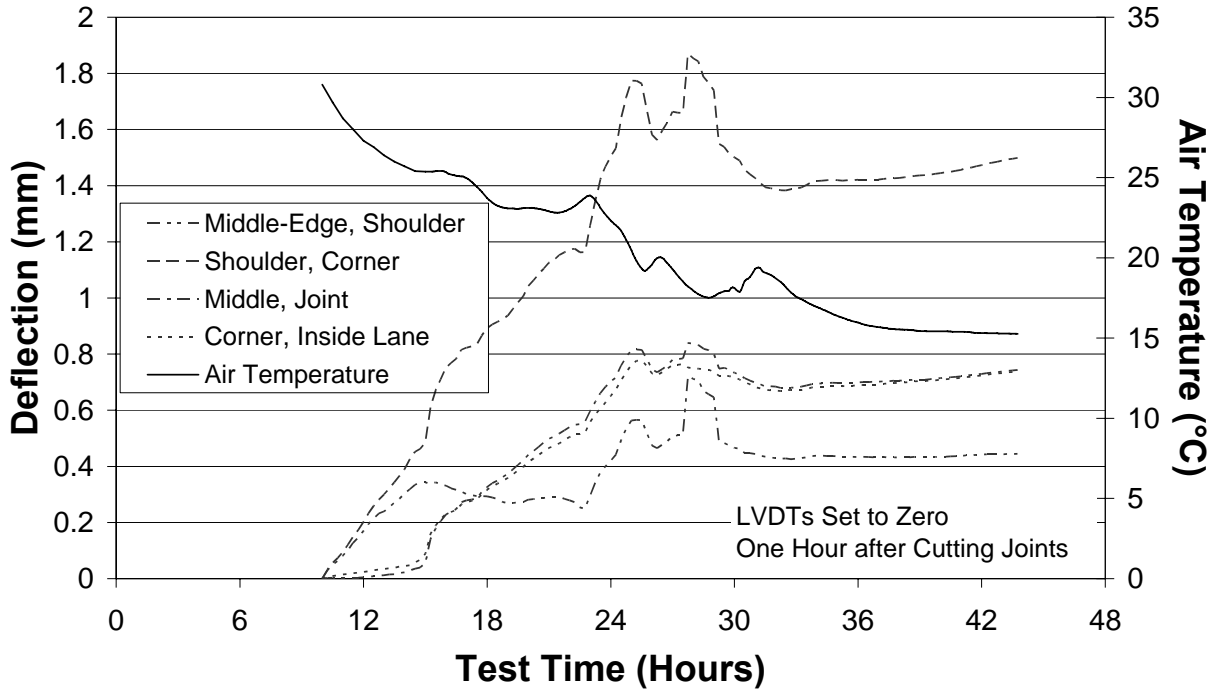


Figure 21. Deep reference LVDT data, June 11, 2002 (1mm = 39 mil; air temperature scale range is from 32°F to 95°F)

The largest rise occurred at the corner next to the shoulder because the shoulder was not yet poured and the slab was not constrained by tie bars. The greatest deformation occurred between test hours 24 to 30, which coincided with the time period when the greatest negative temperature gradient occurred in the center of the slab.

4.2.3 Dipstick®

Dipstick® surveys were taken of both slabs after the joints were sawcut. These dipstick surveys were calibrated to LVDT data collected at that time such that the Dipstick® plot deformations at the deep LVDT locations coincide. Figure 22 shows the deformation of Slab 1 at the test time of 30 hours. It can be seen that the lifting at the corners relative to the center of the slab is nearly 2 mm (79 mil). This is due to the high shrinkage rates and large temperature gradients that occur in concrete pavement placed in hot weather.

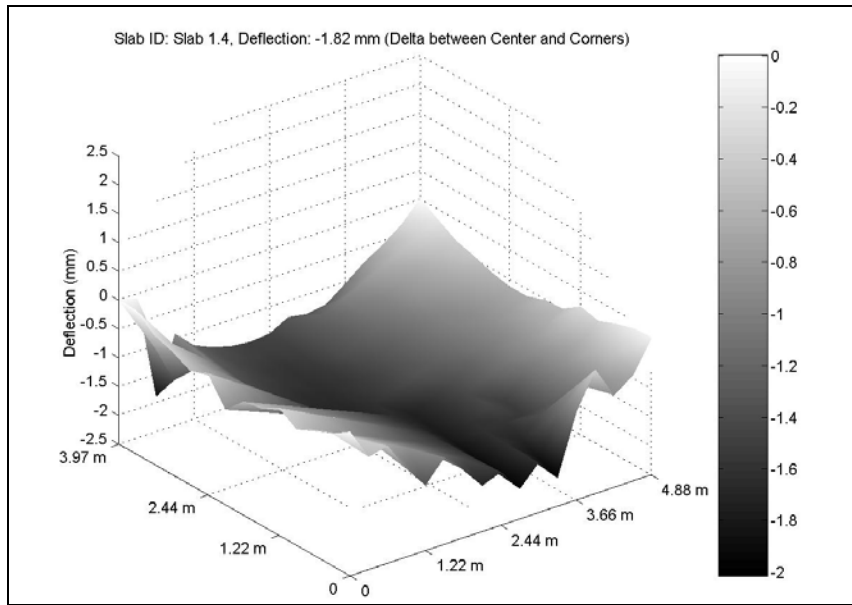


Figure 22. Slab 1 profile at 3pm, June 12, 2002, referenced after joints were sawcut (1m=3.28 ft; 1 mm=39 mil)

As seen in Figure 23, not much change in slab shape occurred between the 30 hour and 48 hour test times. During the 48 hour test time the pavement had a more negative temperature gradient than it did at the 30 hour test time, which alone would result in more downward curling. However, this downward curling was offset by the upward warping caused by the curing process. Slab 2 followed the same trends as Slab 1, and additional plots of Dipstick[®] profiles for Slabs 1 and 2 can be found in Appendix A.

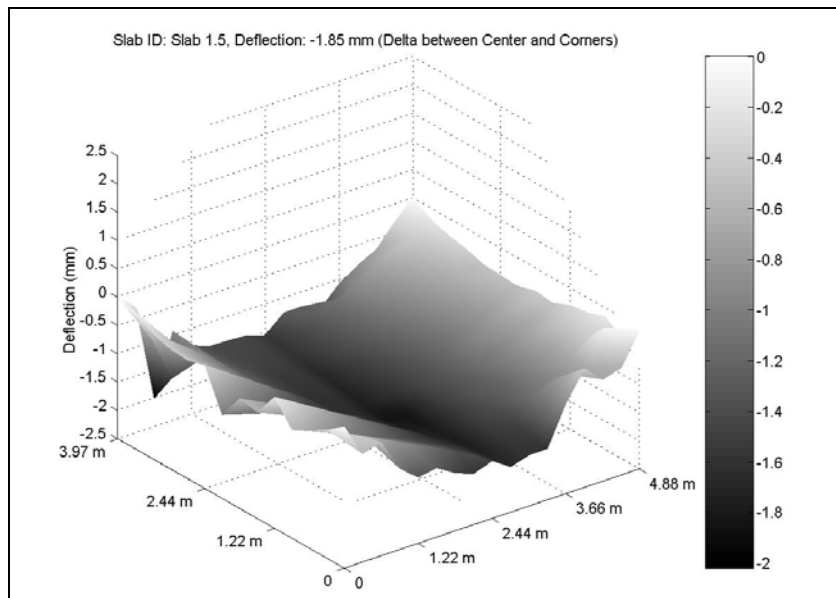


Figure 23. Slab 1 profile at 9am, June 13, 2002, referenced after joints were sawcut (1m=3.28 ft; 1 mm=39 mil)

4.3 I-490 West July 2002 24 Hour Monitoring Period

Five weeks after the pavement was placed, the test slabs were monitored to study environmental responses. This monitoring period took place before the road was opened to traffic and before the tied shoulder was installed. The 24 hour monitoring period began at 9:15 pm on the 37th day after placement, July 16, 2002. During this monitoring period, the LVDTs, thermocouples, and strain gages were monitored. Gaps in data collection occurred between 3:00 am and 6:00 am due to power supply malfunctions, otherwise data were collected at 15 minute intervals. Dipstick surveys were taken at times of maximum pavement temperature gradients and FWD testing was conducted to determine the loss of support.

4.3.1 Temperature Data

The air temperature and pavement temperature gradients for the 24 hour collection period are presented in Figure 24.

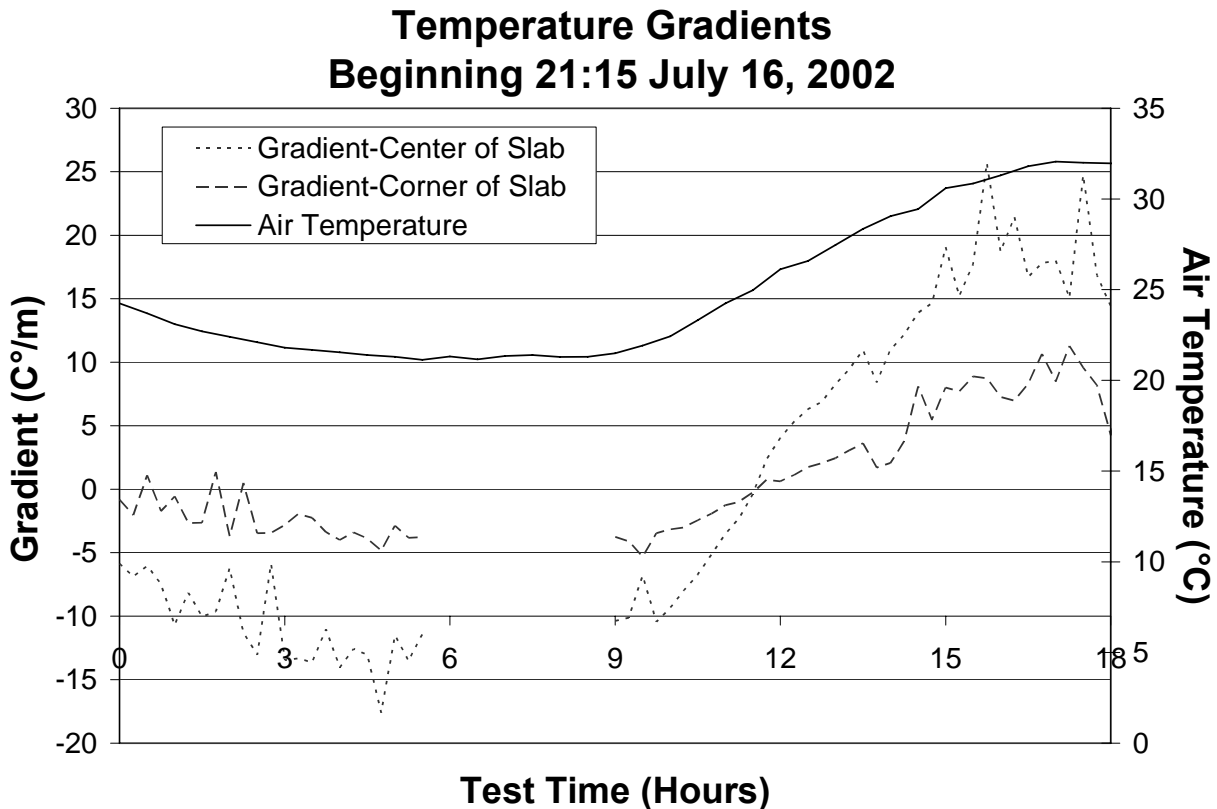


Figure 24. Temperature gradients and air temperature, July 17, 2002 (1C°/m = 0.046°F/in; air temperature scale range is from 32°F to 95°F)

The air temperature during this collection period was similar to that when the pavement was placed over a month earlier. The greatest negative temperature gradient occurred at about 2:00 am (test hour 5) and the greatest positive temperature gradient occurred around 2:00 pm (test hour 17).

4.3.2 Deep LVDT

The deep LVDT data were collected throughout the 24 hour collection period and provides information on the curling experienced by the pavement. In Figure 25 the air temperature is plotted versus deep LVDT deflections.

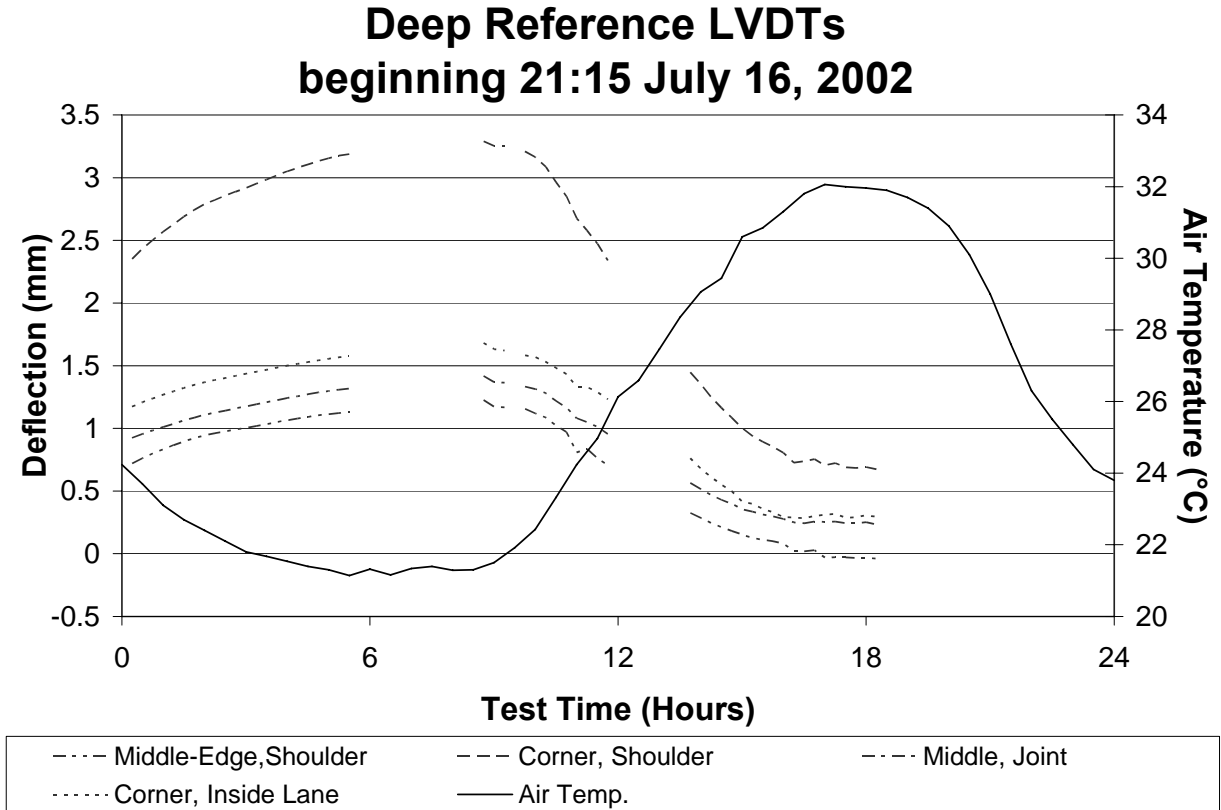


Figure 25. Deep reference LVDT data, July 17, 2002 (1mm = 39 mil; air temperature scale range is from 68°F to 93°F)

At the extreme low air temperature the LVDTs were at peak deflection and at the peak air temperature the LVDTs were least deflected. This indicates that the changes in slab shape were due to the change in ambient temperature. The LVDT at the corner near the shoulder experienced the most deflection at all times, showing the influence of the slab not being constrained on this side.

4.3.3 Shallow LVDTs

Readings were taken of the shallow LVDT deflections on both the 2nd and 37th days after the pavement was poured; the temperature gradient in the pavement was $-9.1\text{C}^{\circ}/\text{m}$ ($-0.42^{\circ}\text{F}/\text{in}$) at the time of both readings. As shown in Table 4, in the five weeks between the two sets of readings the deflection readings for each of the LVDTs increased around 100 percent. At the time that the second set of readings was collected the warp had increased around 100 percent from the first reading. At the time the second readings were taken, the loss of support is determined more by the warping than by the built in gradient, solar radiation, or high concrete temperatures.

Table 4. Warping with Time at Varying Slab Locations

LVDT Number	Reading on 2nd Day		Reading on 37th Day		Warping Difference	
	(mm)	(mil)	(mm)	(mil)	(mm)	(mil)
LVDT 1	0.4	16	1.1	43	0.7	28
LVDT 2	1.5	59	3.2	126	1.7	67
LVDT 3	0.7	28	1.3	51	0.6	24
LVDT 4	0.7	28	1.6	63	0.8	31

4.3.4 Dipstick[®]

Dipstick[®] surveys were taken twice: when the pavement temperature gradient was at the maximum positive and maximum negative values. In Figure 26 and Figure 27 the differences between the extreme gradients are shown. The deformation between the center and corners is 2.79 mm (110 mil) for slab 1 and 2.90 mm (114 mil) for slab 2. As was previously shown with the LVDT data, the slabs experienced the greatest deformation along the unconstrained shoulder edge.

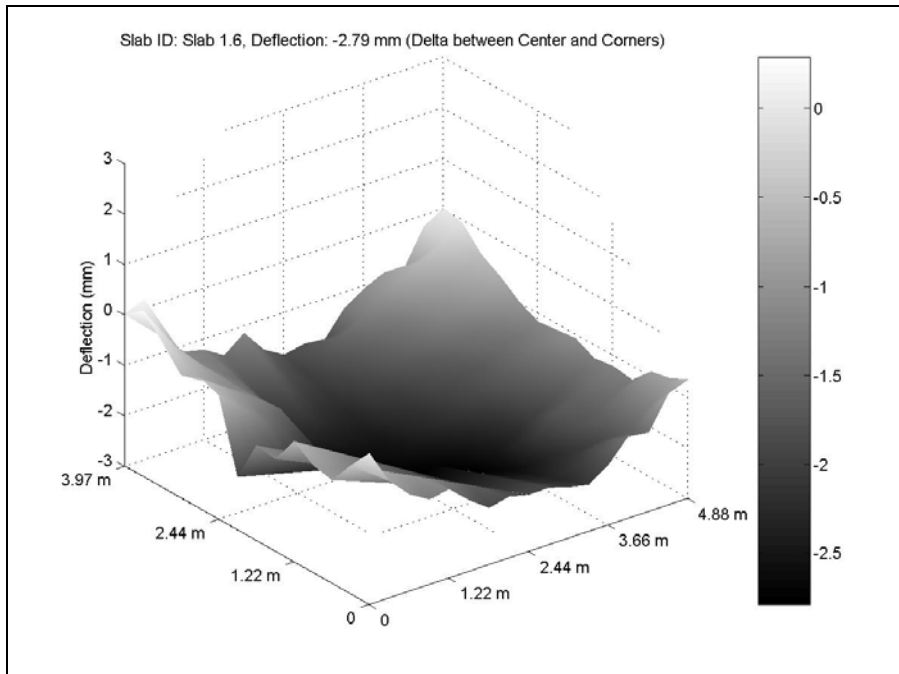


Figure 26. Slab 1 profile difference between extreme gradients, July 17, 2002 (1m=3.28 ft; 1 mm=39 mil)

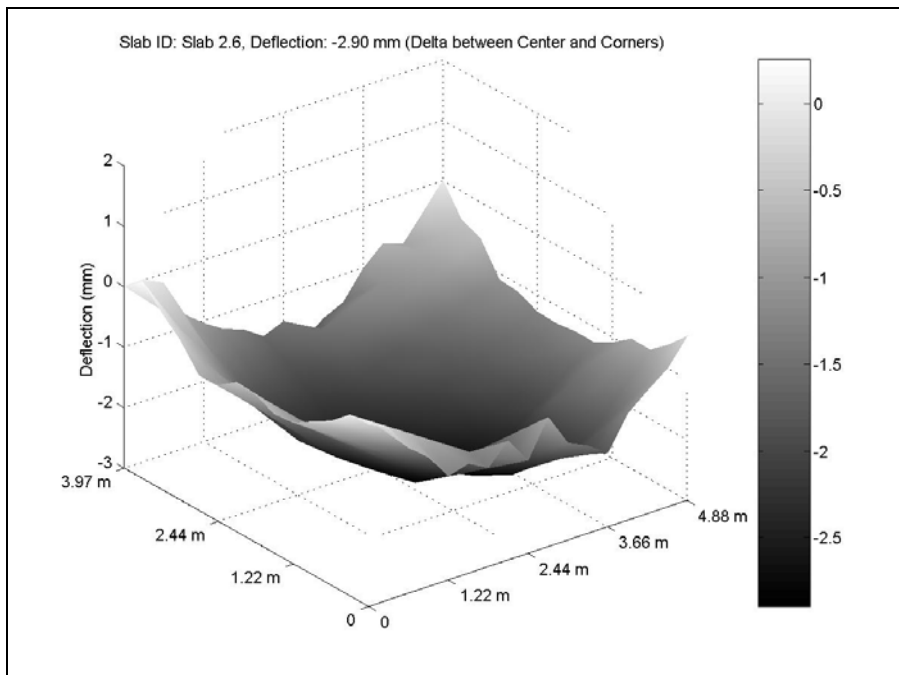


Figure 27. Slab 2 profile differences between extreme gradients, July 17, 2002 (1m=3.28 ft; 1 mm=39 mil)

4.3.5 Falling Weight Deflectometer

Falling Weight Deflectometer testing was conducted at the times of both extreme temperature gradients to investigate slab loss of support. The weights were dropped according to the pattern previously shown in Figure 19. The maximum deflections at both extreme gradients for an approximately 71 kN load are shown in Figure 28 and Figure 29 for Slab 1, and in Figure 30 and Figure 31 for Slab 2. At the times when the slabs were known to be curled, the slab edges acted in a cantilever manner when the load was applied. When the slab was not warped the slab edge deflection reduced significantly. Additionally, the influence of the missing shoulder is evident by the increase in deflection along the shoulder edge. The deflection at the slab center does not change much between the two testing times. When compared to the slab shape data, it is assumed that the center of the slab stays in contact with the base which reduces deflection.

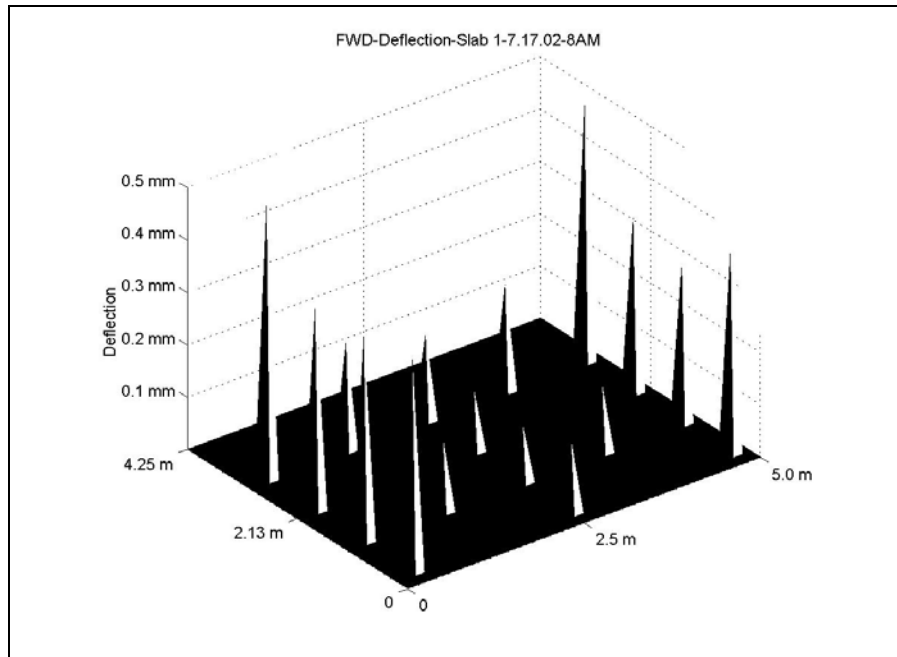


Figure 28. Slab 1 deflection from FWD at 8am, July 17, 2002 (1m=3.28 ft; 1 mm=39 mil)

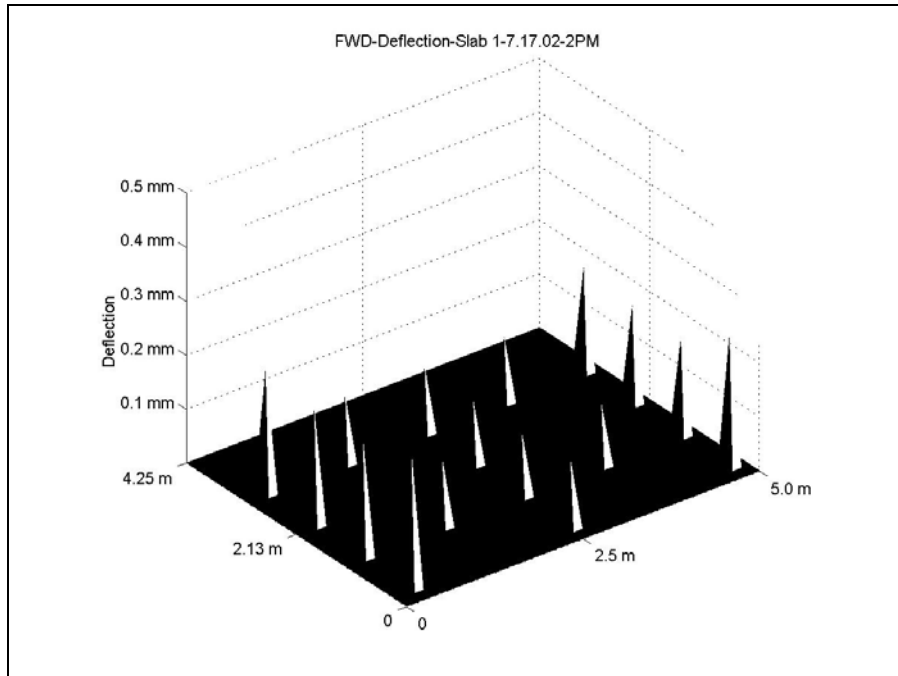


Figure 29. Slab 1 deflection from FWD at 2pm, July 17, 2002 (1m=3.28 ft; 1 mm=39 mil)

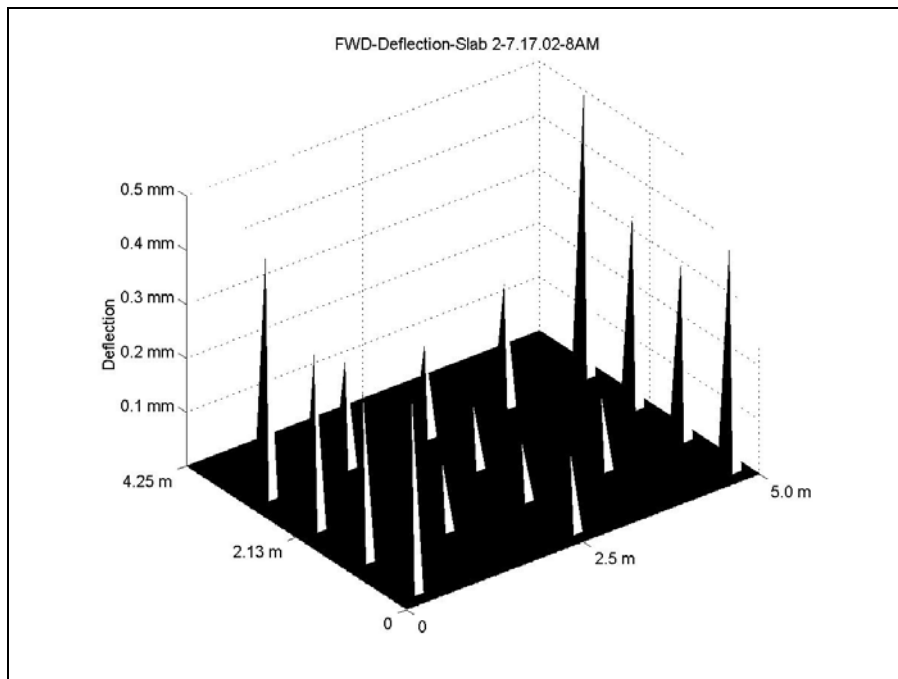


Figure 30. Slab 2 deflection from FWD at 8am, July 17, 2002 (1m=3.28 ft; 1 mm=39 mil)

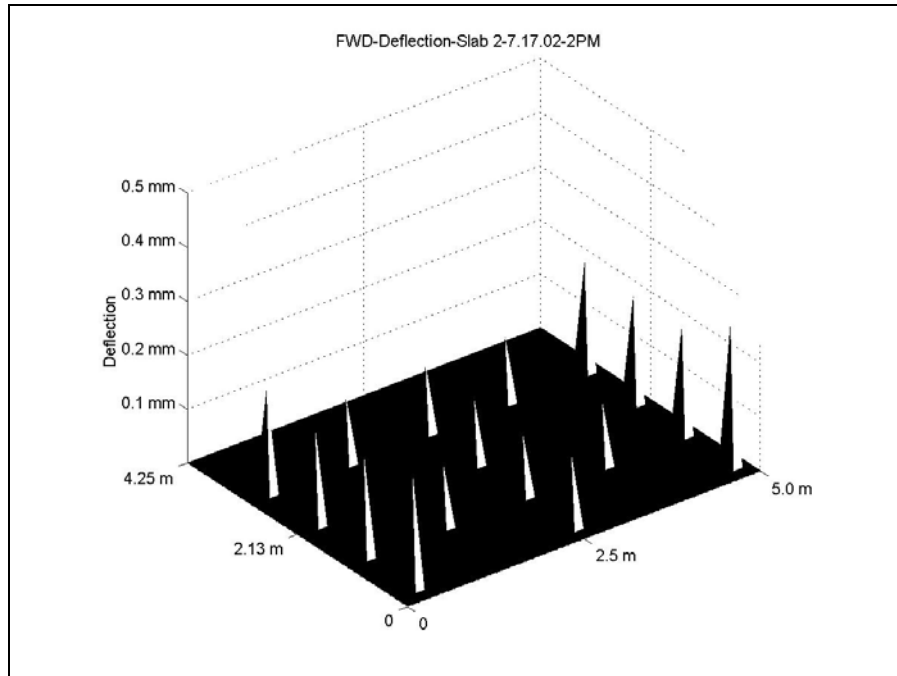


Figure 31. Slab 2 deflection from FWD at 2pm, July 17, 2002 (1m=3.28 ft; 1 mm=39 mil)

4.3.6 Vibrating Wire

The vibrating wire strain gages were monitored throughout the 24 hour test period to study the effect of pavement stresses due to curling. While the absolute stresses in the concrete slab cannot be determined, the strain gage readings can be used to calculate the increase of tensile stresses due to upward curling in the top strata of the pavement. The strain experienced by the slab generally follows the 24-hour ideal thermal strain cycle, which is defined as the temperature differential times the coefficient of thermal expansion of concrete. However, the dead load of the concrete slab prevents this model from being completely accurate. A plot of the ideal thermal strain versus the actual strain calculated from the vibrating wire strain gage data in the left wheel path of the slab is shown in Figure 32.

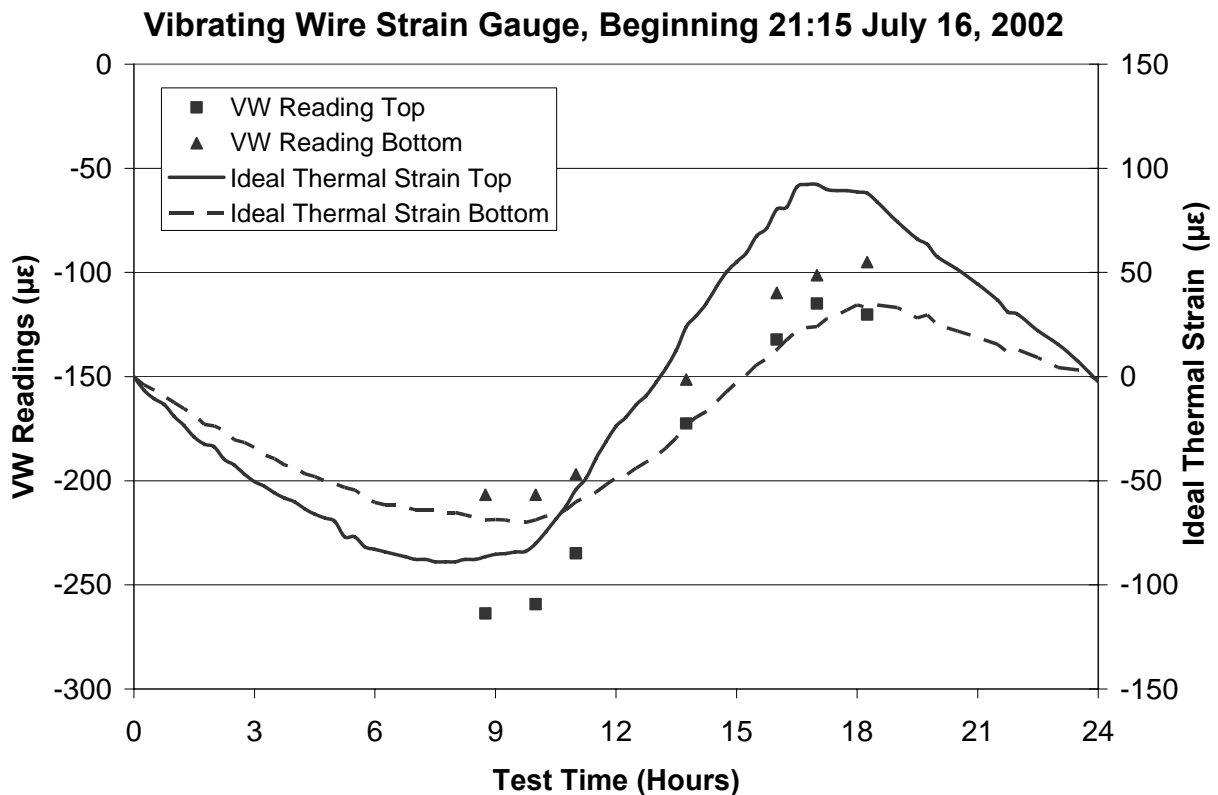


Figure 32. Ideal thermal strain versus actual strain readings in left wheel path

These results are characteristic of actual thermal strain with the maximum and minimum strain lower than the ideal calculations at the top of the slab and higher than the ideal calculations at the bottom of the slab. This is due to the increase in tensile stress on the top of the slab when the slab cools, which results in an effective negative temperature gradient throughout the depth of the slab.

At times of the extreme temperature gradients, the strain due to the slab curling can be calculated in the following manner:

$$\varepsilon_{\text{curling}} = \Delta\varepsilon_{\text{ideal thermal}} - \Delta\varepsilon_{\text{actual}} \quad \text{Equation 4.1}$$

Where:

$\Delta\varepsilon_{\text{ideal thermal}}$ = difference in ideal thermal strain based on temperatures at extreme gradients

$\Delta\varepsilon_{\text{actual}}$ = difference in actual strain readings at extreme gradients

The longitudinal stress due to curling can then be calculated using Equation 4.1, the vibrating wire strain gage readings collected in the field, and the material properties determined in the lab. These calculations result in curling stresses of 0.8 MPa (116 psi) at the center of the slab and 1.0 MPa (145 psi) near the edge of the slab. This is a significant amount of stress for the slab to experience due only to environmental factors. The tensile stress the slab actually experiences is much higher than these calculated stresses as it also includes stresses resulting from slab curling and loss of support.

4.4 I-490 West June 2003 40 Hour Monitoring Period

Approximately one year after the pavement placement, the two westbound instrumented slabs were monitored for a period of 40 hours. This environmental response monitoring period was to evaluate the pavement loss of support after the road had been opened to traffic for about a year and the tied shoulder had been placed. The readings began at 8:30 am on June 17, 2003; the deep LVDTs and strain gages were monitored continuously for the next 40 hours, with data collected every ten minutes. It was found that the thermocouples were no longer functioning. In place of the thermocouple data, the temperature data collected from thermistors built into the vibrating wire strain gages, located at 3.8 cm (1.5 in) from the top and bottom of the slab, were substituted. Additionally it was found that the deep LVDT located at the shoulder corner was no longer functioning. Dipstick surveys were taken at times of maximum pavement temperature gradient and FWD testing was done to evaluate the loss of support.

4.4.1 Temperature Data

The temperature gradients across the 18 cm (7.1 in) gap between the vibrating wire strain gages calculated for the 40 hour collection period are presented in Figure 33. The temperature data followed a similar trend to that of the previous data collection periods.

4.4.2 Deep LVDT

Past the eighth week of curing moisture losses from the pavement have little effect on the pavement shape. Therefore, the pavement deflections measured in this monitoring period are a result of curling due to slab temperature changes. As seen in Figure 34, the LVDTs located along the tied shoulder show little movement throughout the monitoring period.

Upon later removal of the LVDTs in October 2004, it was found that a tie rod had been inserted through the LVDT housing. This prevented the LVDT from moving after the shoulder had been placed, and made the data collected from the corner shoulder LVDT unusable. It can be seen from Figure 34 that the LVDT located at the inside corner deflected upward most at the coolest temperatures and deflected downward during the peak temperatures. This is consistent with findings from previous test periods.

4.4.3 Dipstick[®]

Dipstick[®] surveys were taken at 6:00 am, 8:00 am, and 2:00 pm to capture the slab shape during both extreme slab temperature gradients. The differences in slab deflection between the maximum and minimum slab temperature gradients are depicted in Figure 35 and Figure 36 for Slab 1 and Slab 2 respectively.

Temperature gradients measured with Vibrating Wire strain gauge, beginning 8:30 June 17, 2003

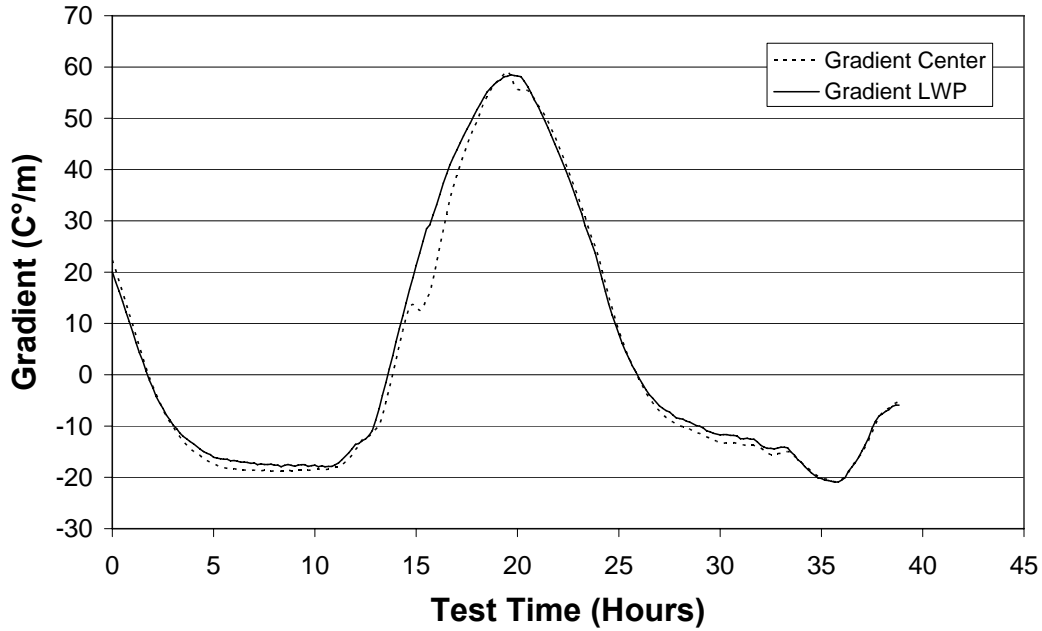


Figure 33. Temperature gradients in slab as measured using thermistors in vibrating wire strain gauges, June 17, 2003 (1C°/m = 0.046°F/in)

**Deep Reference LVDTs
Beginning 8:30 June 17, 2003**

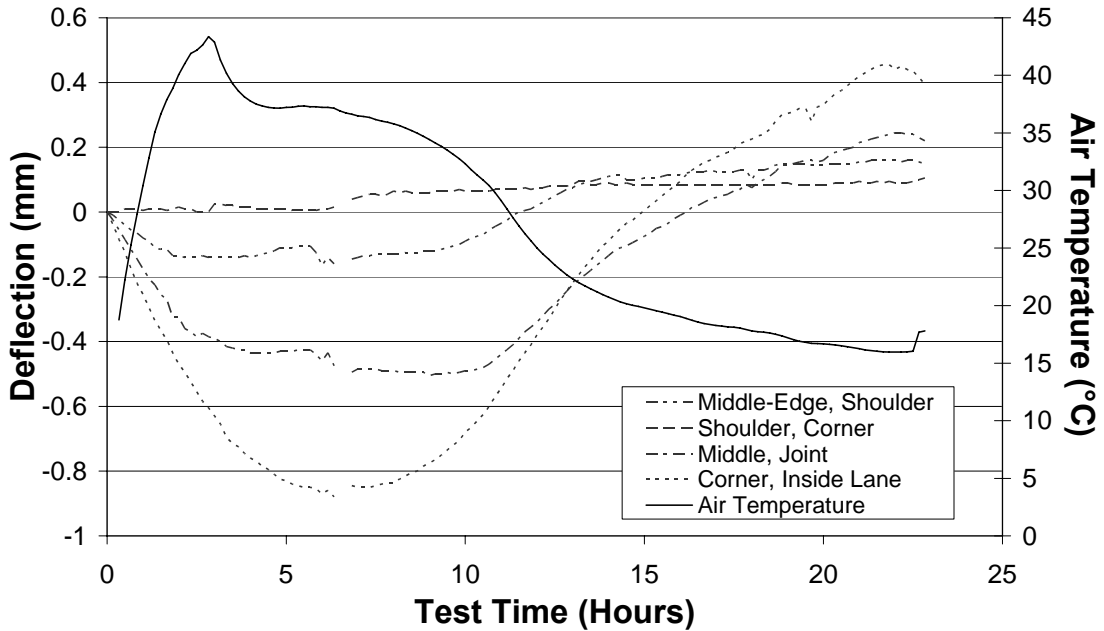


Figure 34. Deep reference LVDT data, June 17, 2003 (1 mm = 39 mil; air temperature scale range is from 32°F to 113°F)

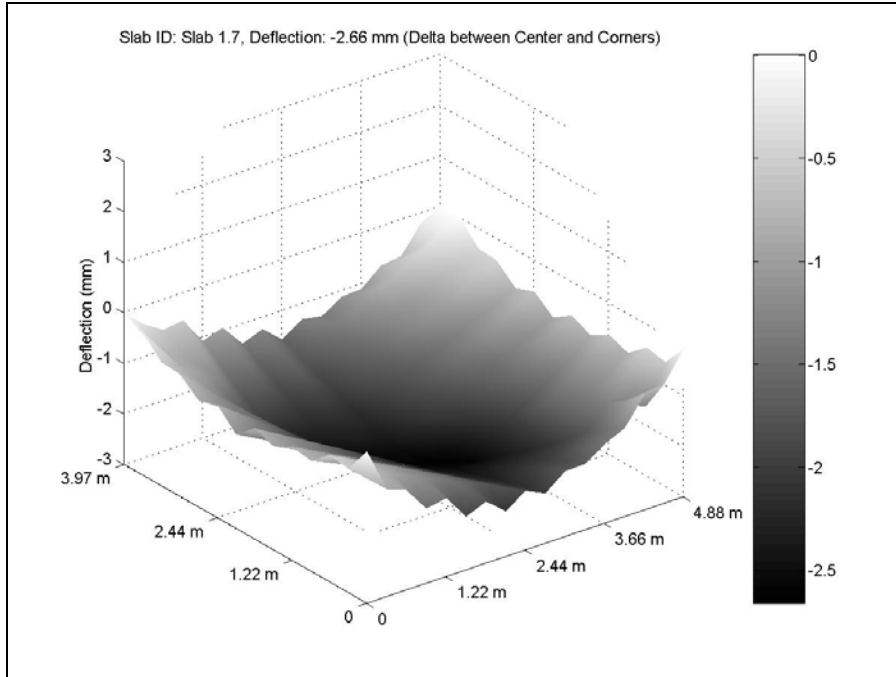


Figure 35. Slab 1 profile difference between extreme gradients, June 18, 2003 (1m=3.28 ft; 1 mm=39 mil)

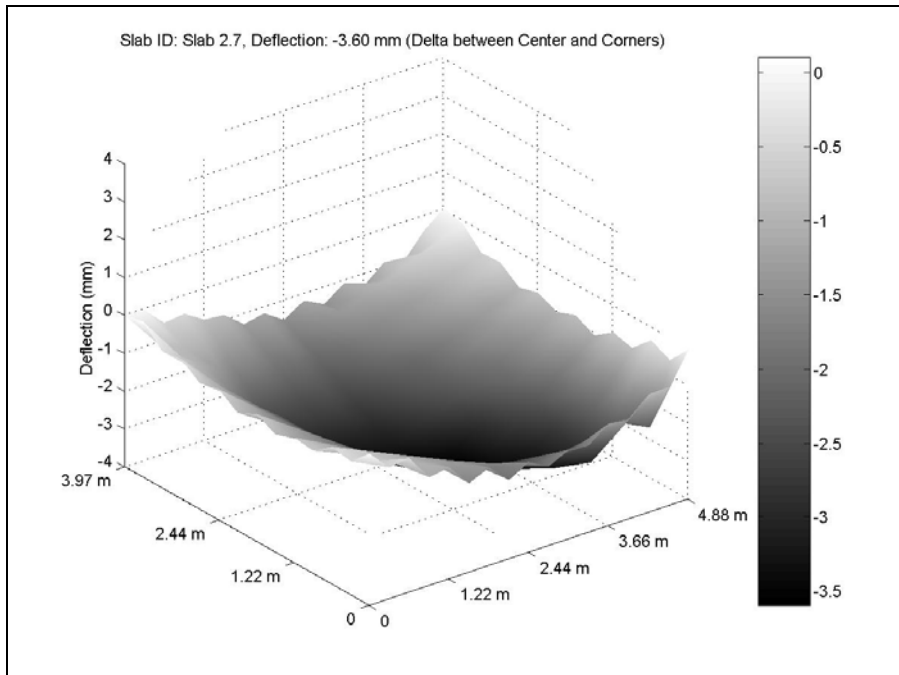


Figure 36. Slab 2 profile difference between extreme gradients, June 18, 2003 (1m=3.28 ft; 1 mm=39 mil)

4.4.4 Falling Weight Deflectometer

FWD readings were taken at 10:00 am and 2:00 pm (at test times 1.5 hours and 5.5 hours) are depicted in Figure 37 and Figure 38 respectively for Slab 1 and in Figure 39 and Figure 40 respectively for Slab 2. The 2:00 pm readings were taken during the extreme positive temperature gradient, but readings were not taken at the extreme negative gradient at 6:00 am because the FWD machine malfunctioned. At 10:00 am when the negative gradient was still present, the deflection was higher at the corners than the center for both slabs. This further verifies that while the addition of the shoulder did constrain the slab, the slab was still able to curl and the readings from the LVDT at the corner near the shoulder were inaccurate. The FWD data from the 2:00 pm readings show relatively uniform deflection throughout the slab, indicating that the slab corners as well as the slab center were in contact with the base.

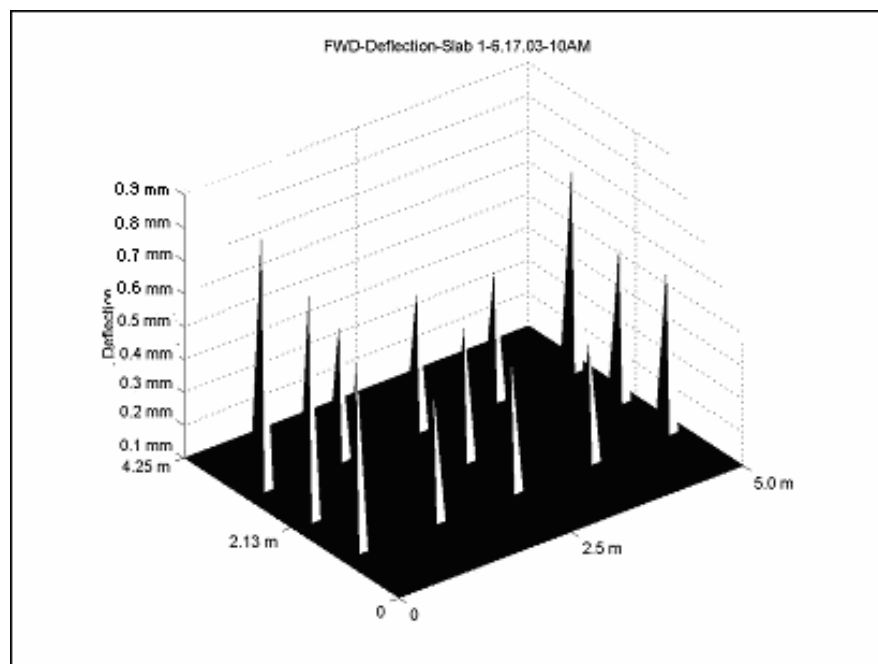


Figure 37. Slab 1 deflection from FWD at 10am, June 17, 2003 (1m=3.28 ft; 1 mm=39 mil)

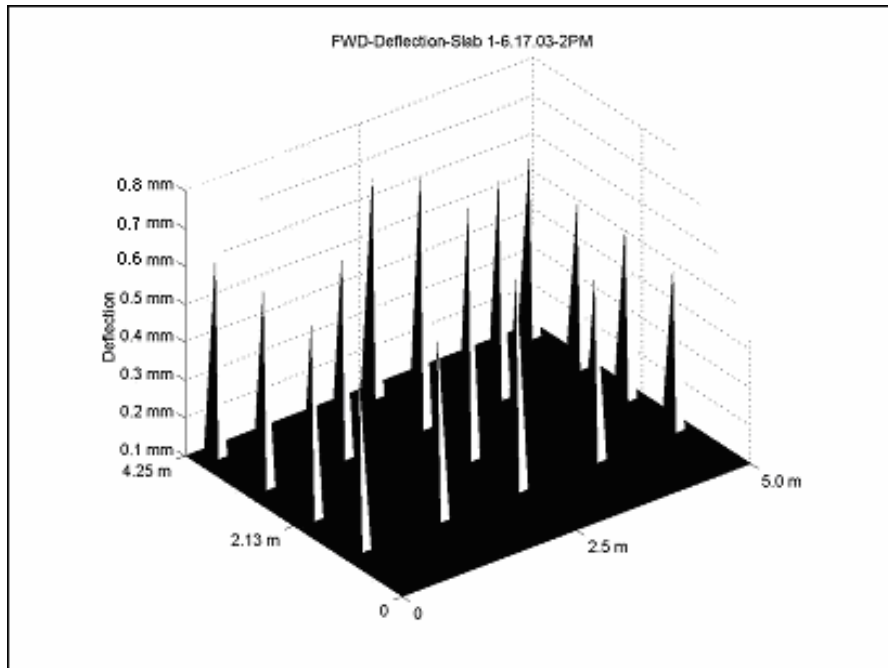


Figure 38. Slab 1 deflection from FWD at 2pm, June 17, 2003 (1m=3.28 ft; 1 mm=39 mil)

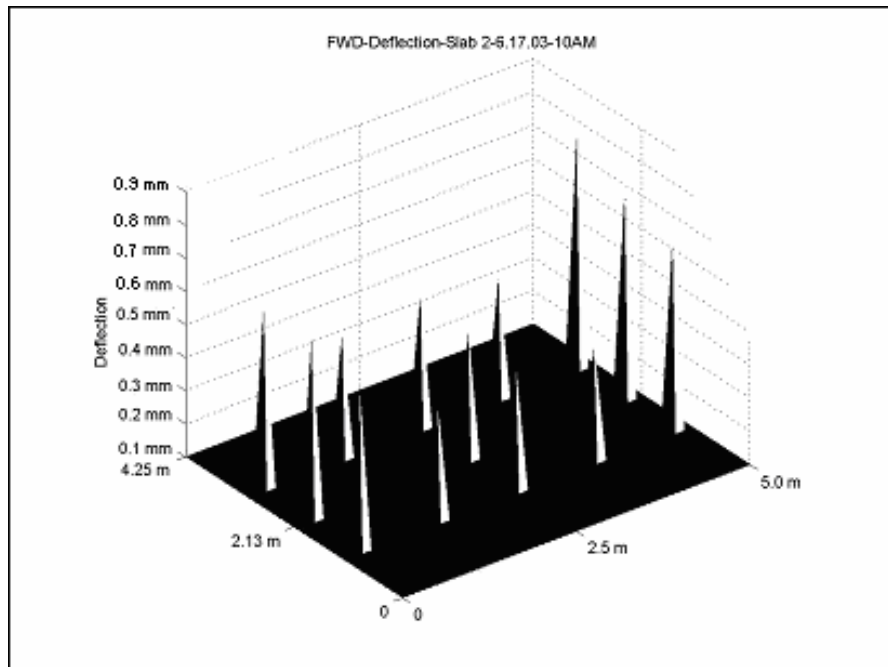


Figure 39. Slab 2 deflection from FWD at 10am, June 17, 2003 (1m=3.28 ft; 1 mm=39 mil)

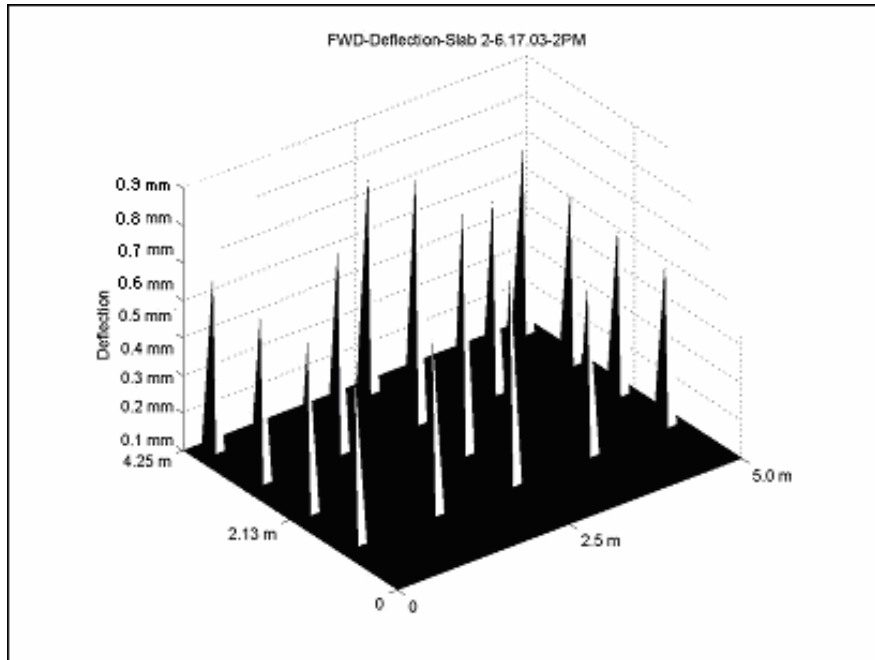


Figure 40. Slab 2 deflection from FWD at 2pm, June 17, 2003 (1m=3.28 ft; 1 mm=39 mil)

4.4.5 Vibrating Wire

The strain was measured throughout the 40 hour monitoring period, and the data were used to calculate stresses in the pavement. It was found that the maximum stresses coincide with the maximum temperature gradients while the maximum strains lag the maximum temperature gradients by about 4 hours. The maximum tensile stresses in the slab occurred at the top strata of the slab in the left wheel path. The maximum tensile stresses in the bottom strata of the pavement were in the bottom of the left wheel path. These strains are presented in Figure 41 and Figure 42 for the center and left wheel path respectively. The corresponding stresses are graphed in Figure 43 and Figure 44 for the center and left wheel path.

**Vibrating Wire change in strain in center
beginning 8:30 June 17, 2003**

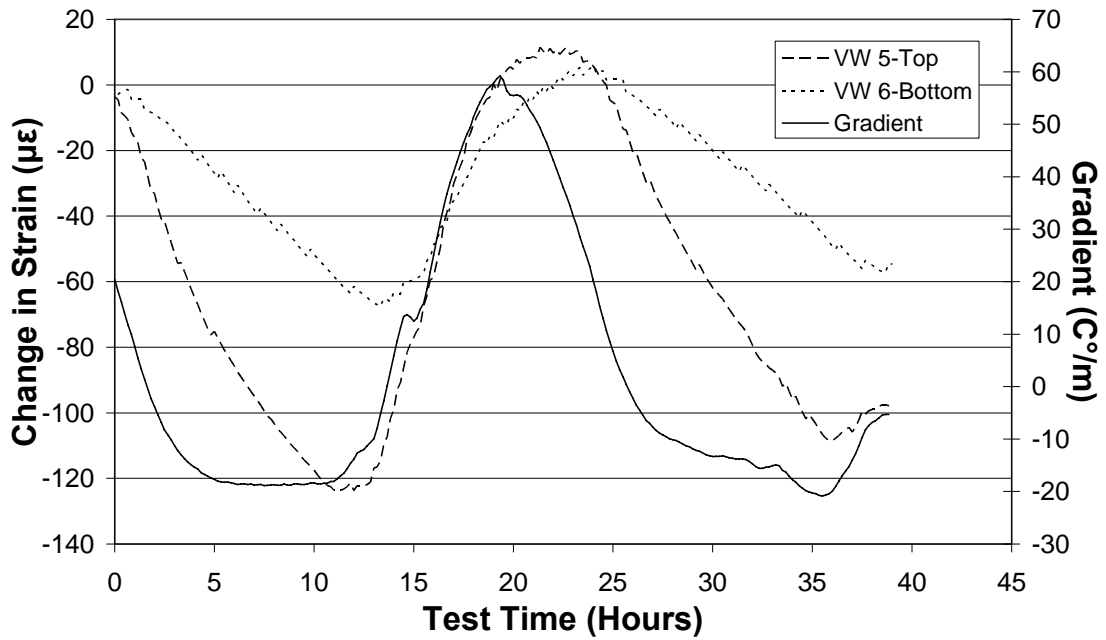


Figure 41. Vibrating wire strain, center of slab, June 17, 2003 ($1\text{C}^\circ/\text{m} = 0.046^\circ\text{F}/\text{in}$)

**Vibrating Wire change in strain in left wheel path
beginning 8:30 June 17, 2003**

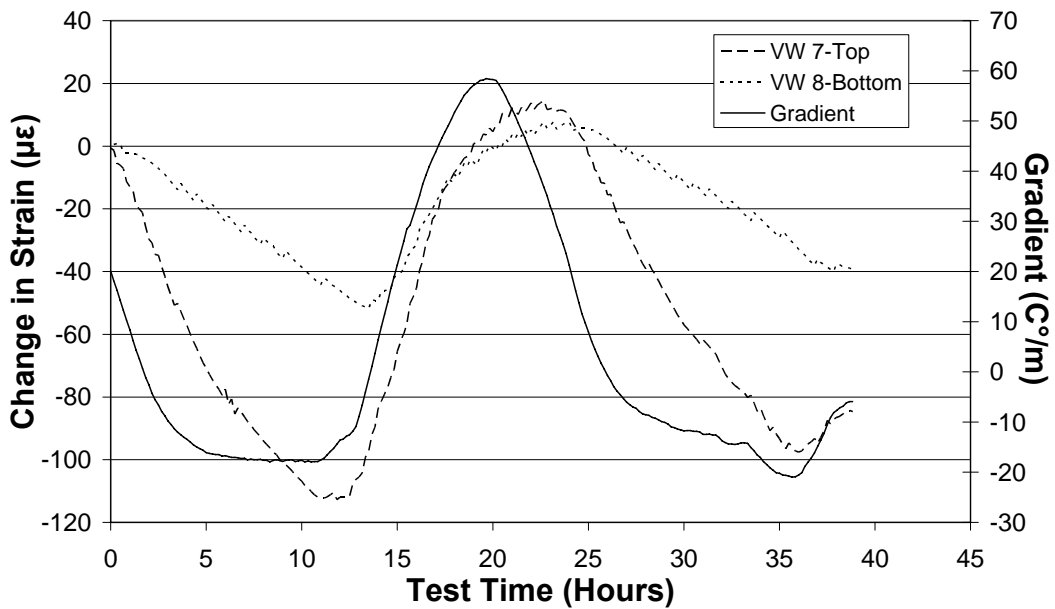


Figure 42. Vibrating wire strain, left wheel path, June 17, 2003 ($1\text{C}^\circ/\text{m} = 0.046^\circ\text{F}/\text{in}$)

**Change in stress at center of slab
Vibrating Wire, beginning 8:30 June 17, 2003**

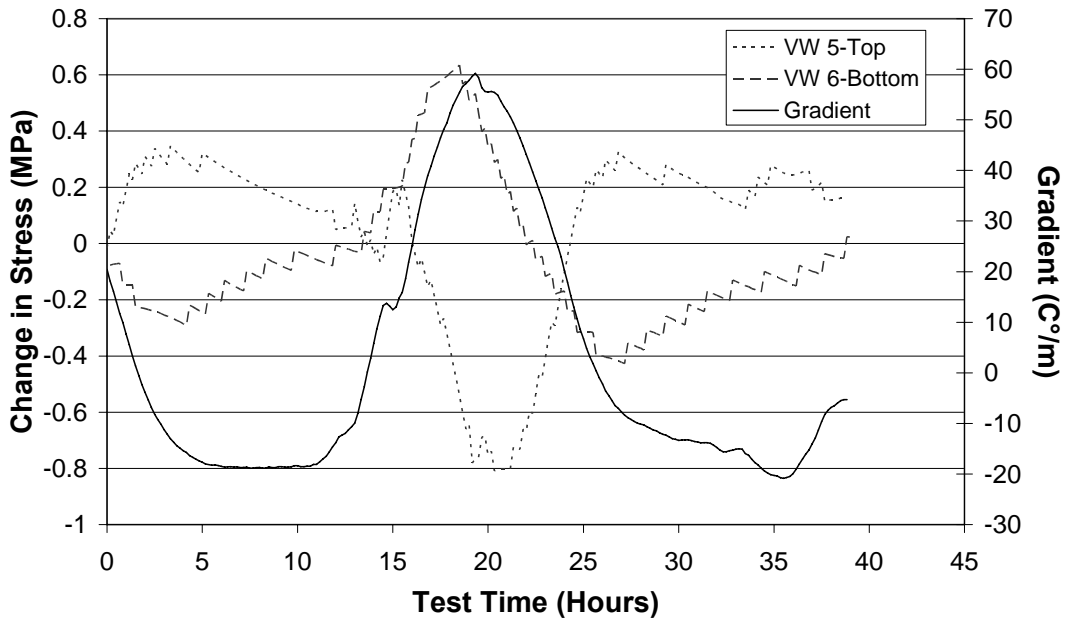


Figure 43. Vibrating wire stress, center of slab, June 17, 2003 (1 MPa = 145 psi; 1C°/m = 0.046°F/in)

**Change In stress in left wheel path
Vibrating Wire, beginning 8:30 June 17, 2003**

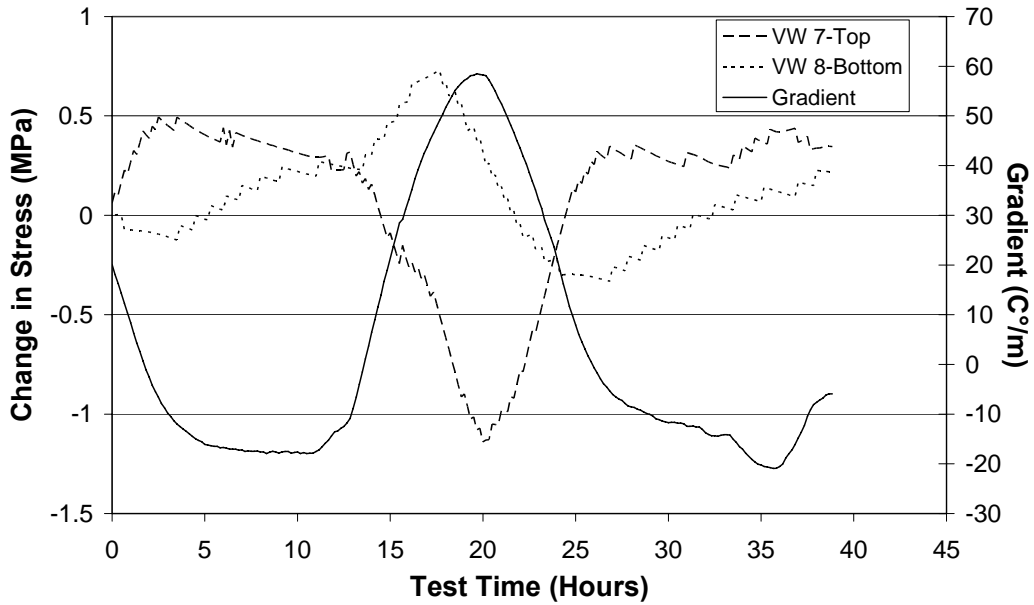


Figure 44. Vibrating wire stress, left wheel path, June 17, 2003 (1 MPa = 145 psi; 1C°/m = 0.046°F/in)

4.5 I-490 West September 2003 24 Hour Monitoring Period

The two instrumented slabs were monitored again for a 24 hour period beginning at 8:50 am September 30, 2003. During this time the strain gage data and thermocouple data were collected every ten minutes. No deep LVDT data were collected because it was found that all four LVDTs had stopped functioning. Additionally, the Dipstick[®] trigger malfunctioned, making that device unusable. FWD tests were conducted to evaluate the loss of support.

4.5.1 Temperature Data

Data collected from the thermistors installed with the vibrating wire strain gages were processed; the pavement temperature gradient at the center of the slab and left wheel path are presented in Figure 45. Because there was little change in the air temperature during the collection period, the slab temperature gradient experienced very little variation.

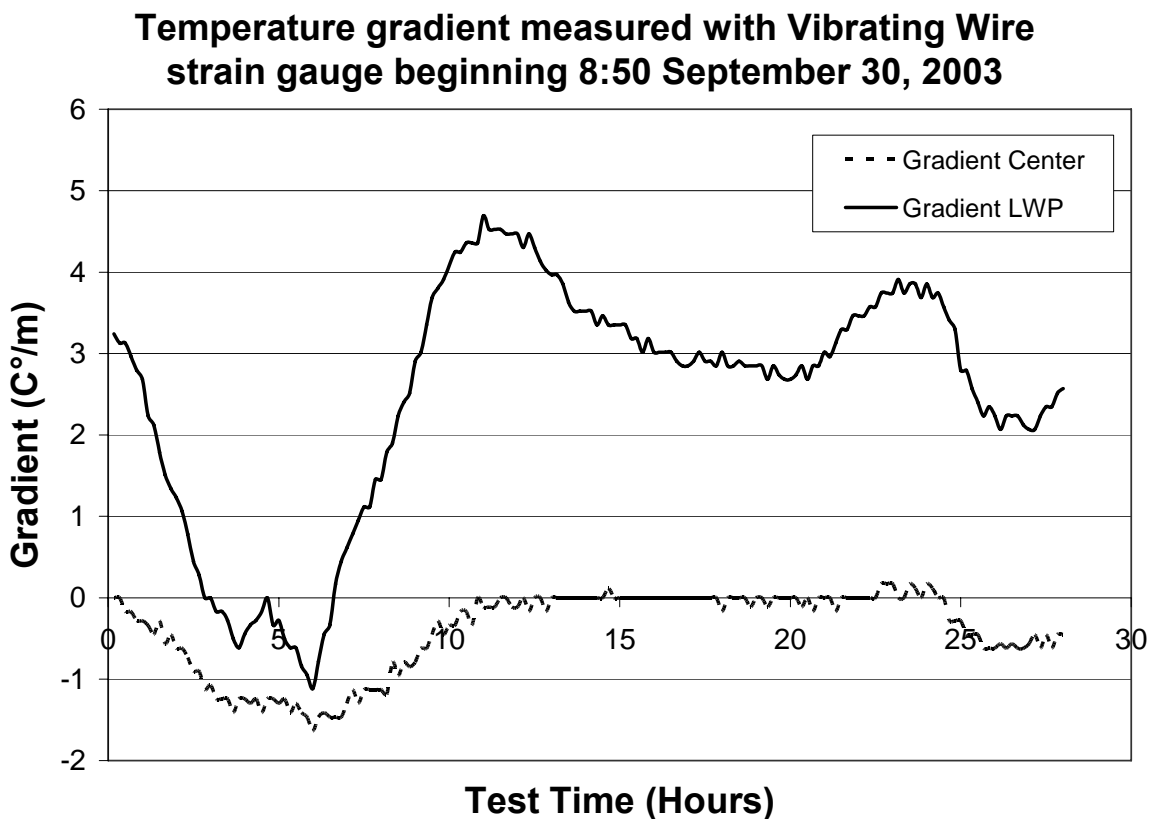


Figure 45. Thermistor gradients, September 30 - October 1, 2003 ($1\text{C}^{\circ}/\text{m} = 0.046^{\circ}\text{F}/\text{in}$)

4.5.2 Falling Weight Deflectometer

FWD data were collected at 10:00 am and 1:00 pm (Test Times 1.16 hours and 4.16 hours respectively) on the first day of the monitoring period and at 9:30 am on the second day of the monitoring period (Test Time 24.67 hours). Plots of the data collected from Slab 1 for both the morning and afternoon of the first day are presented in Figure 46 and Figure 47 respectively. These data are typical of both slabs for this monitoring period; there was little change in

deflection between the test times due to the relatively constant temperature. Additional FWD data plots for Slab 1 and Slab 2 can be found in Appendix D.

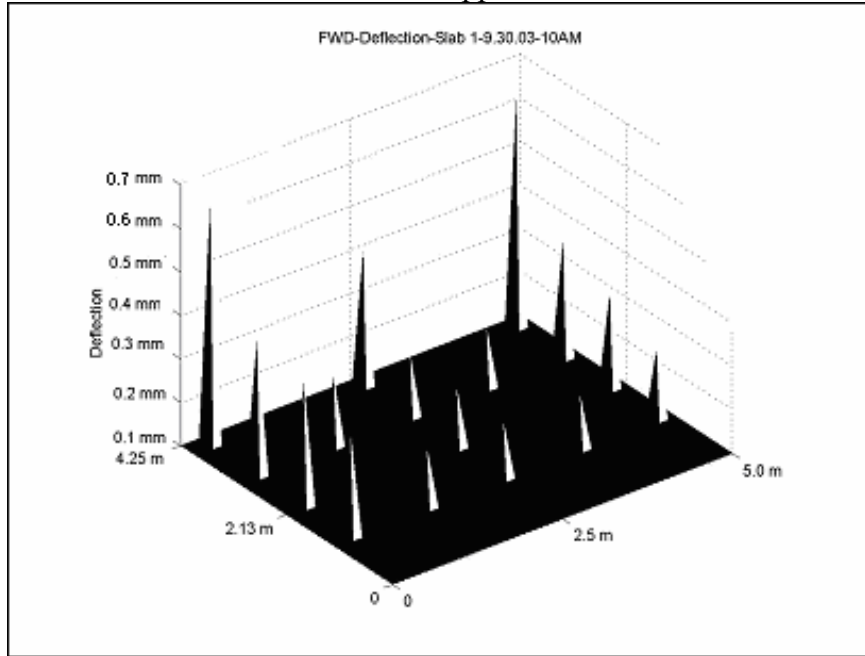


Figure 46. Slab 1 deflection from FWD at 10am, September 30, 2003 (1m=3.28 ft; 1 mm=39 mil)

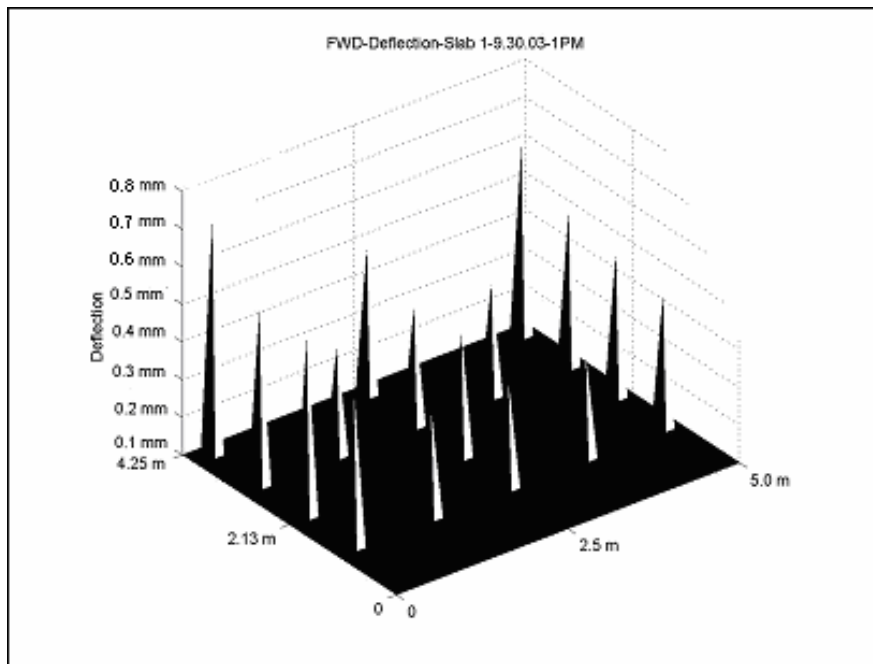


Figure 47. Slab 1 deflection from FWD at 1pm, September 30, 2003 (1m=3.28 ft; 1 mm=39 mil)

4.5.3 Vibrating Wire Strain Gages

Data from the vibrating wire strain gages were collected continuously throughout the monitoring period. As with the previous monitoring periods, the collected strain data were used to calculate the environmentally induced stresses in the concrete. The calculated stresses for both the center of the slab and the left wheel path are presented below in Figure 48 and Figure 49 respectively. Due to the minimal temperature changes throughout the test period, the stress changed less than 0.3 MPa (44 psi) for all of monitored locations. Plots of the strain data are located in Appendix D.

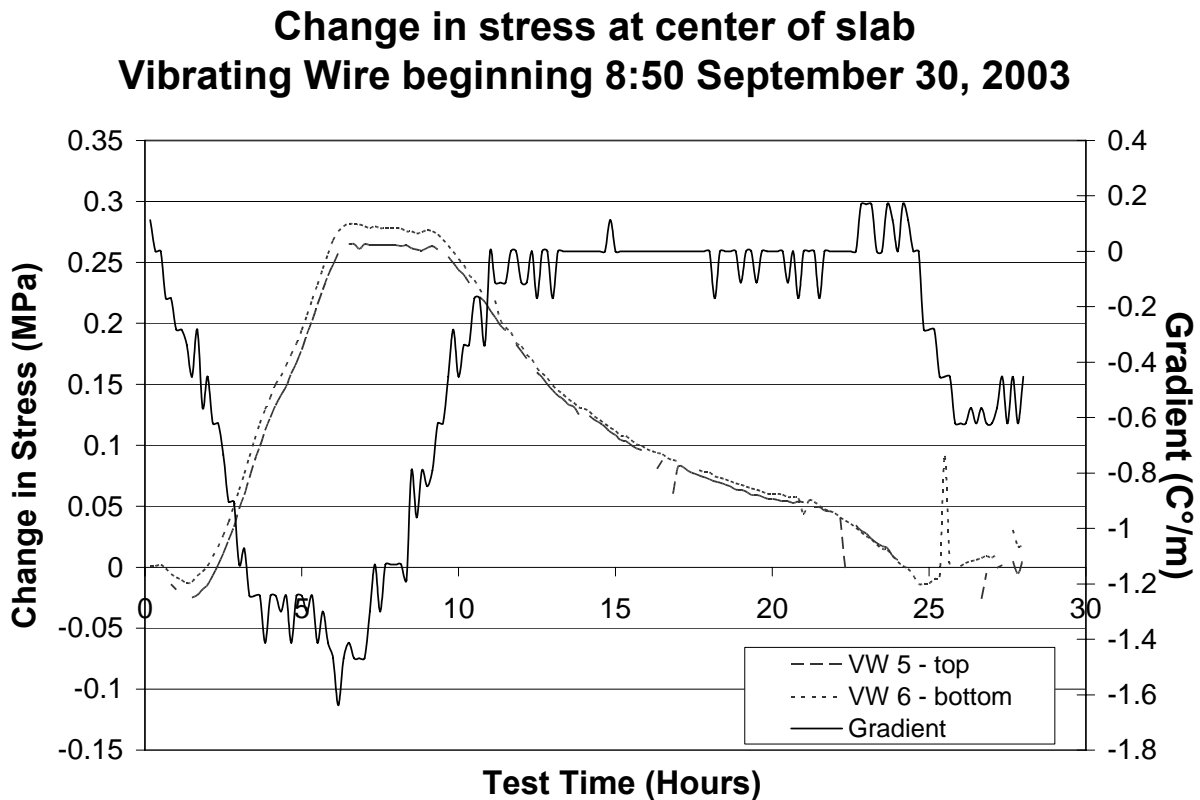


Figure 48. Vibrating wire stress, center of slab, September 30 - October 1, 2003 (1 MPa = 145 psi; 1C°/m = 0.046°F/in)

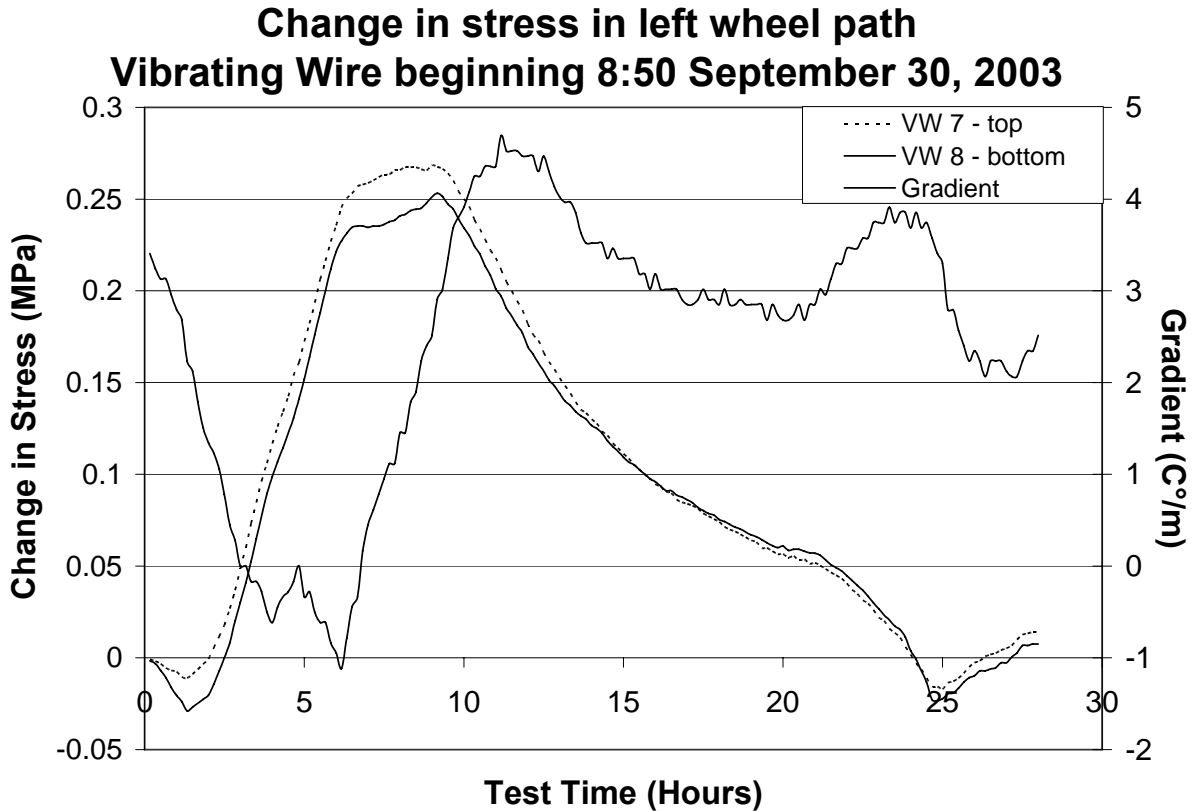


Figure 49. Vibrating wire stress, left wheel path, September 30 - October 1, 2003 (1 MPa = 145 psi; 1C°/m = 0.046°F/in)

4.6 I-490 West October 2004 Testing

Instrumentation maintenance activities were performed on the two instrumented slabs in October 26-27, 2004. After cleaning the deep LVDTs, monitoring equipment was set up to collect vibrating wire strain gage readings, deep LVDT deflection data, and air temperature, with data collected every ten minutes starting at 9:20 AM on the 27th. After the 24-hour monitoring period, environmental data were collected every ten minutes over the next three months, during which data were periodically downloaded from the CR7 for processing. Upon inspection of the data, the vibrating wire strain gage data were found to be faulty. Additionally, during the October monitoring period several measurements were taken of the shallow LVDT deflections and Dipstick[®] surveys were taken at the times of extreme gradients.

The temperature gradients during the first 25 hours and 40 minutes are shown in Figure 50.

Temperature Gradient measured with Vibrating Wire strain gauges, Beginning 9:20 October 27, 2004

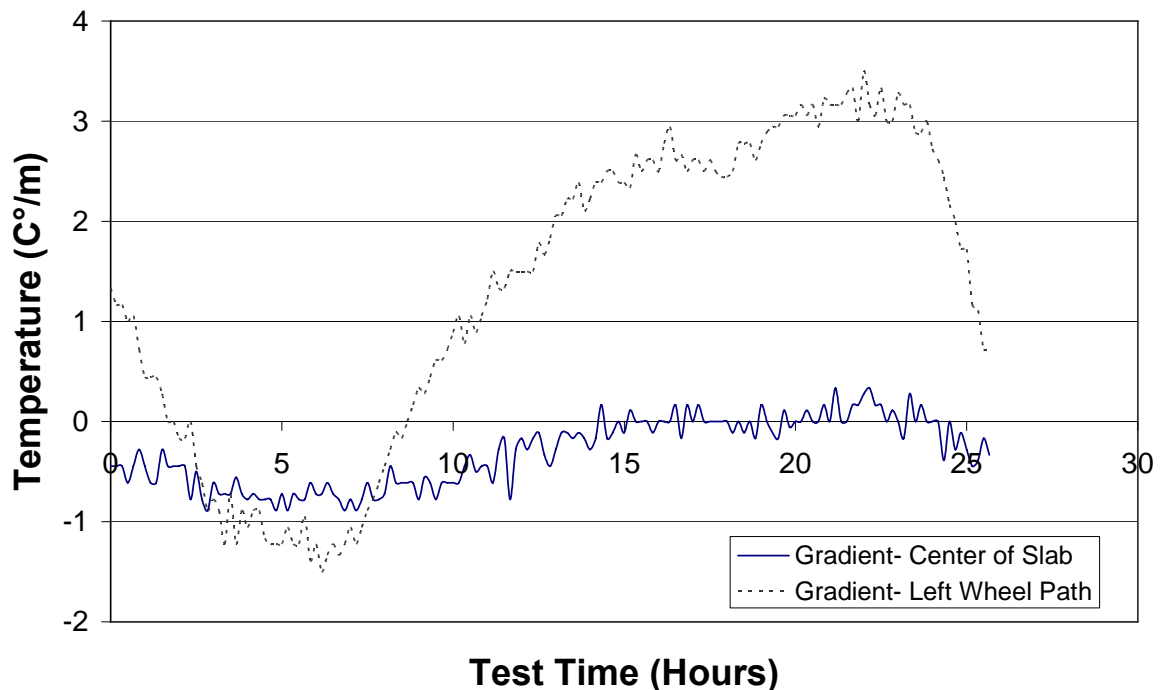


Figure 50. Temperature gradients in slab as measured using thermistors in vibrating wire strain gauges, October 27, 2004 (1C°/m = 0.046°F/in)

4.6.1 Deep LVDTs

Because all four deep LVDTs were found to be no longer functioning in October 2003, the LVDTs were cleaned prior to data collection. This was accomplished by coring the approximately 2.5 cm (1 in) of concrete covering the LVDT caps and removing the LVDTs. Because the LVDT located at the corner by the shoulder had a tie bar inserted through the casing when the shoulder was placed, this LVDT could not be restored to a functional state. The three other deep LVDTs were removed, cleaned, replaced, and their cored holes were refilled with hydraulic grout. When the data were analyzed it was found that the LVDT located at the middle of the shoulder was still not providing usable data. The data collected from the remaining two LVDTs confirmed the findings of previous monitoring sessions. Over the previous three months, the data collected showed there was little fluctuation in the air temperature. However, when the air temperature was lowest the LVDT deflection indicated the pavement was curled and when the air temperature was highest the LVDT deflections indicated that the pavement had flattened. Two typical days of LVDT deflection data along with air temperature from October are depicted in Figure 51 and Figure 52.

Deep Reference LVDTs Day 303

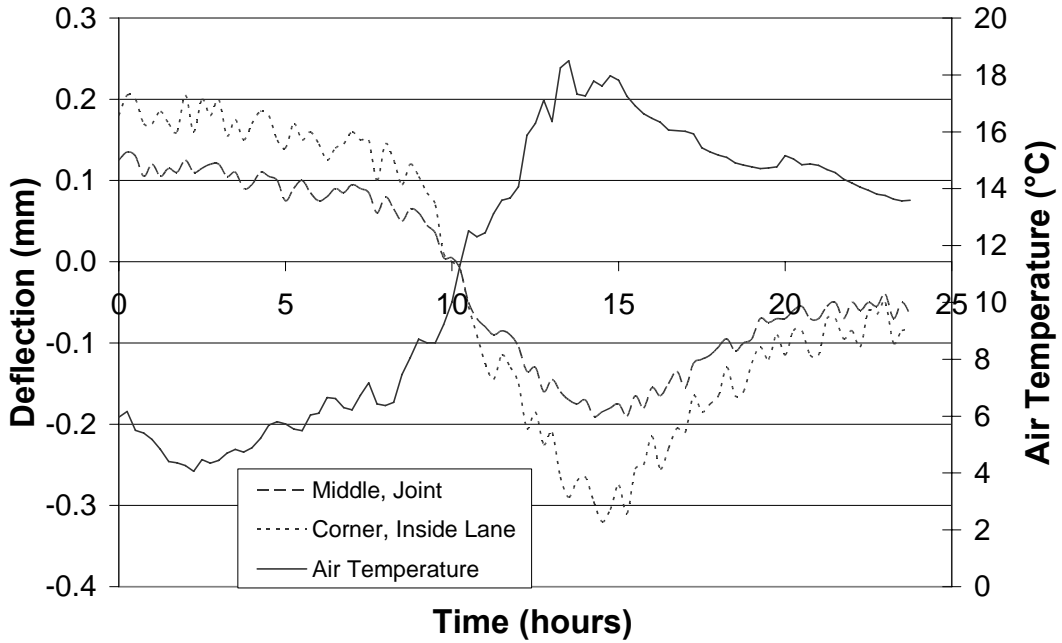


Figure 51. I490 West LVDT Deflection and Air Temperature Data October 29, 2004 (0.1mm = 3.9 mil; air temperature scale range is from 32°F to 68°F)

Deep Reference LVDTs Day 304

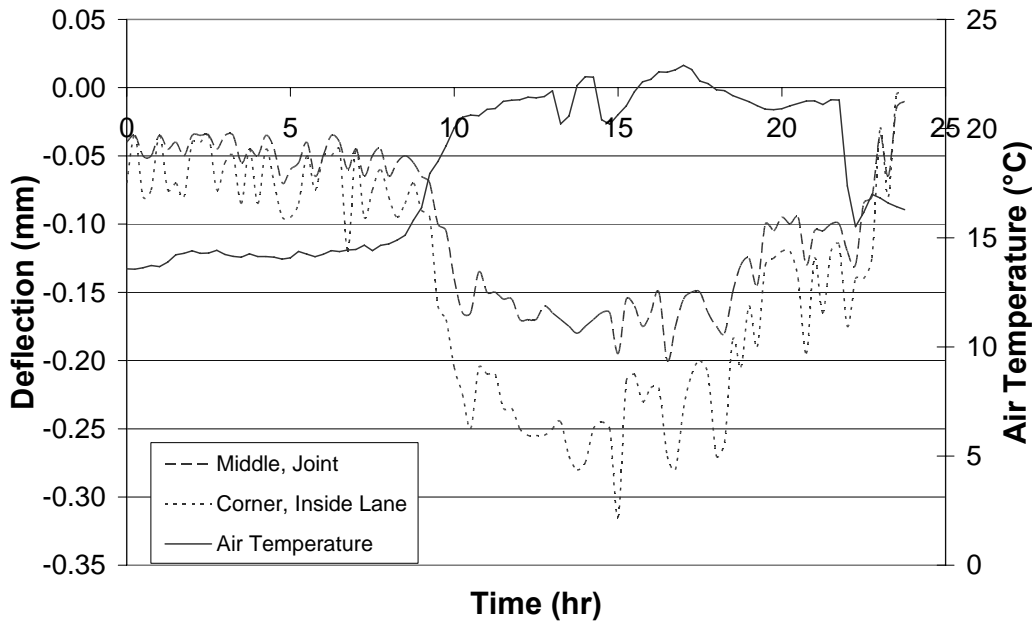


Figure 52. I490 West LVDT Deflection and Air Temperature Data October 30, 2004 (0.1mm = 3.9 mil; air temperature scale range is from 32°F to 77°F)

4.6.2 Shallow LVDTs

Measurements of the shallow LVDT deflection were taken at air temperatures of 7.2° C (45°F), 11.1° C (52°F), and 15.6° C (60°F). The slab temperature gradient at the time of each data collection was determined using the vibrating wire thermistor data. At each of the air temperatures the slab gradient was nearly 0C° (0°F). The slab shape measured by the shallow LVDT deflections is shown in Figure 53. At each of the test temperatures the slab shape follows the same trend with little deflection between collection periods. The slab shape shows the edge of the slab higher than the middle of the slab. The general shape of the slab as indicated by the shallow LVDT deflections coincides with deep LVDT data and Dipstick® profiles.

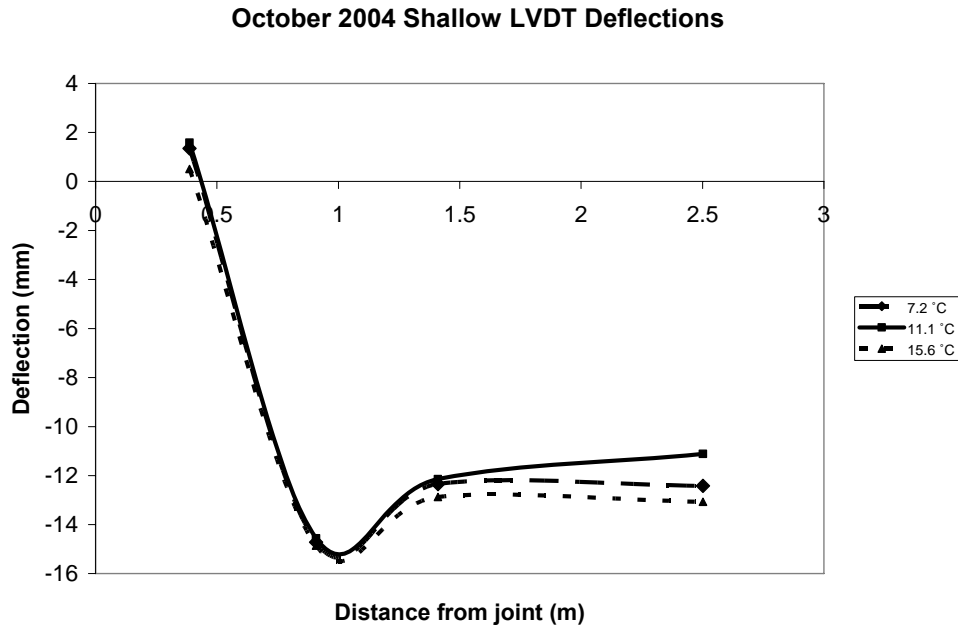


Figure 53. Shallow LVDT Readings, October 2004 (1m=3.28 ft; 1 mm=39 mil; Temperatures are: 7.2° C (45°F), 11.1° C (52°F), and 15.6° C (60°F))

4.6.3 Dipstick®

Dipstick® surveys were taken at 10:30 am and 1:30 pm on the first day of testing as well as at 10:30 am on the second day of testing, October 27. All deflections were plotted relative to the initial slab shape measured immediately after the joints were cut. Morning and afternoon deflections from the first day of testing for Slab 2 are shown in Figure 54 and Figure 55. Additional Dipstick® plots for Slab 1 and Slab 2 are located in Appendix E. The overall displacement between the slab center and corners since the joints were cut is around 4 to 5 mm (0.16 to 0.20 in). Because there was little temperature fluctuation between the two readings, the slab shape remained nearly constant. Figure 56 shows the relative displacement between the morning and afternoon Dipstick® surveys for Slab 2.

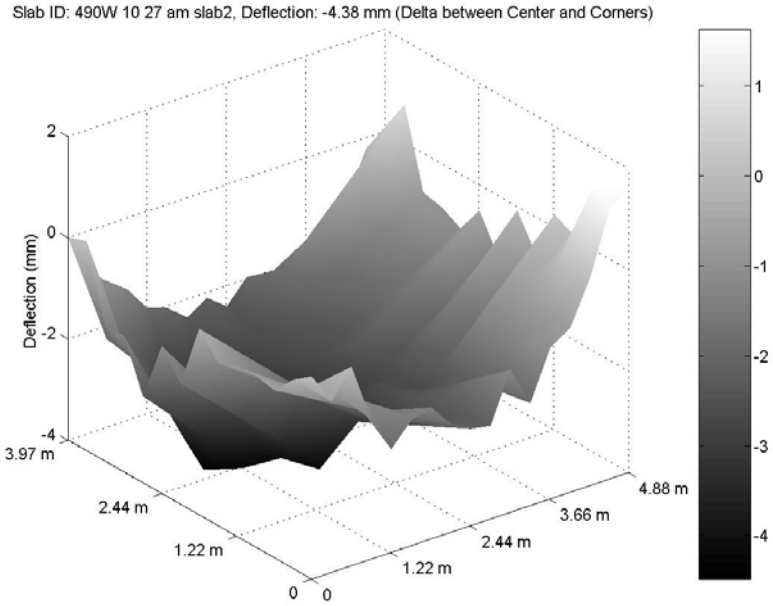


Figure 54. Slab 2 profile at 10:30 am, referenced after joints sawcut (1m=3.28 ft; 1 mm=39 mil)

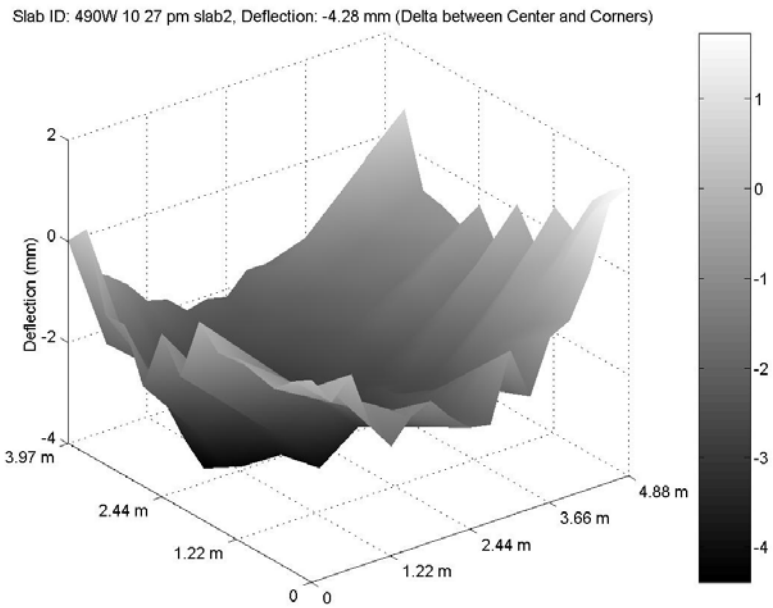


Figure 55. Slab 2 profile at 1:30 pm, referenced after joints sawcut (1m=3.28 ft; 1 mm=39 mil)

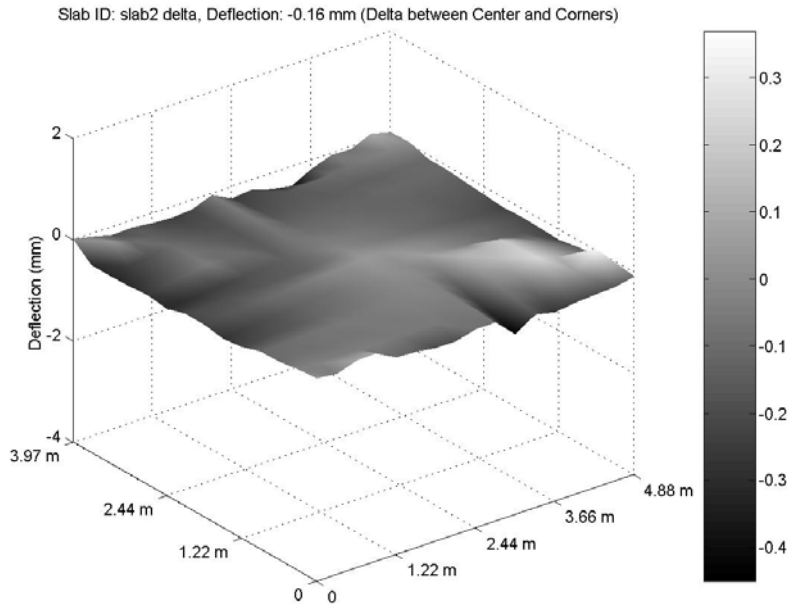


Figure 56. Slab 2 difference between 10:30 am and 1:30 pm profiles (1m=3.28 ft; 1 mm=39 mil)

4.7 I-490 East October 2004 Dowel Bar Testing

In October 26-27, 2004 the slab shapes of the sections in I490 eastbound containing the varied dowel bar arrangements were measured using the Profilometer. Additionally, FWD testing was conducted at each of the test joints.

4.7.1 Slab Profiles

The eighty-five slab profiles were recorded continuously beginning at 10:00 am and ending at 1:30 pm. Instrumentation to continuously monitor air temperature was not available. However, the initial pavement surface temperature at the beginning of testing was 13° C (55.4°F) in the sun and 10° C (50°F) in the shade. By the end of the testing period, the pavement surface temperature had risen to 20° C (68°F). The effect of this temperature change was evident in the slab profiles. While the profile for each slab was measured only once, the dowel bar arrangements were repeated at 10 slab intervals making it possible to compare the reaction of the same dowel bar arrangement throughout the testing period. At the beginning of the testing period all the slabs had significant amounts of curling and warping, causing differences in deflections ranging from an average of 3.1 mm (0.12 in) for the E2 slabs to 3.6 mm (0.14 in) for the STD slabs. As the day progressed and the temperature increased, the slabs generally flattened out with the slab deflection differences in the afternoon averaging from 1.9 mm (0.075 in) to 2.1 mm (0.083 in) for all dowel bar arrangements. The elevation or deflection differences between the center and corner of each slab are presented in Table 5 in metric units and in Table 6 in English units.

When comparing sections containing different dowel bar arrangements that were tested close to the same time, it is noted that for the group from slab 1 to slab 25 as well as the group from slab 26 through slab 55, the STD slab sections had the highest average curl, followed by the E1 sections. The slab group from slab 56 to slab 85 had a nearly consistent curl for all dowel bar arrangements, with the E1 sections curling an average of 0.2 mm (8 mils) more than the STD and

E2 sections. This reduction in curl for all slabs corresponds to the rising temperature throughout the test period which is assumed to increase the temperature gradient throughout the depth of the slab. Unfortunately, it is impossible to separate the effects of temperature on the slabs (“curling”) from the effects of moisture loss during curing (“warping”).

Table 5. I490 East Estimated Differences in Deflection Due to Environmental Factors for Individual Slabs (metric units)

Dowel Bar Spacing Configuration	STD	Slab No.	1	2	3	4	5	--	--	--	--	--	μ	σ
		Net Deflection (mm)	3.6	4.1	3.3	3.3	3.6	--	--	--	--	--	--	3.58
	E1	Slab No.	6	7	8	9	10	11	12	13	14	15	μ	σ
		Net Deflection (mm)	3	2.3	3.8	3.6	3.3	3.6	2.8	4.1	3.6	3.8	3.2	0.59
	E2	Slab No.	16	17	18	19	20	21	22	23	24	25	μ	σ
		Net Deflection (mm)	4.3	2.3	3	2.8	4.3	2.5	2.5	3.3	3.6	2.3	3.34	0.91
	STD	Slab No.	26	27	28	29	30	31	32	33	34	35	μ	σ
		Net Deflection (mm)	2.3	3.6	4.3	3.8	3.6	4.1	4.6	3.6	4.1	2.5	3.52	0.74
	E1	Slab No.	36	37	38	39	40	41	42	43	44	45	μ	σ
		Net Deflection (mm)	2	1.8	2.3	3	3	2.8	2.5	2	3.3	4.3	2.42	0.56
	E2	Slab No.	46	47	48	49	50	51	52	53	54	55	μ	σ
		Net Deflection (mm)	3.3	2.3	2	2.5	2.8	2.3	2.3	2.5	2.3	2.8	2.58	0.50
	STD	Slab No.	56	57	58	59	60	61	62	63	64	65	μ	σ
		Net Deflection (mm)	1.5	2	1.8	1.5	2.8	2.3	2	1.5	2	1.5	1.92	0.54
	E1	Slab No.	66	67	68	69	70	71	72	73	74	75	μ	σ
		Net Deflection (mm)	4.1	2.3	2.8	2	1.5	1.5	2	1.8	2	1	2.54	0.99
E2	Slab No.	76	77	78	79	80	81	82	83	84	85	μ	σ	
	Net Deflection (mm)	1.3	2	2.3	2.5	2.3	1.8	1.5	1.3	2	1.5	2.08	0.47	

Table 6. I490 East Estimated Differences in Deflection Due to Environmental Factors for Individual Slabs (English units)

Dowel Bar Spacing Configuration	STD	Slab No.	1	2	3	4	5	--	--	--	--	--	μ	σ
		Net Deflection (in)	0.142	0.161	0.130	0.130	0.142	--	--	--	--	--	--	0.141
	E1	Slab No.	6	7	8	9	10	11	12	13	14	15	μ	σ
		Net Deflection (in)	0.118	0.091	0.150	0.142	0.130	0.142	0.110	0.161	0.142	0.150	0.126	0.023
	E2	Slab No.	16	17	18	19	20	21	22	23	24	25	μ	σ
		Net Deflection (in)	0.169	0.091	0.118	0.110	0.169	0.098	0.098	0.130	0.142	0.091	0.131	0.036
	STD	Slab No.	26	27	28	29	30	31	32	33	34	35	μ	σ
		Net Deflection (in)	0.091	0.142	0.169	0.150	0.142	0.161	0.181	0.142	0.161	0.098	0.139	0.029
	E1	Slab No.	36	37	38	39	40	41	42	43	44	45	μ	σ
		Net Deflection (in)	0.079	0.071	0.091	0.118	0.118	0.110	0.098	0.079	0.130	0.169	0.095	0.022
	E2	Slab No.	46	47	48	49	50	51	52	53	54	55	μ	σ
		Net Deflection (in)	0.130	0.091	0.079	0.098	0.110	0.091	0.091	0.098	0.091	0.110	0.102	0.020
	STD	Slab No.	56	57	58	59	60	61	62	63	64	65	μ	σ
		Net Deflection (in)	0.059	0.079	0.071	0.059	0.110	0.091	0.079	0.059	0.079	0.059	0.076	0.021
	E1	Slab No.	66	67	68	69	70	71	72	73	74	75	μ	σ
		Net Deflection (in)	0.161	0.091	0.110	0.079	0.059	0.059	0.079	0.071	0.079	0.039	0.100	0.039
	E2	Slab No.	76	77	78	79	80	81	82	83	84	85	μ	σ
		Net Deflection (in)	0.051	0.079	0.091	0.098	0.091	0.071	0.059	0.051	0.079	0.059	0.082	0.019

4.7.2 Falling Weight Deflectometer (FWD) Testing

Falling Weight Deflectometer (FWD) testing was conducted on the joints of 84 of the 85 slabs in the test section beginning at 10:30 am and continuing until 2:00 pm. In several cases, particularly those using the 37.4 kN (8.41 kip) load, the collected data are clearly inaccurate because the calculated load transfer efficiencies (LTE) are significantly greater than the maximum possible LTE of 100 percent. For FWD readings with the 37.4 kN (8.41 kip) load, this problem affects either the approach or leave (or perhaps both) measurements for 47 slabs, and all but 5 of those have LTEs > 105%. For the FWD readings with the 50.3 kN (11.3 kip) load, only 8 are affected, and of these only 6 have LTEs > 105%; These six slabs are 12-16 and 19, and the high LTEs are all leave values. These discrepancies most likely result from faulty FWD testing equipment or improper placement of the geophones. For analysis purposes, all LTE values greater than 105% are considered inaccurate and are eliminated from the averages. Because of the great number of problematic readings with the 37.4 kN (8.41 kip) load, those readings are presented, the entire set of readings at this weight are suspect. The LTE, deflection in $\mu\text{m}/\text{kN}$, and Joint Support Ratio (JSR) of the different dowel bar test sections for both the 37.4 kN (8.41 kip) and the 50.3 kN (11.3 kip) test loads are compared in Table 7 through Table 12. LTEs larger than 100% are shaded.

Results for the STD, E1 and E2 sections from Slab 1 to Slab 25 are tabulated in Table 7 and Table 8. The E2 sections deflected the least while the STD sections deflected the most in both the approach and leave positions for both test weights. This corresponds to the average slab curl, with the STD slabs warped 0.5 mm (0.02 in) more than the E2 sections. The JSR for these sections also follows this trend, with the E2 sections having the highest JSR, E1 sections in the middle and STD sections the lowest JSR. When the LTE data is examined for these sections, the previously established trend is not followed as closely. The E2 joints had the highest LTE under 50.3 kN (11.3 kip) load, but the differences between the joint treatment averages are less than the standard deviations.

Upon examining the data for the joints from slab 26 to slab 55 in Table 9 and Table 10, it can be seen that the E2 sections once again deflected the least. However, the E1 sections deflected slightly more than the STD sections in this group. The JSR results for the 50.3 kN (11.3 kip) test correspond to this data with the E2 and STD slabs having higher JSRs than the E1 slabs. The E2 joints clearly have the highest LTE under the 50.3 kN (11.3 kip) load, with the STD and E1 following.

The deflection data from the joints between slabs 56 to 84 displayed in Table 12 consistently show the E1 slabs deflecting the least. Under the 50.3 kN (11.3 kip) test weight the E2 slabs deflected slightly less than the STD slabs. This is not what is expected from the slab shapes; the E1 section had an average warp of 2.1 mm (0.083 in) while both the STD and E2 sections had an average warp of 1.9 mm (0.75 in) so the E1 section would be expected to deflect the most. However, when these curling measurements are compared with the original curl of the slabs of up to 3.6 mm (0.14 in), the difference of 0.2 mm (0.008 in) between all three slab types becomes negligible. Therefore since the slab curl is nearly the same for the three dowel bar arrangements, the differences in slab performance during this testing time is based primarily on the differences in dowel bar arrangement.

For the 50.3 kN (11.3 kip) testing, the E2 sections again had the highest LTE followed closely by the STD sections then the E1 sections, but again the differences are less than the

standard deviations within each joint type. Within both approach and leave efficiencies test categories for both test weights, and disregarding defective values, the difference between the three dowel bar arrangements never exceeded 4.6%. In contrast, the LTE difference in test sections 26 to 55 approached 11%. The relatively close LTEs of slab sections 56 to 84 reinforces that the relaxation of the slabs due to temperature gradient increase resulted in similar slab reactions.

Table 7. I-490 East 37.4 kN (8.41 kip) FWD, Slabs 1-25, October 26, 2004

Joint Number	Joint Approach			Joint Leave			JSR
	Deflection ($\mu\text{m/kN}$)	Deflection (mil/kip)	LTE (%)	Deflection ($\mu\text{m/kN}$)	Deflection (mil/kip)	LTE (%)	
STD Dowel Bar Arrangement							
1	0.623	0.109	83.8	0.47	0.082	96.1	0.75
2	0.53	0.093	64.6	0.548	0.096	83.6	1.03
3	0.507	0.089	97.9	0.502	0.088	89.7	0.99
4	0.484	0.085	83.6	0.432	0.076	88.3	0.89
5	0.434	0.076	107	0.44	0.077	95.1	1.01
μ	0.536	0.094	82.47	0.488	0.085	89.42	0.92
σ	0.061	0.011	13.69	0.049	0.009	5.17	0.12
E1 Dowel Bar Arrangement							
6	0.444	0.078	91.8	0.414	0.073	86	0.93
7	0.432	0.076	97.9	0.432	0.076	93.6	1
8	0.446	0.078	90.8	0.432	0.076	90.8	0.97
9	0.398	0.070	106.9	0.46	0.081	86.4	1.15
10	0.432	0.076	95.8	0.395	0.069	91.9	0.92
11	0.382	0.067	95.2	0.368	0.064	88.8	0.96
12	0.392	0.069	92.2	0.426	0.075	97.5	1.09
13	0.345	0.060	110.2	0.392	0.069	270.4	1.14
14	0.411	0.072	94.8	0.379	0.066	85.9	0.92
15	0.426	0.075	88.9	0.415	0.073	147.8	0.97
μ	0.421	0.074	93.41	0.413	0.072	90.11	0.97
σ	0.024	0.004	2.98	0.031	0.005	4.16	0.06
E2 Dowel Bar Arrangement							
16	0.357	0.063	97.9	0.38	0.067	147.4	1.06
17	0.369	0.065	95.5	0.437	0.077	72.7	1.18
18	0.374	0.065	95.5	0.359	0.063	90.2	0.96
19	0.275	0.048	115.6	0.333	0.058	230.7	1.21
20	0.366	0.064	92.1	0.374	0.065	79.6	1.02
21	0.333	0.058	89	0.35	0.061	86	1.05
22	0.316	0.055	91.8	0.27	0.047	106.8	0.86
23	0.278	0.049	115.9	0.369	0.065	85.5	1.33
24	0.35	0.061	91.3	0.301	0.053	97.5	0.86
25	0.337	0.059	91	0.33	0.058	93.1	0.98
μ	0.350	0.061	92.99	0.360	0.063	86.37	1.01
σ	0.020	0.004	2.97	0.042	0.007	8.32	0.11

LTE=Load Transfer Efficiency

JSR=Joint Support Ratio

Averages (μ) and standard deviations (σ) include only slabs with LTE less than 105%

Table 8. I-490 East 50.3 kN (11.3 kip) FWD, Slabs 1-25, October 26, 2004

Joint Number	Joint Approach			Joint Leave			JSR
	Deflection ($\mu\text{m/kN}$)	Deflection (mil/kip)	LTE (%)	Deflection ($\mu\text{m/kN}$)	Deflection (mil/kip)	LTE (%)	
STD Dowel Bar Arrangement							
1	0.619	0.108	85.1	0.61	0.107	87.3	0.99
2	0.601	0.105	86	0.581	0.102	85.7	0.97
3	0.626	0.110	82	0.61	0.107	80.4	0.97
4	0.553	0.097	83.2	0.552	0.097	81.5	1
5	0.555	0.097	87.3	0.561	0.098	81.6	1.01
μ	0.591	0.103	84.73	0.583	0.102	83.32	0.99
σ	0.035	0.006	2.14	0.027	0.005	3.03	0.02
E1 Dowel Bar Arrangement							
6	0.505	0.088	86.3	0.482	0.084	81.6	0.96
7	0.498	0.087	89.3	0.528	0.092	83	1.06
8	0.504	0.088	81.8	0.509	0.089	81	1.01
9	0.502	0.088	88.2	0.504	0.088	84.5	1
10	0.512	0.090	88	0.505	0.088	80.2	0.99
11	0.472	0.083	79.6	0.478	0.084	78.4	1.01
12	0.518	0.091	74.6	0.48	0.084	198.8	0.93
13	0.481	0.084	85.8	0.495	0.087	181.9	1.03
14	0.515	0.090	81.7	0.492	0.086	139	0.95
15	0.506	0.089	82.1	0.489	0.086	105.8	0.97
μ	0.501	0.088	83.74	0.501	0.088	81.46	1
σ	0.014	0.002	4.63	0.018	0.003	2.13	0.03
E2 Dowel Bar Arrangement							
16	0.472	0.083	81.7	0.455	0.080	143.1	0.96
17	0.439	0.077	89.9	0.464	0.081	91.9	1.06
18	0.444	0.078	87	0.459	0.080	85.1	1.03
19	0.38	0.067	89.6	0.392	0.069	291.3	1.03
20	0.433	0.076	82.9	0.42	0.074	79.2	0.97
21	0.378	0.066	89.8	0.385	0.067	86.1	1.02
22	0.338	0.059	98.3	0.395	0.069	81.9	1.17
23	0.434	0.076	82.5	0.4	0.070	85.5	0.92
24	0.383	0.067	89.3	0.371	0.065	88.4	0.97
25	0.418	0.073	82.9	0.404	0.071	83.4	0.97
μ	0.412	0.072	87.39	0.412	0.072	85.2	1.01
σ	0.041	0.007	5.13	0.034	0.006	3.9	0.08

LTE=Load Transfer Efficiency

JSR=Joint Support Ratio

Averages (μ) and standard deviations (σ) include only slabs with LTE less than 105%

Table 9. I-490 East 37.4 kN FWD, Slabs 26-55, October 26, 2004

Joint Number	Joint Approach			Joint Leave			JSR
	Deflection ($\mu\text{m/kN}$)	Deflection (mil/kip)	LTE (%)	Deflection ($\mu\text{m/kN}$)	Deflection (mil/kip)	LTE (%)	
STD Dowel Bar Arrangement							
26	0.331	0.058	98.6	0.345	0.060	89.8	1.04
27	0.308	0.054	100	0.336	0.059	85.5	1.09
28	0.414	0.073	70.8	0.339	0.059	81.1	0.82
29	0.339	0.059	97.3	0.334	0.058	100.5	0.99
30	0.334	0.058	94.5	0.316	0.055	92.8	0.95
31	0.313	0.055	86.8	0.307	0.054	85.6	0.98
32	0.322	0.056	88.2	0.269	0.047	106.3	0.83
33	0.325	0.057	83.1	0.284	0.050	87.1	0.87
34	0.278	0.049	84.1	0.232	0.041	100	0.84
35	0.243	0.043	101.9	0.302	0.053	78.8	1.25
μ	0.321	0.056	90.53	0.311	0.054	89	0.98
σ	0.044	0.008	9.72	0.036	0.006	7.6	0.13
E1 Dowel Bar Arrangement							
36	0.405	0.071	53.6	0.377	0.066	65.2	0.93
37	0.328	0.057	91.6	0.356	0.062	82	1.08
38	0.365	0.064	87	0.261	0.046	117	0.72
39	0.289	0.051	106.9	0.302	0.053	101.5	1.05
40	0.276	0.048	114.9	0.275	0.048	111.7	0.99
41	0.33	0.058	97.2	0.385	0.067	77.4	1.17
42	0.29	0.051	96.8	0.282	0.049	101.6	0.97
43	0.298	0.052	94.4	0.29	0.051	96.8	0.97
44	0.278	0.049	98.9	0.276	0.048	92.3	0.99
45	0.246	0.043	113.7	0.316	0.055	85	1.29
μ	0.328	0.057	88.51	0.323	0.057	87.73	1.02
σ	0.045	0.008	15.91	0.043	0.008	12.78	0.09
E2 Dowel Bar Arrangement							
46	0.286	0.050	91.4	0.275	0.048	98.3	0.96
47	0.263	0.046	107.6	0.247	0.043	119.8	0.94
48	0.273	0.048	117.3	0.301	0.053	102	1.1
49	0.256	0.045	116.1	0.24	0.042	117.2	0.93
50	0.249	0.044	122.1	0.261	0.046	113.5	1.05
51	0.27	0.047	119.8	0.292	0.051	107.9	1.08
52	0.255	0.045	122.2	0.324	0.057	99.5	1.27
53	0.289	0.051	107.4	0.34	0.060	88.8	1.18
54	0.235	0.041	133.8	0.205	0.036	147	0.87
55	0.331	0.058	94	0.299	0.052	108.2	0.9
μ	0.308	0.054	92.73	0.31	0.054	97.17	0.96
σ	0.032	0.006	1.81	0.029	0.005	5.8	-

LTE=Load Transfer Efficiency

JSR=Joint Support Ratio

Averages (μ) and standard deviations (σ) include only slabs with LTE less than 105%

Table 10. I-490 East 50.3 kN FWD, Slabs 26-55, October 26, 2004

Joint Number	Joint Approach			Joint Leave			JSR
	Deflection ($\mu\text{m/kN}$)	Deflection (mil/kip)	LTE (%)	Deflection ($\mu\text{m/kN}$)	Deflection (mil/kip)	LTE (%)	
STD Dowel Bar Arrangement							
26	0.394	0.069	91.1	0.397	0.070	85.1	1.01
27	0.381	0.067	88.4	0.394	0.069	80.1	1.03
28	0.385	0.067	82.3	0.383	0.067	78.9	0.99
29	0.386	0.068	92.9	0.427	0.075	82.7	1.11
30	0.396	0.069	86.5	0.383	0.067	86.9	0.97
31	0.334	0.058	89.1	0.364	0.064	79.8	1.09
32	0.362	0.063	86.8	0.359	0.063	85.1	0.99
33	0.333	0.058	87.4	0.356	0.062	76.8	1.07
34	0.342	0.060	80.1	0.354	0.062	74	1.04
35	0.336	0.059	80.1	0.346	0.061	75.4	1.03
μ	0.365	0.064	86.47	0.376	0.066	80.49	1.03
σ	0.027	0.005	4.4	0.025	0.004	4.4	0.05
E1 Dowel Bar Arrangement							
36	0.463	0.081	52.9	0.435	0.076	60.3	0.94
37	0.386	0.068	85.3	0.371	0.065	84.7	0.96
38	0.401	0.070	85.8	0.426	0.075	78.1	1.06
39	0.396	0.069	86.5	0.415	0.073	80.3	1.05
40	0.381	0.067	90.8	0.395	0.069	83.6	1.04
41	0.384	0.067	87.3	0.4	0.070	83.5	1.04
42	0.37	0.065	82.5	0.373	0.065	82.1	1.01
43	0.367	0.064	86.7	0.36	0.063	83.9	0.98
44	0.337	0.059	87.2	0.341	0.060	84	1.01
45	0.336	0.059	90.2	0.342	0.060	87	1.02
μ	0.382	0.067	83.53	0.386	0.068	80.76	1.01
σ	0.036	0.006	11	0.034	0.006	7.59	0.04
E2 Dowel Bar Arrangement							
46	0.328	0.057	89.6	0.337	0.059	85.5	1.03
47	0.349	0.061	92.8	0.352	0.062	91.3	1.01
48	0.369	0.065	94.2	0.385	0.067	87.3	1.04
49	0.347	0.061	91.5	0.352	0.062	87.1	1.01
50	0.318	0.056	102.9	0.339	0.059	93.3	1.07
51	0.364	0.064	94.1	0.369	0.065	90.2	1.01
52	0.351	0.061	97.7	0.366	0.064	92.5	1.04
53	0.37	0.065	89	0.378	0.066	84.4	1.02
54	0.356	0.062	93.6	0.35	0.061	91.9	0.98
55	0.334	0.058	101.4	0.358	0.063	94.9	1.07
μ	0.349	0.061	94.67	0.359	0.063	89.84	1.03
σ	0.018	0.003	4.65	0.016	0.003	3.56	0.03

LTE=Load Transfer Efficiency

JSR=Joint Support Ratio

Averages (μ) and standard deviations (σ) include only slabs with LTE less than 105%

Table 11. I-490 East 37.4 kN (8.41 kip) FWD, Slabs 56-84, October 26, 2004

Joint Number	Joint Approach			Joint Leave			JSR
	Deflection ($\mu\text{m/kN}$)	Deflection (mil/kip)	LTE (%)	Deflection ($\mu\text{m/kN}$)	Deflection (mil/kip)	LTE (%)	
STD Dowel Bar Arrangement							
56	0.311	0.054	97.5	0.272	0.048	109.6	0.87
57	0.299	0.052	110.2	0.301	0.053	109.1	1.01
58	0.331	0.058	97.2	0.304	0.053	99.5	0.92
59	0.319	0.056	91.4	0.218	0.038	132.9	0.68
60	0.25	0.044	107.3	0.231	0.040	118.5	0.92
61	0.293	0.051	89.1	0.266	0.047	97.1	0.91
62	0.197	0.034	118.6	0.226	0.040	113.5	1.15
63	0.279	0.049	92.9	0.304	0.053	85.4	1.09
64	0.229	0.040	102.7	0.209	0.037	116.1	0.91
65	0.269	0.047	95.5	0.229	0.040	122.7	0.85
μ	0.29	0.051	95.18	0.291	0.051	94.02	0.97
σ	0.035	0.006	4.53	0.022	0.004	7.53	0.1
E1 Dowel Bar Arrangement							
66	0.269	0.047	105.7	0.249	0.044	102.5	0.93
67	0.224	0.039	109.5	0.217	0.038	110.6	0.97
68	0.261	0.046	99.4	0.273	0.048	90.5	1.05
69	0.253	0.044	92.8	0.231	0.040	101.3	0.91
70	0.235	0.041	98.7	0.218	0.038	103.5	0.93
71	0.221	0.039	116.6	0.246	0.043	87.6	1.11
72	0.208	0.036	101.5	0.202	0.035	105.3	0.97
73	0.189	0.033	122.6	0.226	0.040	89.2	1.19
74	0.223	0.039	104.8	0.214	0.037	112.9	0.96
75	0.235	0.041	96.8	0.234	0.041	98	0.99
μ	0.236	0.041	98.98	0.239	0.042	96.08	0.97
σ	0.02	0.004	4.09	0.018	0.003	6.81	0.06
E2 Dowel Bar Arrangement							
76	0.191	0.033	111.2	0.197	0.034	113.2	1.03
77	0.198	0.035	133.1	0.202	0.035	128	1.02
78	0.266	0.047	108.6	0.29	0.051	103.7	1.09
79	0.296	0.052	111.3	0.319	0.056	97.1	1.08
80	0.325	0.057	98.6	0.263	0.046	112.8	0.81
81	0.266	0.047	108	0.305	0.053	93	1.15
82	0.295	0.052	88.1	0.223	0.039	115.8	0.76
83	0.238	0.042	100.6	0.275	0.048	85.6	1.15
84	0.304	0.053	96.5	0.328	0.057	87.9	1.08
μ	0.29	0.051	95.95	0.304	0.053	93.46	1.12
σ	0.037	0.006	5.51	0.022	0.004	7.27	0.05

LTE=Load Transfer Efficiency

JSR=Joint Support Ratio

Averages (μ) and standard deviations (σ) include only slabs with LTE less than 105%

Table 12. I-490 East 50.3 kN FWD, Slabs 56-84, October 26, 2004

Joint Number	Joint Approach			Joint Leave			JSR
	Deflection ($\mu\text{m/kN}$)	(mil/kip)	LTE (%)	Deflection ($\mu\text{m/kN}$)	(mil/kip)	LTE (%)	
STD Dowel Bar Arrangement							
56	0.354	0.062	94.6	0.356	0.062	92.4	1.01
57	0.367	0.064	97.8	0.368	0.064	94.8	1
58	0.397	0.070	84.9	0.378	0.066	87.1	0.95
59	0.361	0.063	88.1	0.376	0.066	84.3	1.04
60	0.354	0.062	85.6	0.356	0.062	81.5	1.01
61	0.337	0.059	85.2	0.338	0.059	83.9	1
62	0.32	0.056	83.3	0.342	0.060	80.4	1.07
63	0.342	0.060	83.1	0.335	0.059	81	0.98
64	0.321	0.056	82.3	0.334	0.058	78.9	1.04
65	0.372	0.065	78.7	0.389	0.068	74.3	1.05
μ	0.353	0.062	86.34	0.357	0.063	83.86	1.01
σ	0.024	0.004	5.79	0.02	0.004	6.16	0.03
E1 Dowel Bar Arrangement							
66	0.328	0.057	94.8	0.358	0.063	76.2	1.09
67	0.317	0.056	84.2	0.329	0.058	80.3	1.04
68	0.343	0.060	82.5	0.346	0.061	79.3	1.01
69	0.317	0.056	82.1	0.319	0.056	80.4	1.01
70	0.338	0.059	76.5	0.313	0.055	79.7	0.93
71	0.301	0.053	97.7	0.301	0.053	78.5	1
72	0.307	0.054	76.7	0.309	0.054	76.8	1.01
73	0.283	0.050	94	0.274	0.048	85.1	0.97
74	0.336	0.059	91.2	0.286	0.050	88.5	0.85
75	0.303	0.053	83.1	0.3	0.053	84.8	0.99
μ	0.317	0.056	86.28	0.313	0.055	80.97	0.99
σ	0.019	0.003	7.61	0.026	0.005	3.93	0.06
E2 Dowel Bar Arrangement							
76	0.297	0.052	81.7	0.299	0.052	80.2	1
77	0.296	0.052	100	0.317	0.056	84.9	1.07
78	0.366	0.064	91.3	0.391	0.068	83.7	1.07
79	0.394	0.069	89.9	0.384	0.067	88.5	0.97
80	0.396	0.069	84.2	0.373	0.065	87.2	0.94
81	0.351	0.061	89	0.366	0.064	84.5	1.04
82	0.341	0.060	85	0.335	0.059	83.7	0.98
83	0.33	0.058	83.5	0.328	0.057	83.4	0.99
84	0.375	0.066	87	0.371	0.065	87.2	0.99
μ	0.35	0.061	87.96	0.351	0.061	84.82	1.01
σ	0.037	0.006	5.52	0.033	0.006	2.51	0.04

LTE=Load Transfer Efficiency

JSR=Joint Support Ratio

Averages (μ) and standard deviations (σ) include only slabs with LTE less than 105%

5 Conclusions

5.1 PCC Pavement Response Conclusions

A significant component of the loss of support observed in this pavement is built-in curling. When pavement is placed in hot weather a positive built-in temperature gradient develops. As a result, significant upward deflections of the pavement corners may develop as early as the second day after placement. This leads to the development of tensile stresses in the top of the pavement, which themselves generally do not contribute to pavement deterioration. However, the resulting loss of support may lead to top-down cracking in the pavement when a heavy load, such as a truck, runs over the inadequately supported area, providing additional tensile stress. The observed loss of support due to built-in curling is so significant that even with the most favorable temperature gradients observed, the pavement will not come into complete contact with the base.

The loss of support measurements based on the LVDTs at selected temperature gradients were validated by the FWD measurements. Where the LVDTs indicated significant loss of support, the FWD measured a large deflection. The deflection due to load, such as that measured from the FWD, was significantly smaller than that resulting from environmental factors. A realistic and rational design approach for rigid pavement must account for the environmental factors that cause warping and curling and the resulting loss of support. Furthermore, the design approach must also address the causes of top-down cracking.

5.2 Dowel Bar Arrangement Conclusions

Throughout the testing period it was found that the STD slabs, with the largest dowel bar diameter, widest spacing, and greatest cross-sectional area of steel throughout one-third of the slab width, exhibited the greatest amount of warping and curling. In contrast, the E2 slabs with the smallest dowel bar diameter, narrowest spacing, and least amount of steel throughout one-third of the slab cross section, warped and curled the least.

When the pavement temperature gradient was negative the LTE varied more among the various dowel bar configurations. The E2 sections typically had the highest LTE with the negative gradient present and also experienced the least deflection. This followed the general trend found throughout the testing period that the slabs with higher LTE performance generally deflected less. The E1 sections deflected less and had higher LTEs than the STD sections for slabs 1 through 25. However, for slabs 26 through 55 the STD sections slightly outperformed the E1 sections. Overall the E2 sections exhibited superior performance with the least curl and deflection as well as the highest LTEs.

After the air temperature rose and the pavement temperature gradient became positive, the LTEs for all dowel bar arrangements became less varied, though again E2 had the highest LTEs. When the pavement was in this state, the E1 sections deflected the least, followed by the E2 sections and finally the STD sections. Pavement performance in this state is not as critical as during the negative temperature gradient because the slab experiences less loss of support. Under higher temperatures, the slabs expand and at the joints there is aggregate interlock, which assists with the load transfer.

One could conclude that dowel bars play a key role in controlling the loss of support as well as assisting in load transfer. This research suggests that the E2 configuration will perform better and result in better slab support than the STD configuration.

5.3 Implementation

New York should design rigid pavements taking into account the mechanisms causing loss of support and top-down cracking. The resulting design process can then be validated via the Mechanistic-Empirical design process. A number of smaller equally-spaced dowel bars, such as the E2 configuration, should result in improved performance of rigid pavements.

6 References

- Armaghani, J.M., Larsen, T.J., & Smith, L.L., (1986). "Temperature Response of Concrete Pavements". *Transportation Research Record*, 1121, 23-33.
- Bradbury, R.D. (1933). "Design of Joints in Concrete Pavement. *Proceedings of the 12th Annual Meeting - Highway Research Board*, Washington DC, 105-141.
- Choubane, B., and Tia, M. (1986). "Analysis and Verification of Thermal-Gradient Effects on Concrete Pavement". *Journal of Transportation Engineering*, 121, 75-81.
- Friberg, B.F. (1938). "Design of Dowels in Transverse Joints in Concrete Pavement". *Proceedings of the American Society of Civil Engineers*, 64,1809-1828.
- Heinrich, K.W., Liu, M.J., Darter, M.I., Carpenter, S.H., and Ioannides, A.M. (1989). *Rigid Pavement Analysis and Design*, Report No. FHWA-RD-88-068, Federal Highway Administration.
- Huang, Y.H. (2004). *Pavement Analysis and Design* (2nd ed.). Upper Saddle River, NJ: Pearson Prentice Hall.
- Hveem, F.N., and Tremper, B. (1957). "Some Factors Influencing Shrinkage of Concrete Pavements". *Journal of the American Concrete Institute*, 28, 781-789.
- Jeong, J.H., and Zollinger, D. G. (2003). "Development of a Test Methodology and Model for Evaluation of Curing Effectiveness in Concrete Pavement Construction". *Transportation Research Record*, Vol. 1861, p. 17.
- Jeong, J.H., and Zollinger, D. G. (2004). "Insights on Early-Age Curling and Warping Behavior for a Fully Instrumented Test Slab System". *Transportation Research Record*, Vol. 1896, p. 66.
- Owusu-Anti, E.B., Meyer, A.H., and Hudson, W.R. (1990). *Assessing Load Transfer Across Joints and Cracks in Rigid Pavements Using the Falling Weight Deflectometer*. Austin: Center for Transportation Research, Bureau of Engineering Research, University of Texas at Austin.
- Portland Cement Association. (1975). *Joint Design for Concrete Highway and Street Pavements*. Portland Cement Association.
- Rollings, R.S., and Pittman, D.W. (1992). "Field Instrumentation and Performance Monitoring of Rigid Pavements". *Journal of Transportation Engineering*, 118, 361-369.
- Sargand, S. (1998). "Measurement of Dowel Bar Response in Rigid Pavement". Technical Note ORITE-1. Ohio Department of Transportation. Columbus, OH.

- Sargand, S. (2001). *Performance of Dowel Bars and Rigid Pavement*. Final report for U.S. Department of Transportation and Federal Highway Administration. Athens, OH: Ohio Research Institute for Transportation and the Environment.
- Sargand, S. (2004). *Evaluation of HPC Pavement in Nelsonville, Ohio*. Final report for U.S. Department of Transportation and Federal Highway Administration. Athens, OH: Ohio Research Institute for Transportation and the Environment.
- Sargand, S., and Abdalla, B. (2006). *Truck/Pavement/Economic Modeling and In-Situ Field Test Data Analysis Applications – Volume 2: Verificiation and Validation of Finite Element Models for Rigid Pavement Using In-Situ Data – Selection of Joint Spacing*. Final report for U.S. Department of Transportation and Federal Highway Administration. Athens, OH: Ohio Research Institute for Transportation and the Environment.
- Sargand, S., and Cindar, E. (1997). *Field Instrumentation of Dowels*. Final report for U.S. Department of Transportation and Federal Highway Administration. Athens, OH: Ohio Research Institute for Transportation and the Environment.
- Sargand, S., Edwards, W., and Khoury, I. (2003). *Evaluation of Forces in Dowel Bars Under Controlled Conditions*. Final report for U.S. Department of Transportation and Federal Highway Administration. Athens, OH: Ohio Research Institute for Transportation and the Environment.
- Smith, G.L. (1922). “Six Construction Mistakes in One Concrete Road”. *Engineering News-Record*, 88 (9), 357-358.
- Tabatabaie, A.M., and Barenberg, E.J. (1980). “Structural Analysis of Concrete Pavement Systems”. *Transportation Engineering Journal*, TE5, 493-506.
- Teller, L.W., and Cashell, H.D. (1958). “Performance of Doweled Joints under Repetitive Loading”. *Public Roads*, 30 (1), 1-24.
- Teller, L.W., and Sutherland, E.C. (1936). “The Structural Design of Concrete Pavements: A Study of the Structural Action of Several Types of Transverse and Longitudinal Joint Designs”. *Public Roads*, 17 (7), 143-171, 175-192.
- Timoshenko, S., and Lessels, J.M. (1925). *Applied Elasticity*. Pittsburgh, PA: Westinghouse Technical Night School Press.
- Westergaard, H.M. (1928). Spacing of dowels. *Proceedings of the Annual Meeting - Highway Research Board*, Washington DC, 154-158.
- Wise, J. (2004). *Environmental Effects on Portland Cement Concrete*. Ohio University Masters thesis.
- Yoder, E.J. (1959). *Principles of Pavement Design*. New York: John Wiley & Sons.

Appendix A: I-490 West Data June 2002

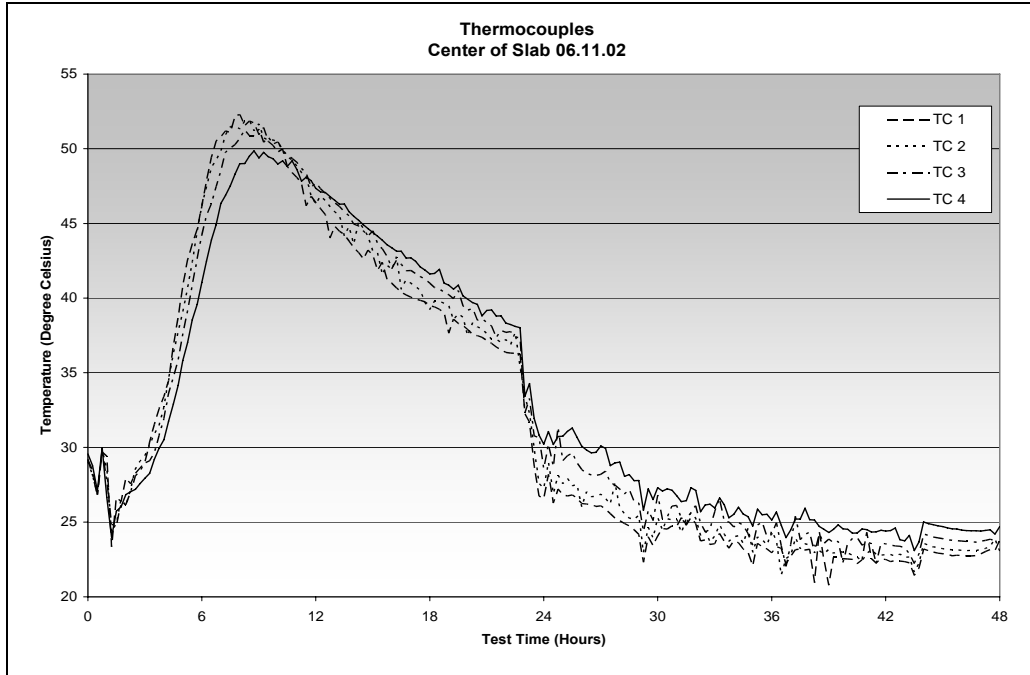


Figure A.1. I-490 Thermocouple readings, center of slab, June 11, 2002 (Temperature range 68°F to 131°F)

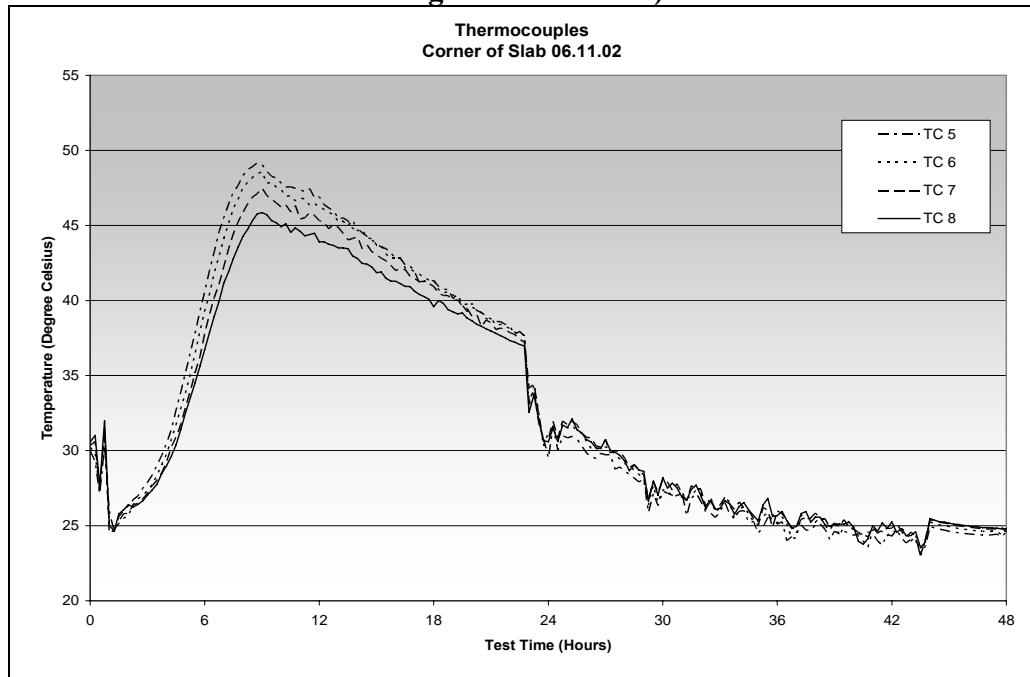


Figure A.2. Thermocouple readings, corner of slab, June 11, 2002 (Temperature range 68°F to 131°F)

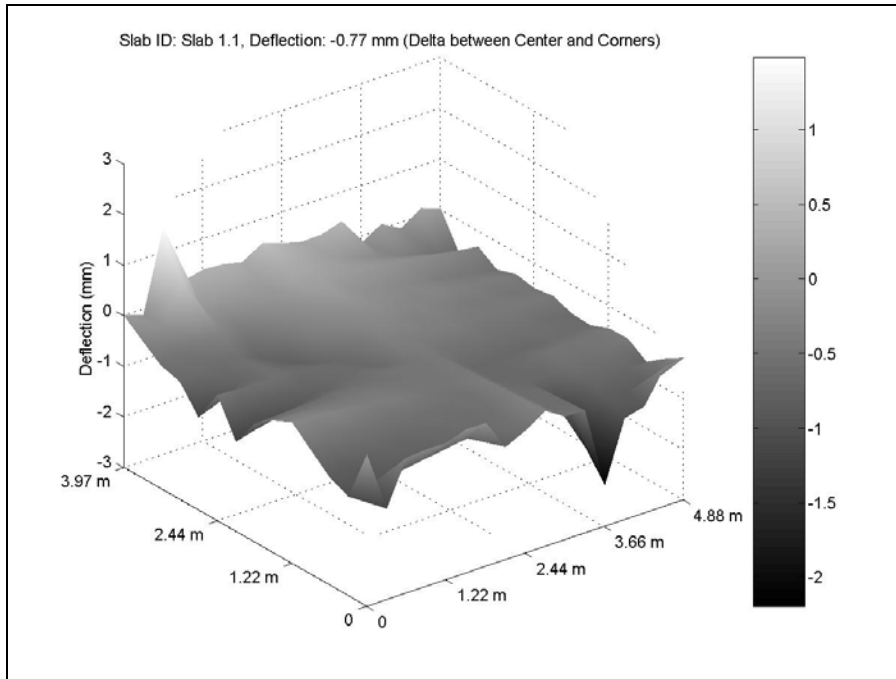


Figure A.3. Slab 1 profile at 7 pm, June 11, 2002, referenced before joints were sawcut (1m=3.28 ft; 1 mm=39 mil)

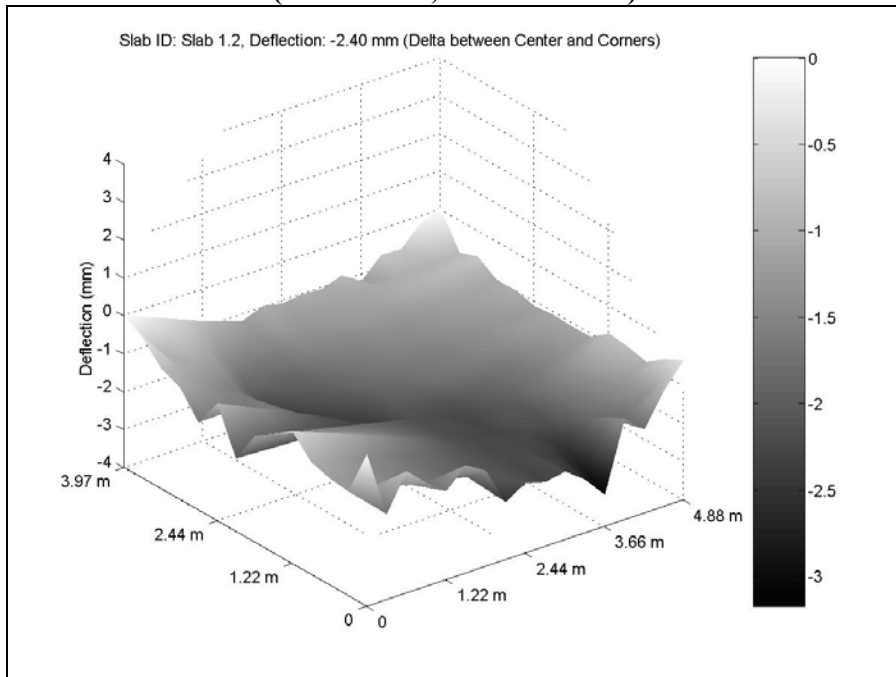


Figure A.4. Slab 1 profile at 3 pm, June 12, 2002, referenced before joints were sawcut (1m=3.28 ft; 1 mm=39 mil)

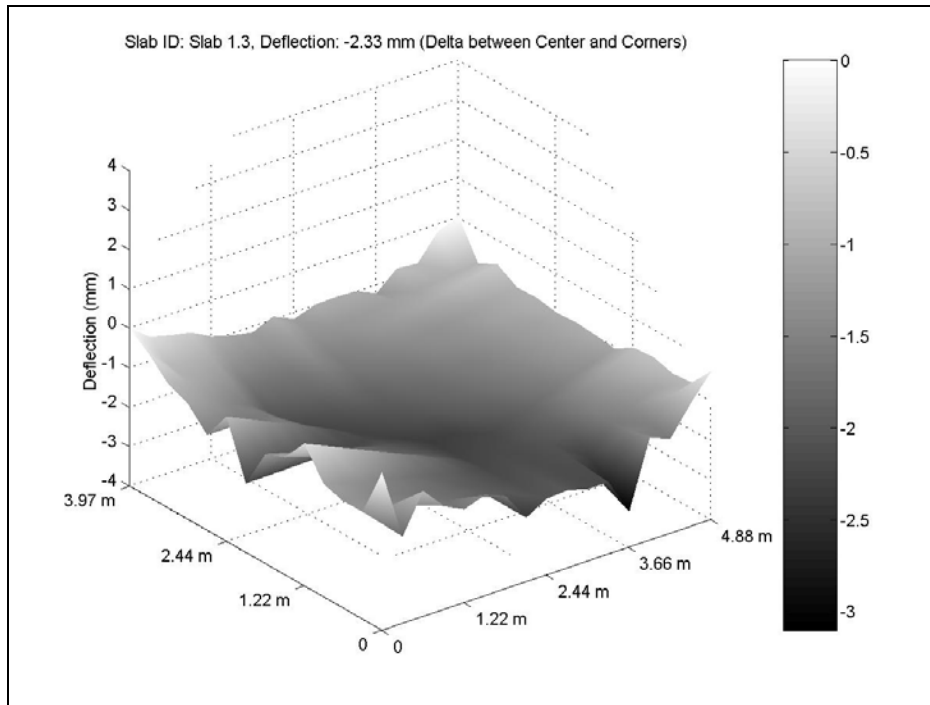


Figure A.5. Slab 1 profile at 9 am, June 13, 2002, referenced before joints were sawcut (1m=3.28 ft; 1 mm=39 mil)

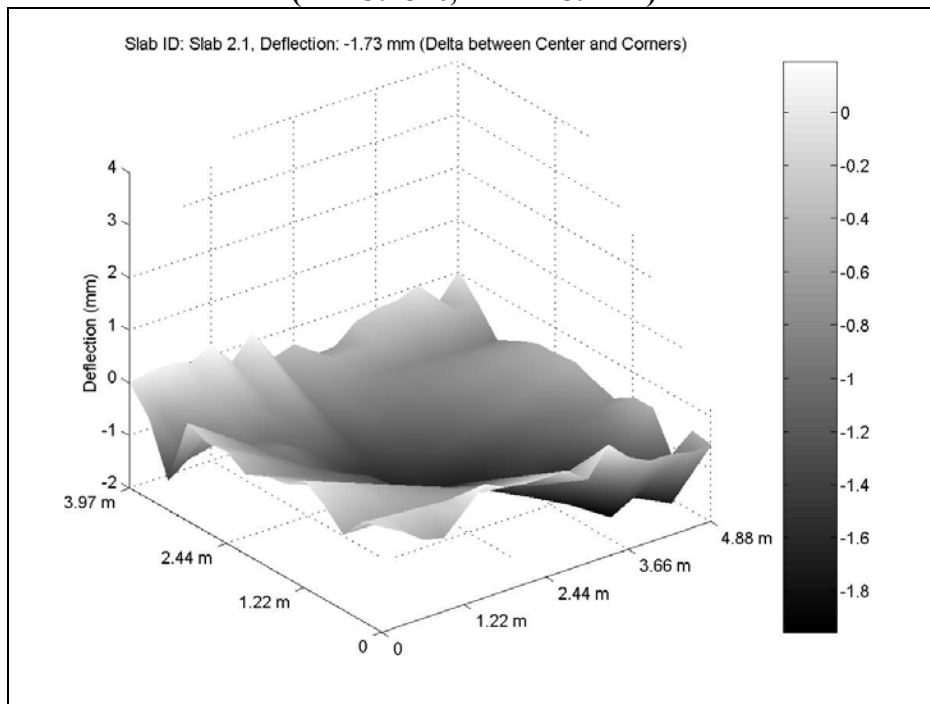


Figure A.6. Slab 2 profile at 7 pm, June 11, 2002, referenced before joints were sawcut (1m=3.28 ft; 1 mm=39 mil)

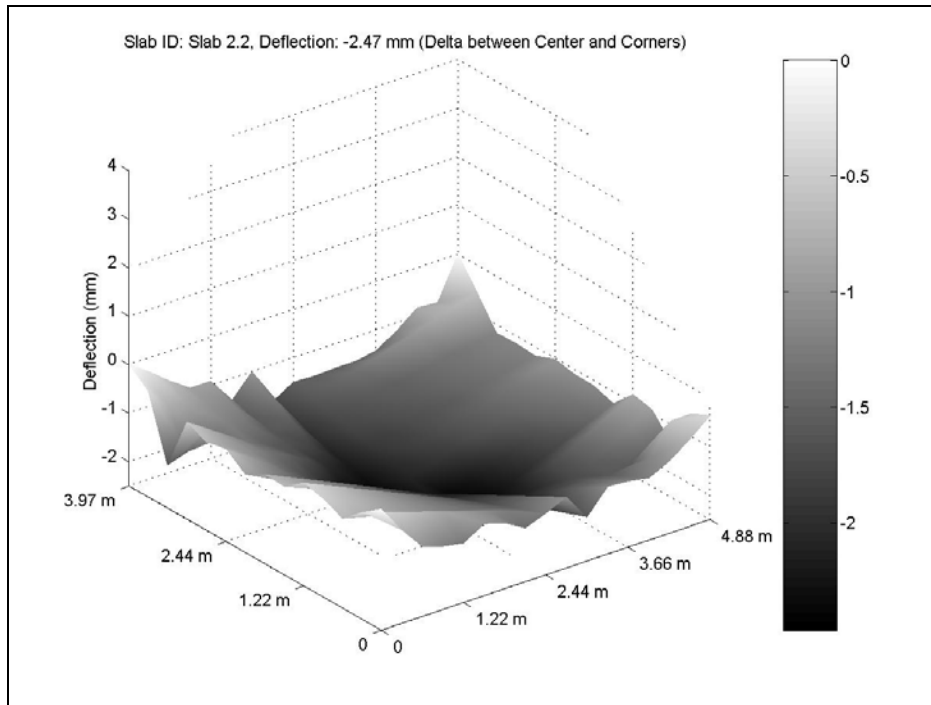


Figure A.7. Slab 2 profile at 3 pm, June 12, 2002, referenced before joints were sawcut (1m=3.28 ft; 1 mm=39 mil)

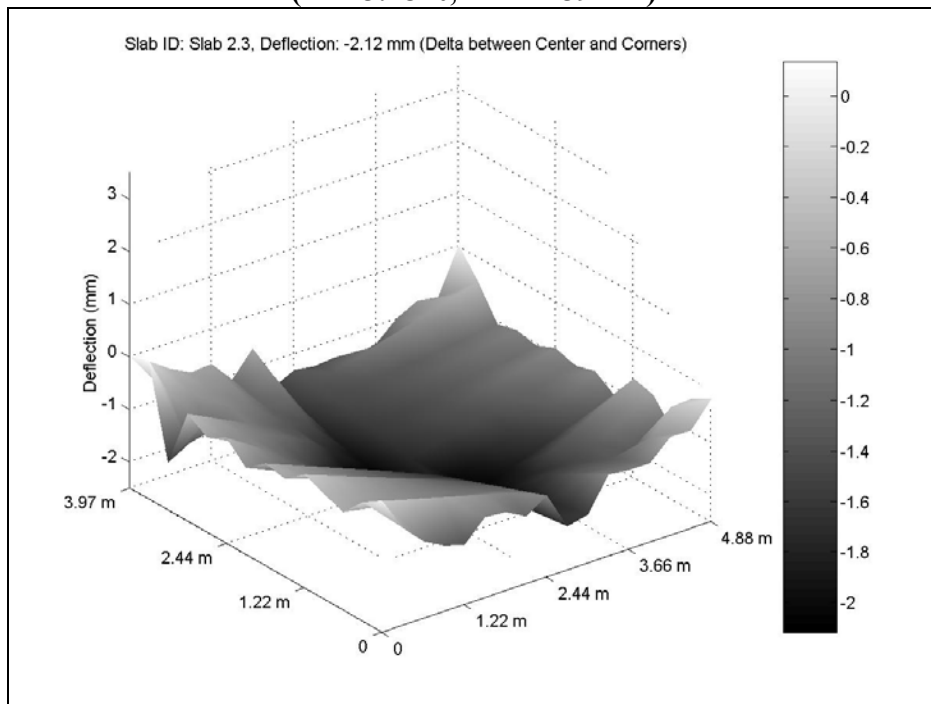


Figure A.8. Slab 2 profile at 9 am, June 13, 2002, referenced before joints were sawcut (1m=3.28 ft; 1 mm=39 mil)

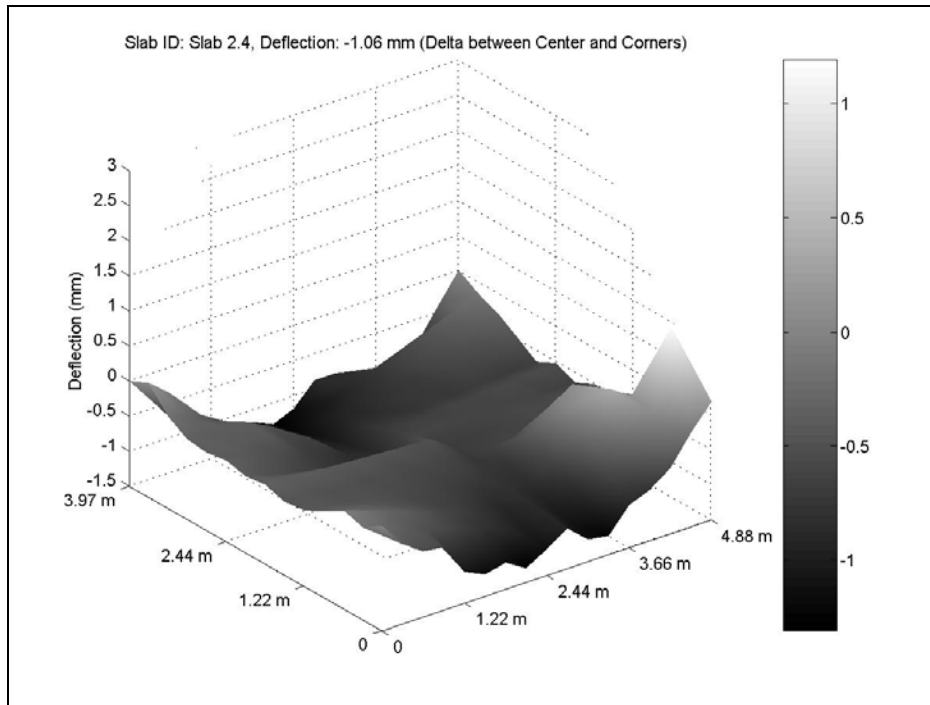


Figure A.9. Slab 2 profile at 3 pm, June 12, 2002, referenced after joints were sawcut (1m=3.28 ft; 1 mm=39 mil)

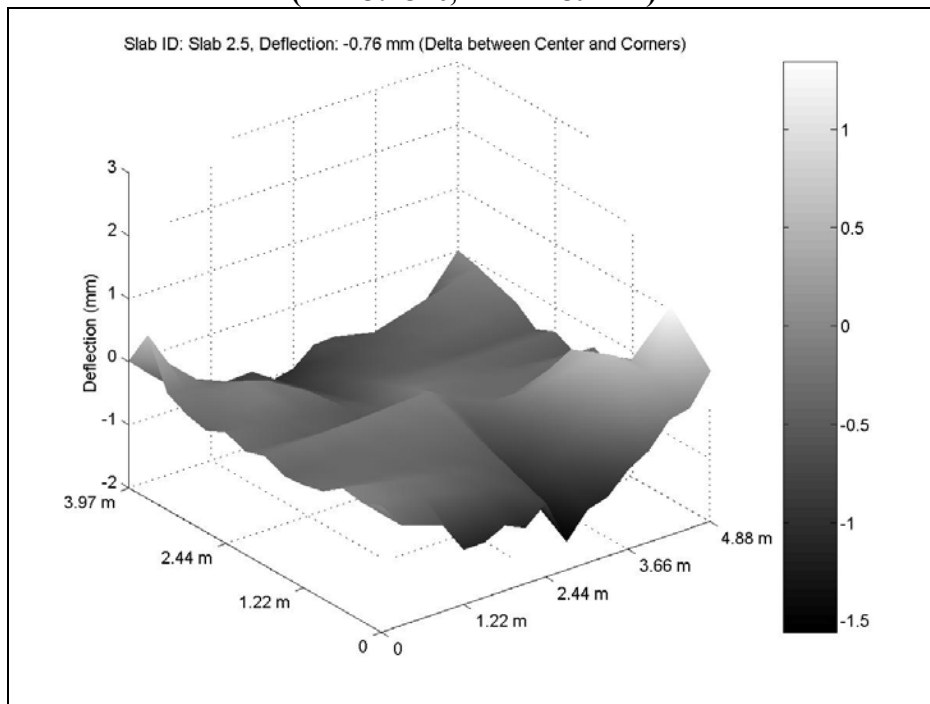


Figure A.10. Slab 2 profile at 9 am, June 13, 2002, referenced after joints were sawcut (1m=3.28 ft; 1 mm=39 mil)

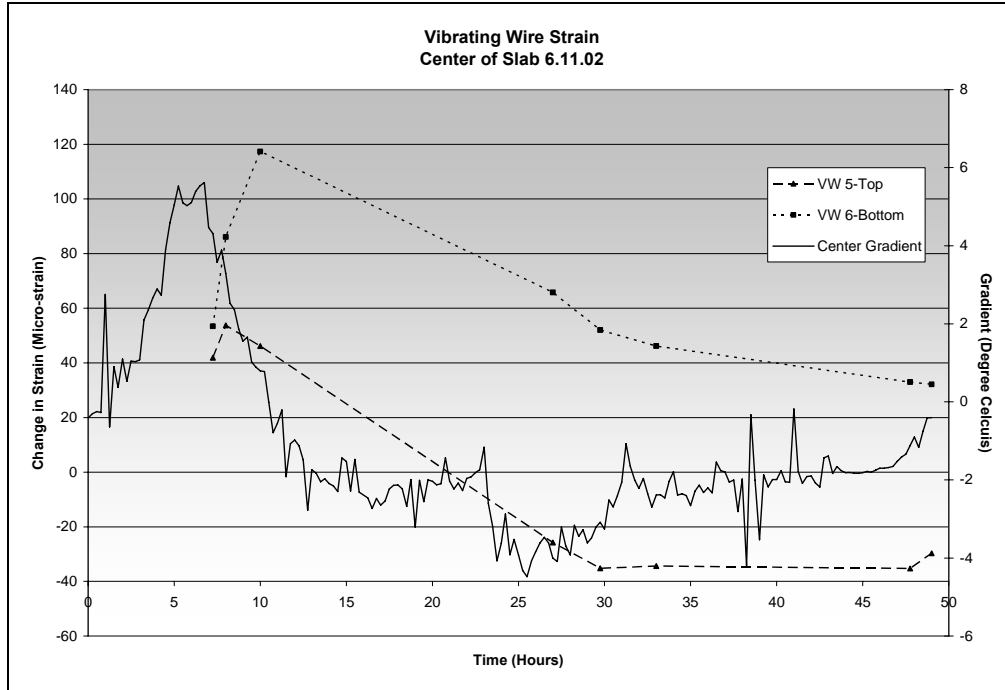


Figure A.11. Vibrating wire strain, center of slab, June 11, 2002 (5C°=9°F)

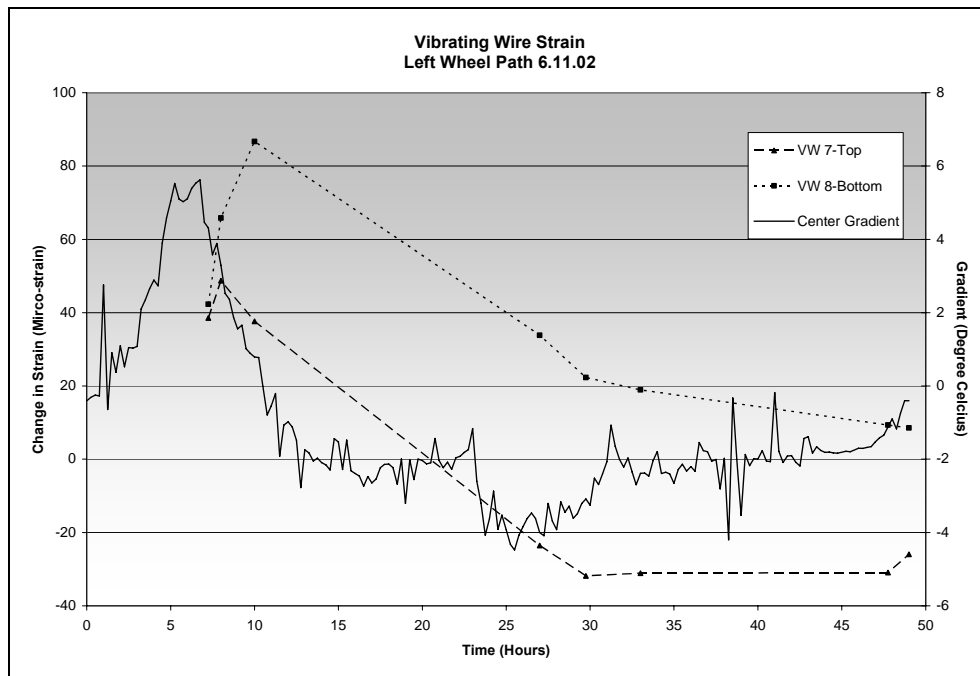


Figure A.12. Vibrating wire strain, left wheel path, June 11, 2002 (5C°=9°F)

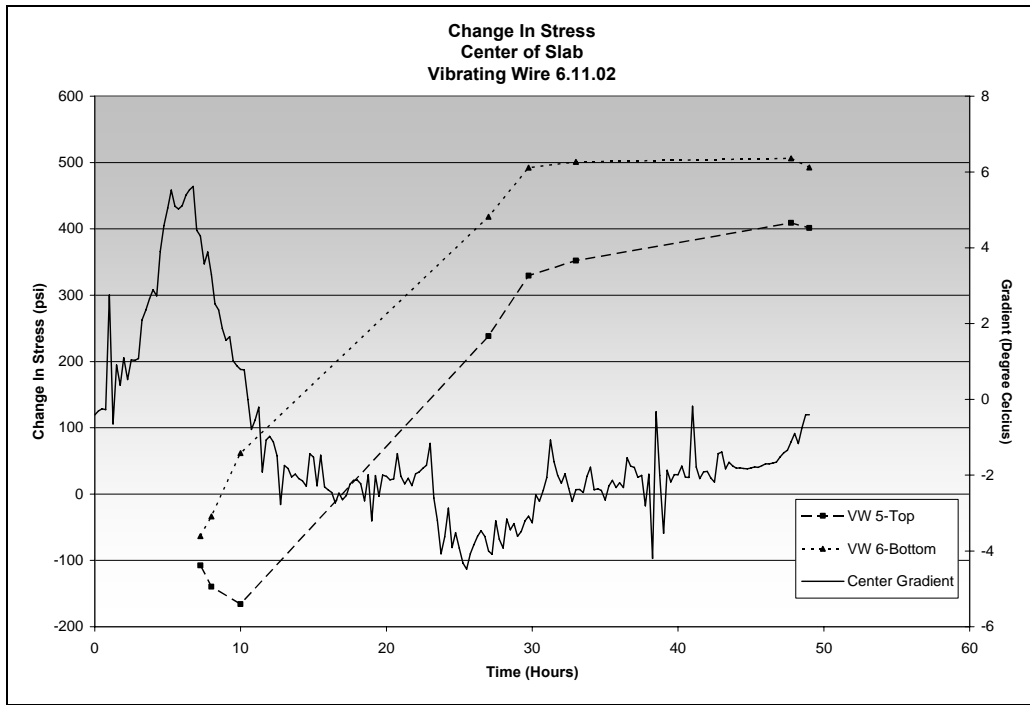


Figure A.13. Vibrating wire stress, center of slab, June 11, 2002 (1 psi = 6.89 Pa, 5C°=9°F)

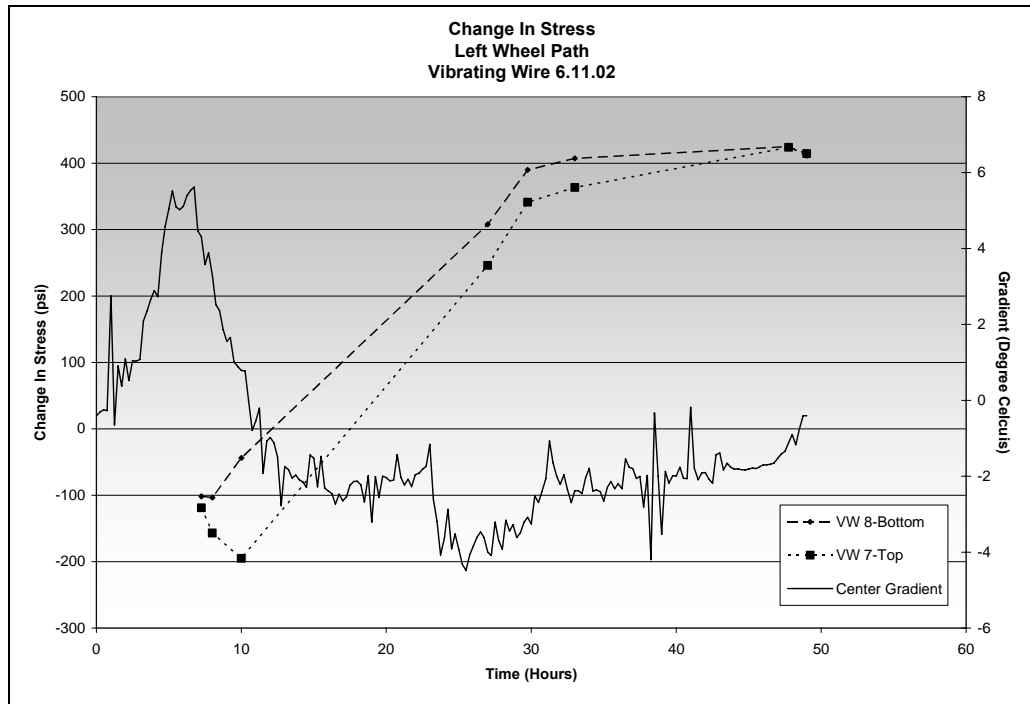


Figure A.14. Vibrating wire stress, left wheel path, June 11, 2002 (1 psi = 6.89 Pa, 5C°=9°F)

Appendix B: I-490 West Data July 2002

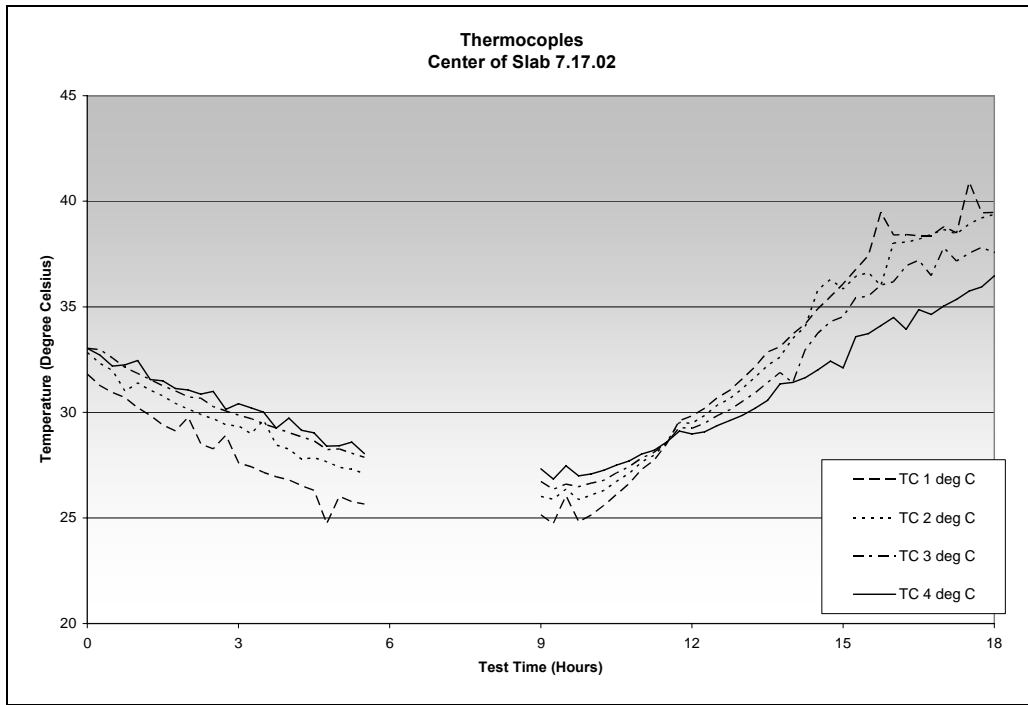


Figure B.1. I-490 thermocouple readings, center of slab, July 17, 2002 (Temperature range 68°F to 113°F)

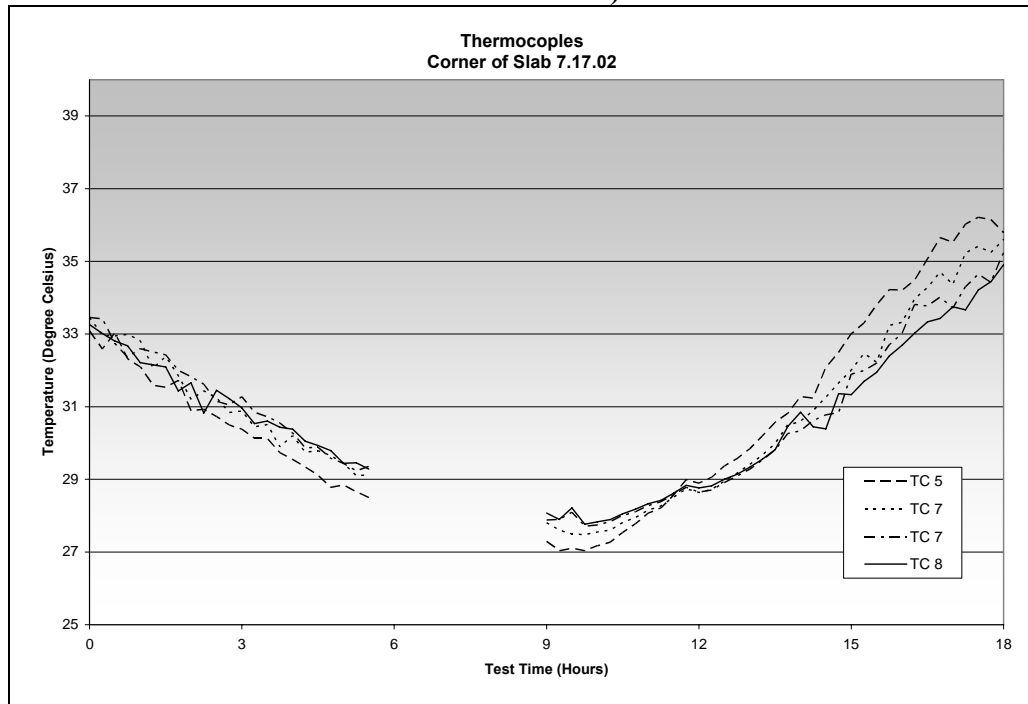


Figure B.2. I-490 thermocouple readings, corner of slab, July 17, 2002 (Temperature range 77°F to 104°F)

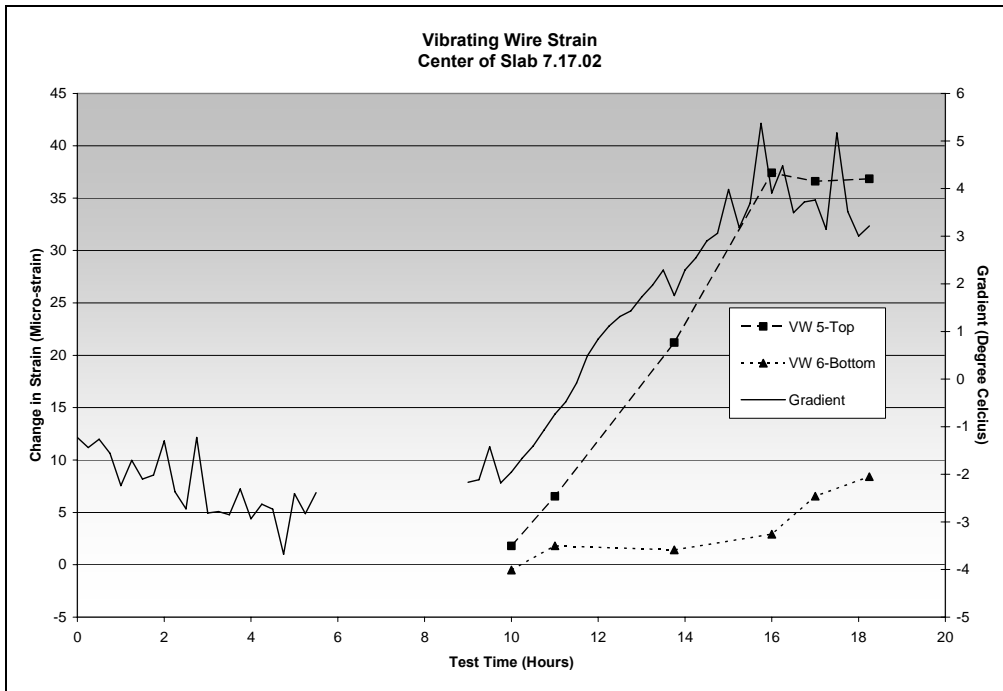


Figure B.3. Vibrating wire strain, center of slab, July 17, 2002 (5C°=9°F)

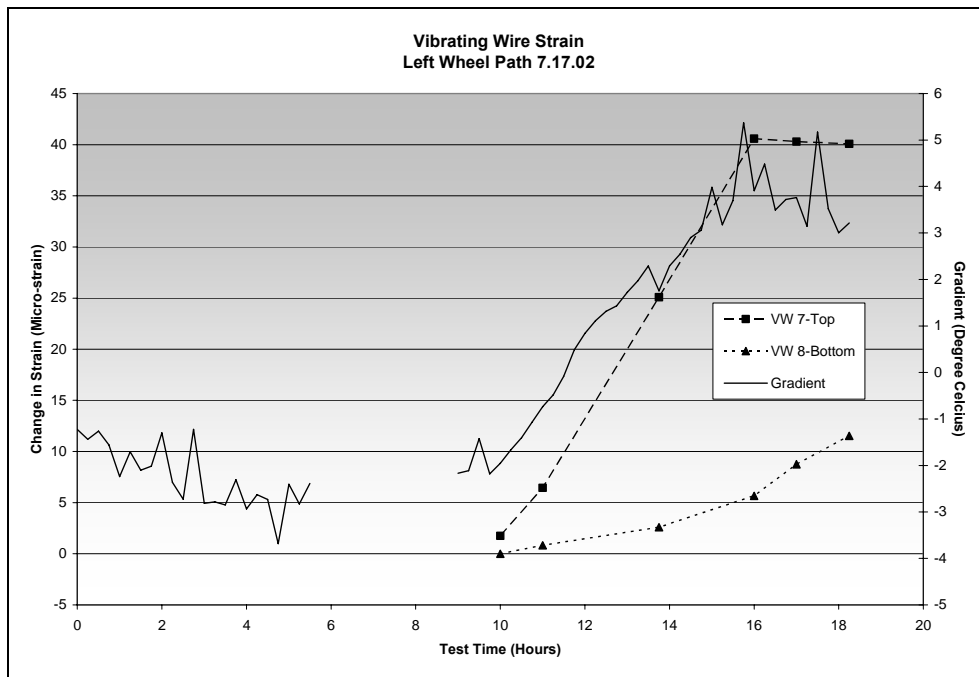


Figure B.4. Vibrating wire strain, left wheel path, July 17, 2002 (5C°=9°F)

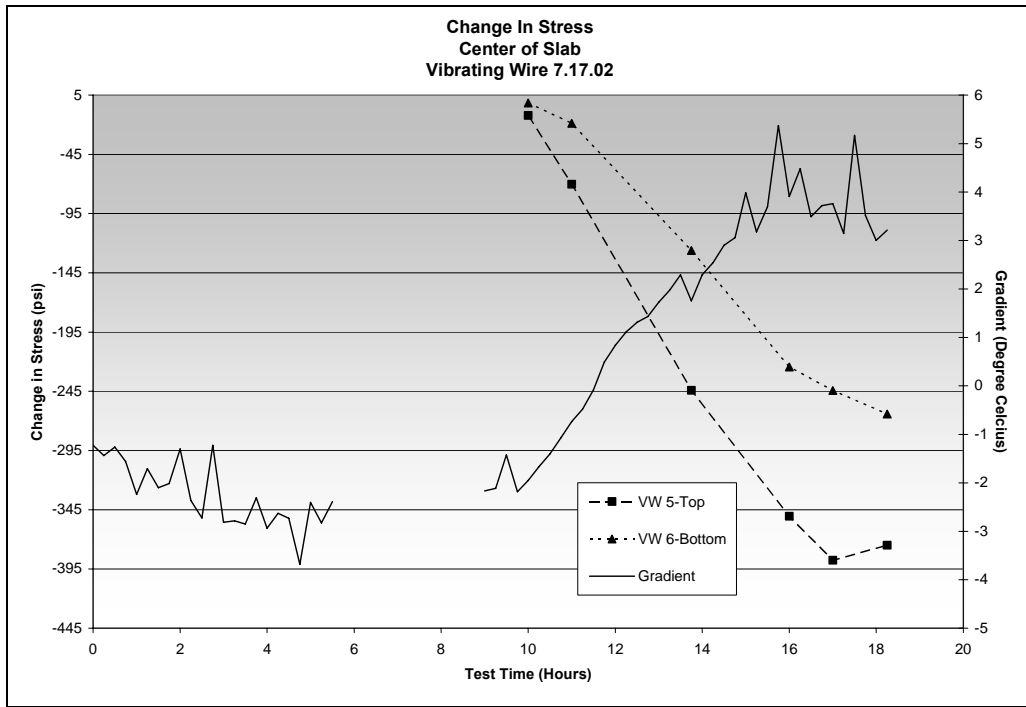


Figure B.5. Vibrating wire stress, center of slab, July 17, 2002 (1 psi = 6.89 Pa, 5C°=9°F)

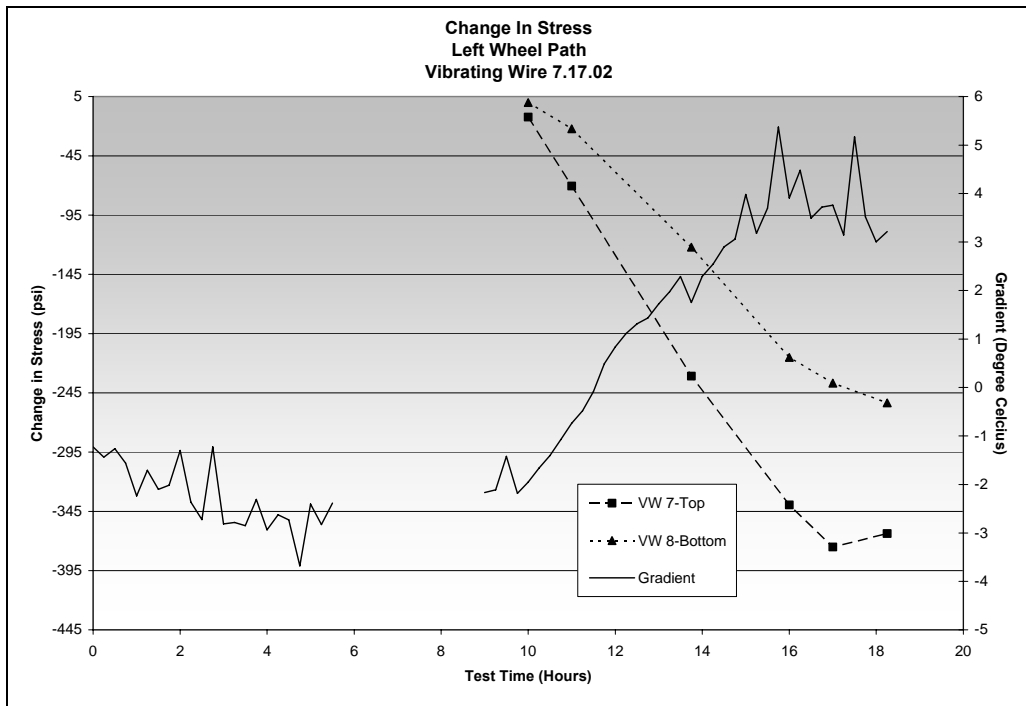


Figure B.6. Vibrating wire stress, left wheel path, July 17, 2002 (1 psi = 6.89 Pa, 5C°=9°F)

Appendix C: I-490 West Data June 2003

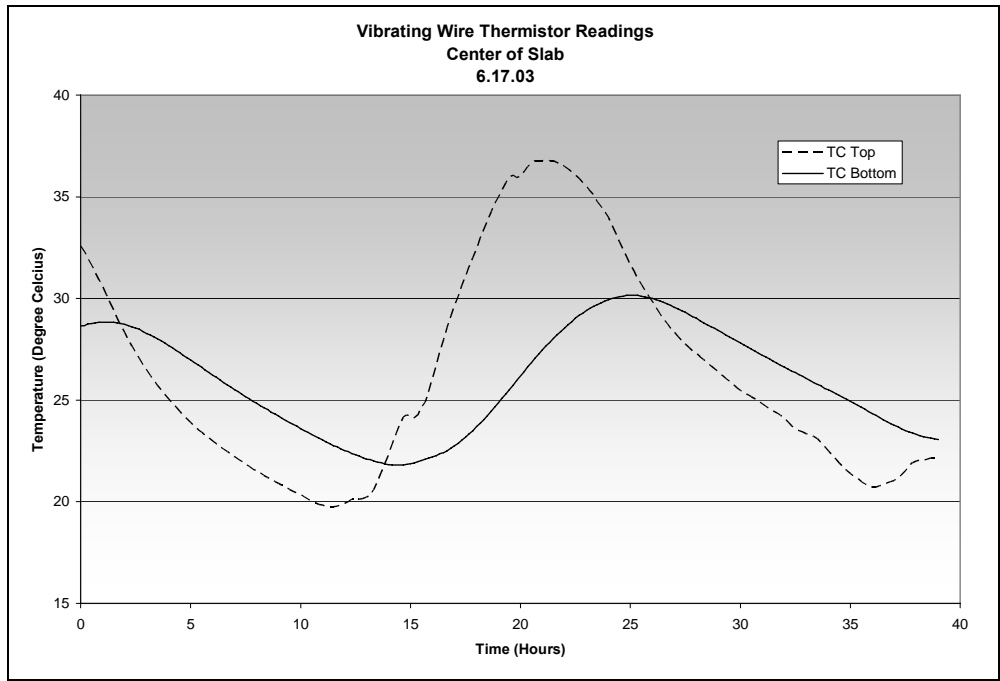


Figure C.1. I-490 vibrating wire thermistor readings, center of slab, June 17, 2003 (Temperature range 59°F to 104°F)

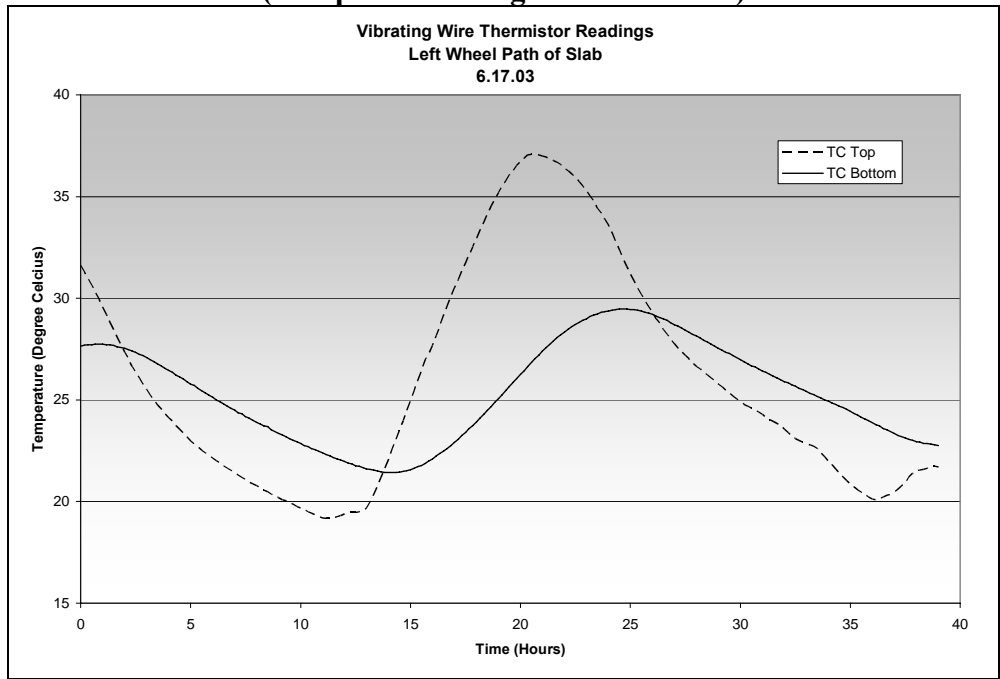
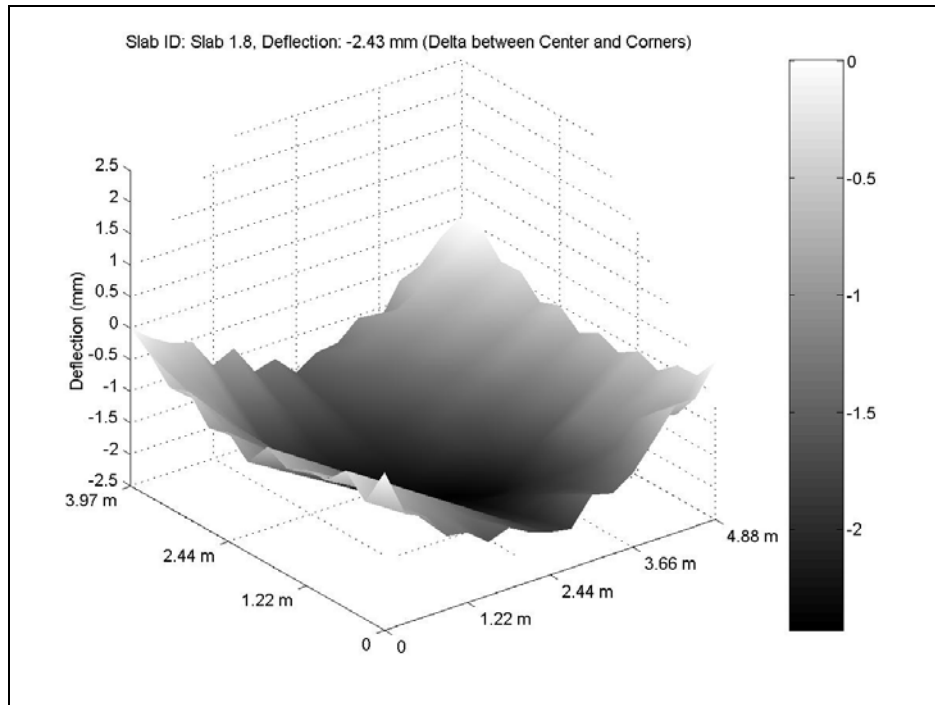
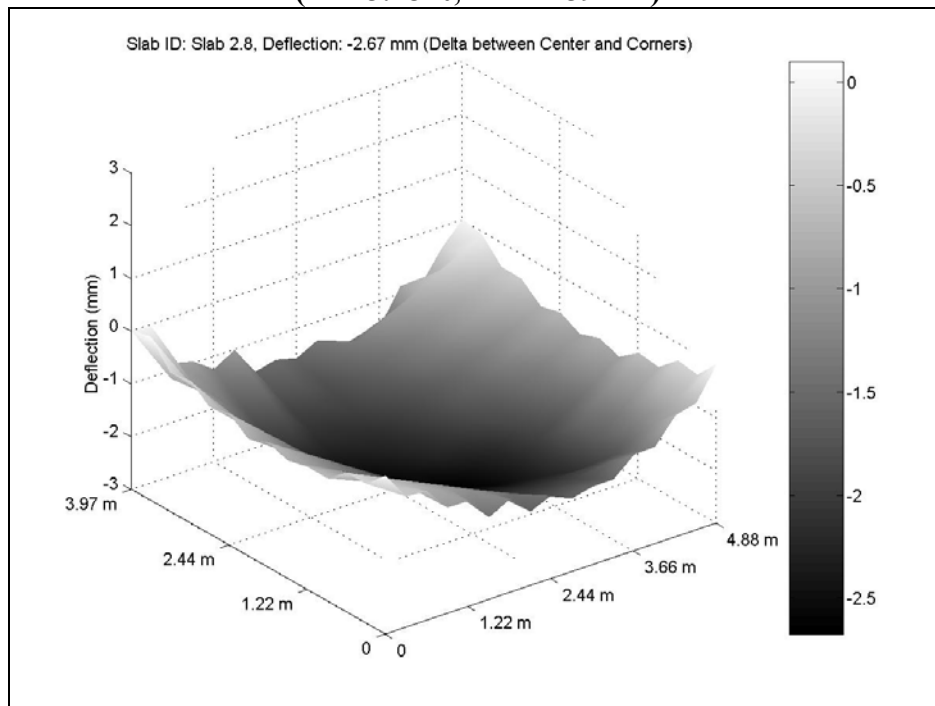


Figure C.2. I-490 vibrating wire thermistor readings, left wheel path, June 15, 2003 (Temperature range 59°F to 104°F)



**Figure C.3. Slab 1 profile difference between extreme gradients, 8 am, June 18, 2003
(1m=3.28 ft; 1 mm=39 mil)**



**Figure C.4. Slab 2 profile difference between extreme gradients, 8 am, June 18, 2003
(1m=3.28 ft; 1 mm=39 mil)**

Appendix D: I-490 West Data October 2003

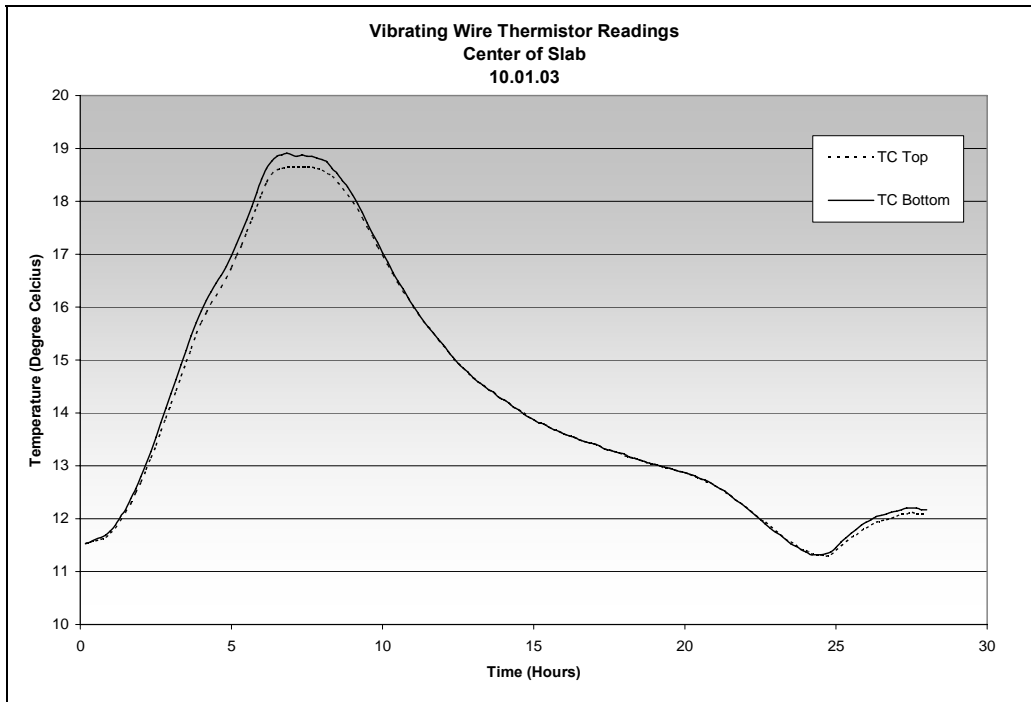


**Figure D.1. I-490 vibrating wire thermistor readings, center of slab, October 1, 2003
(Temperature range 50°F to 68°F)**

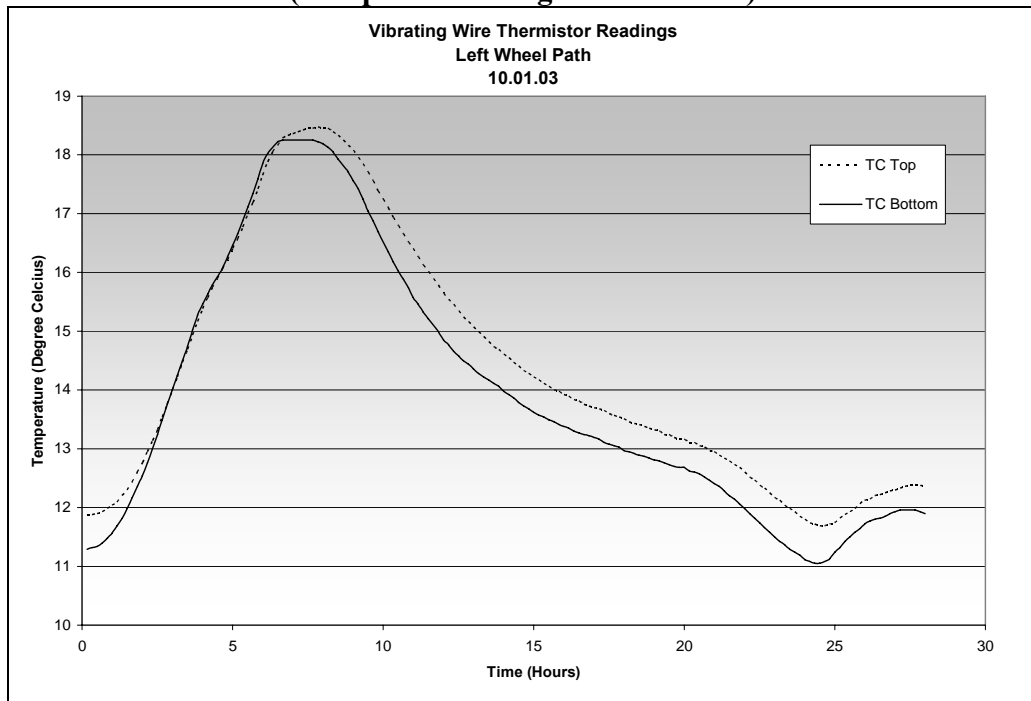


**Figure D.2. I-490 vibrating wire thermistor readings, left wheel path, October 1, 2003
(Temperature range 50°F to 66.2°F)**

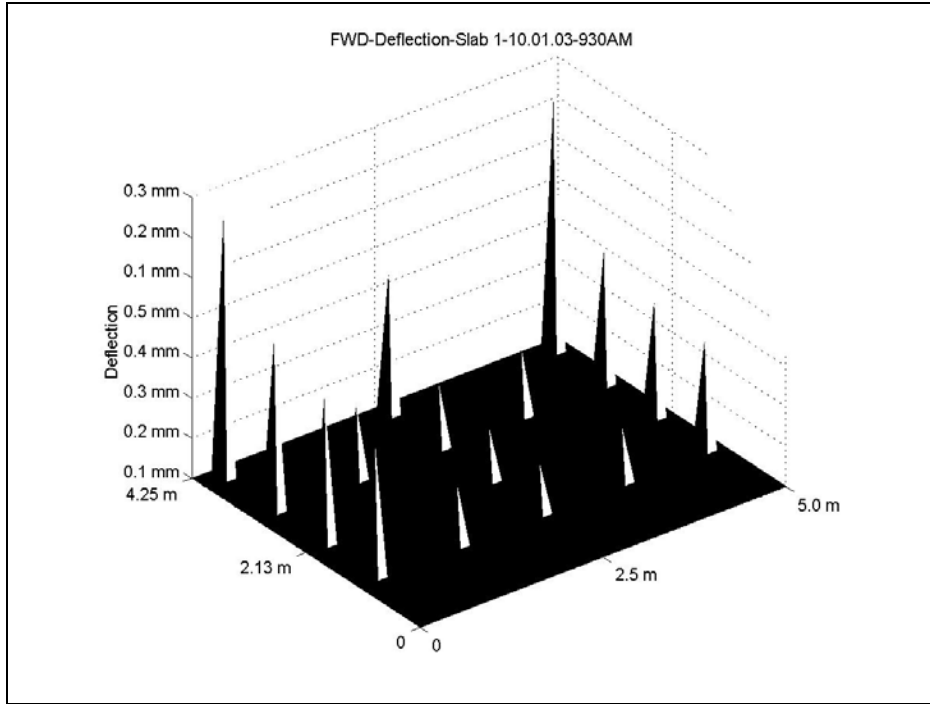


Figure D.3. Slab 1 deflection from FWD at 930 am, October 1, 2003 (1m=3.28 ft; 1 mm=39 mil)

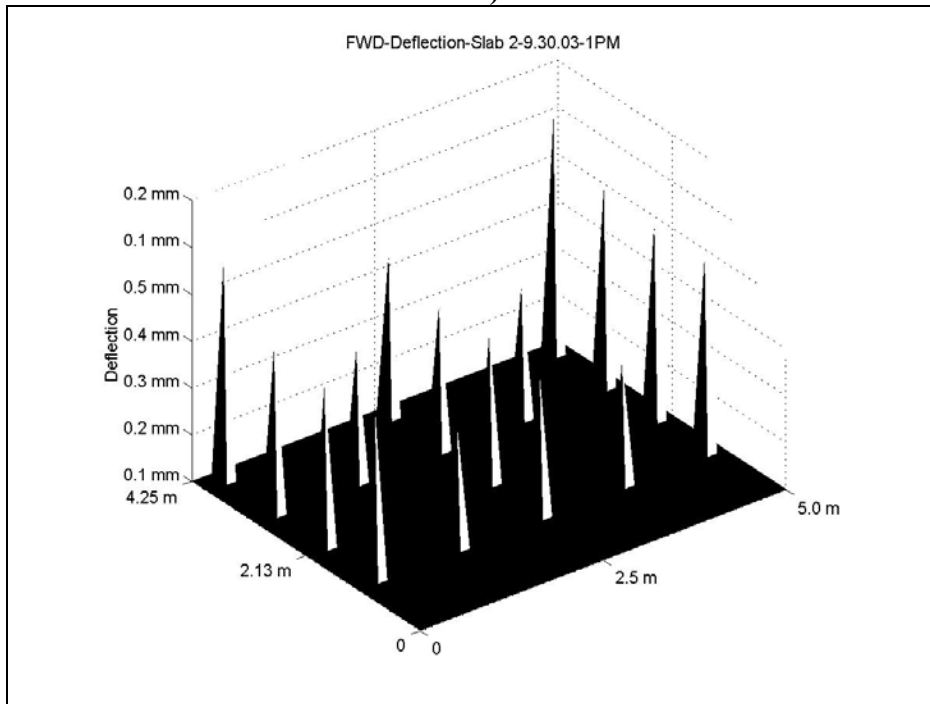


Figure D.4. Slab 2 deflection from FWD at 1 pm, September 30, 2003 (1m=3.28 ft; 1 mm=39 mil)

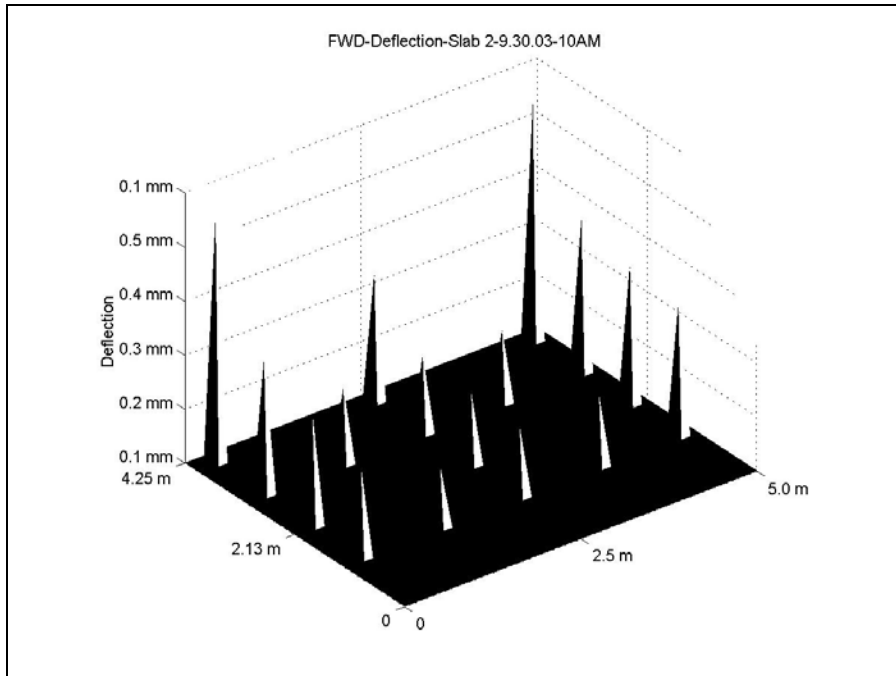


Figure D.5. Slab 2 deflection from FWD at 10 am, September 30, 2003 (1m=3.28 ft; 1 mm=39 mil)

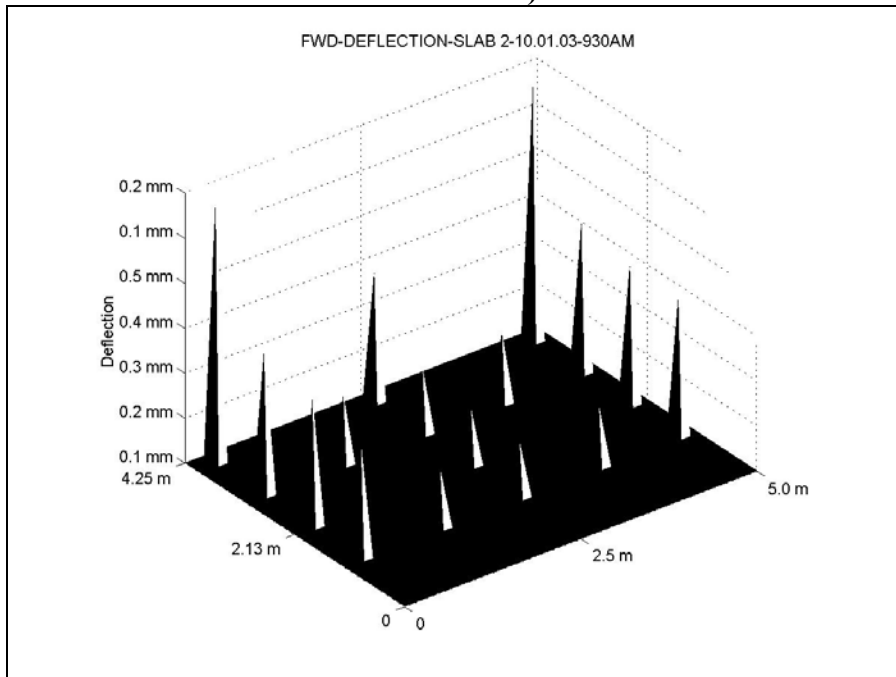


Figure D.6. Slab 2 deflection from FWD at 9:30 am, October 1, 2003 (1m=3.28 ft; 1 mm=39 mil)

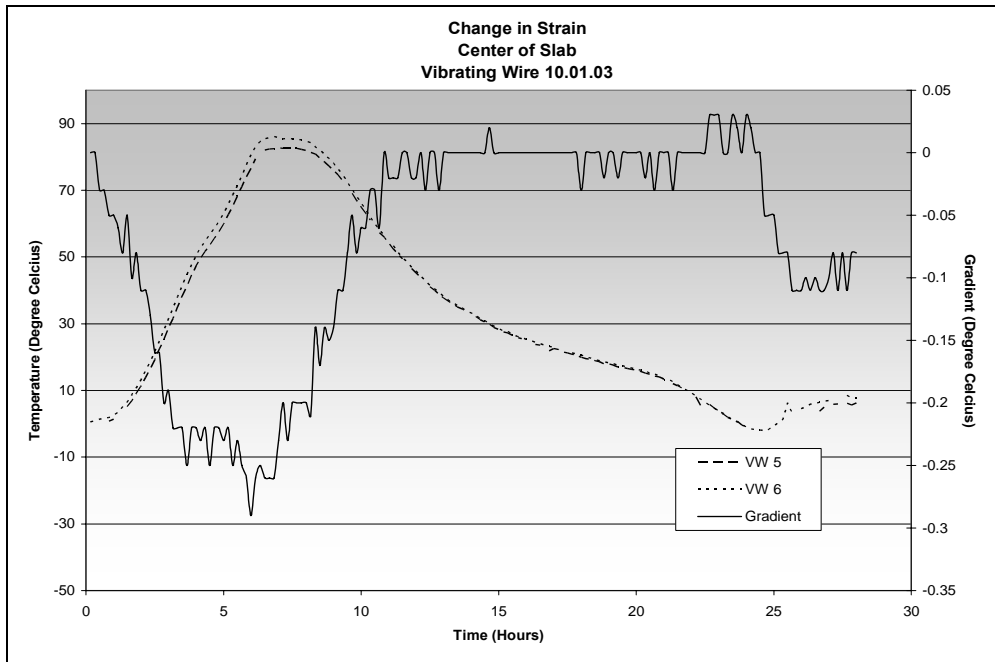


Figure D.7. Vibrating wire strain, center of slab, October 1, 2003 (5C°=9°F)

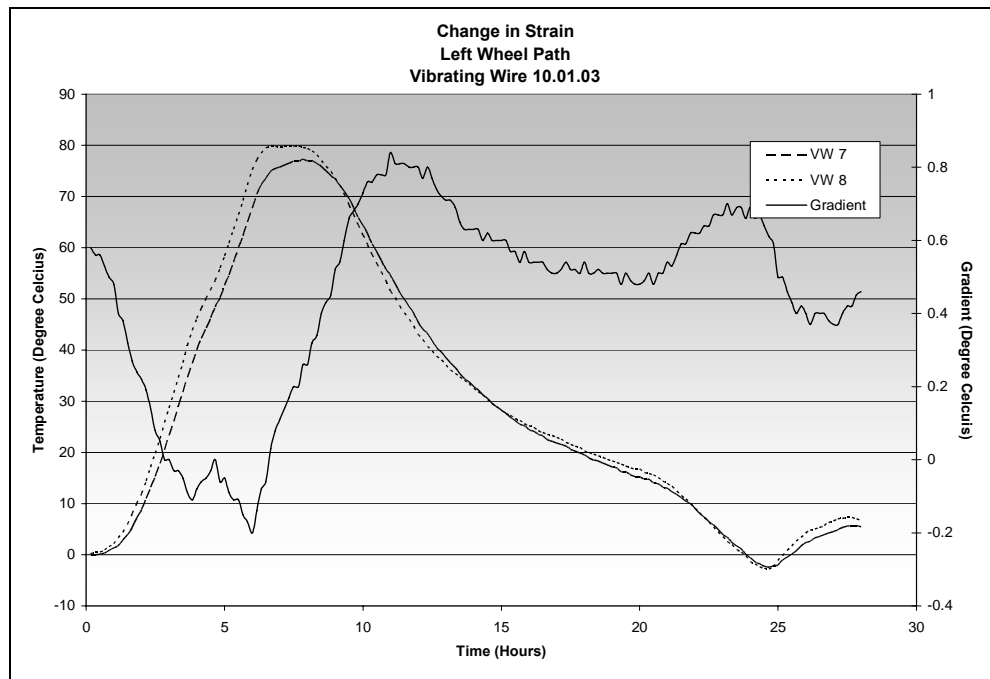


Figure D.8. Vibrating wire strain, left wheel path, October 1, 2003 (5C°=9°F)

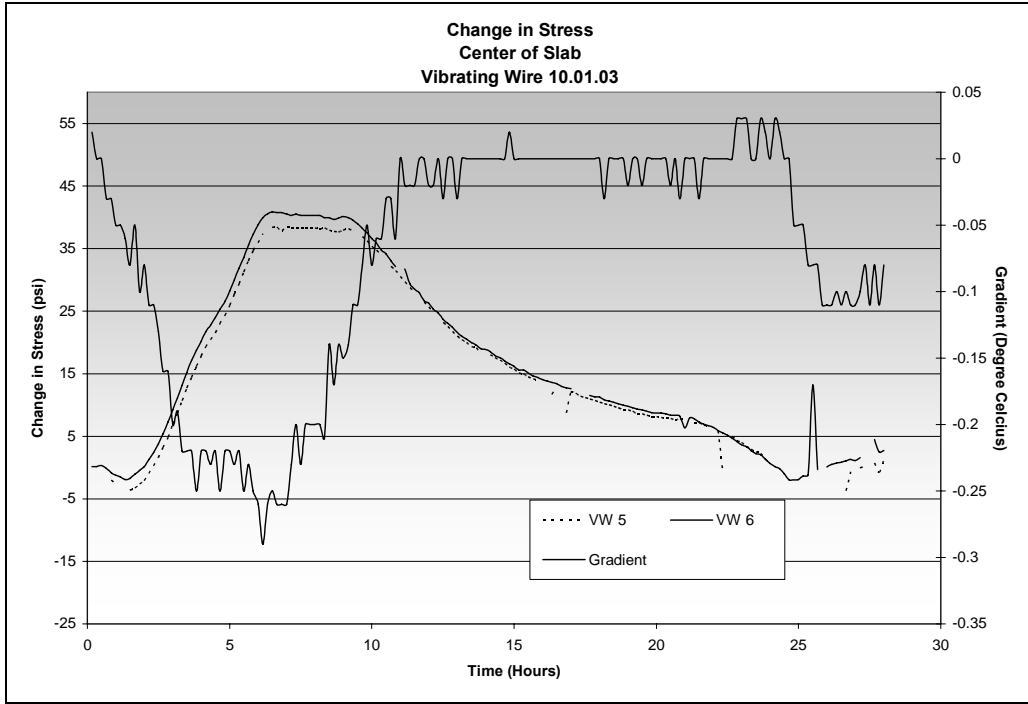


Figure D.9. Vibrating wire stress, center of slab, October 1, 2003 (1 psi = 6.89 Pa, 5C°=9°F)

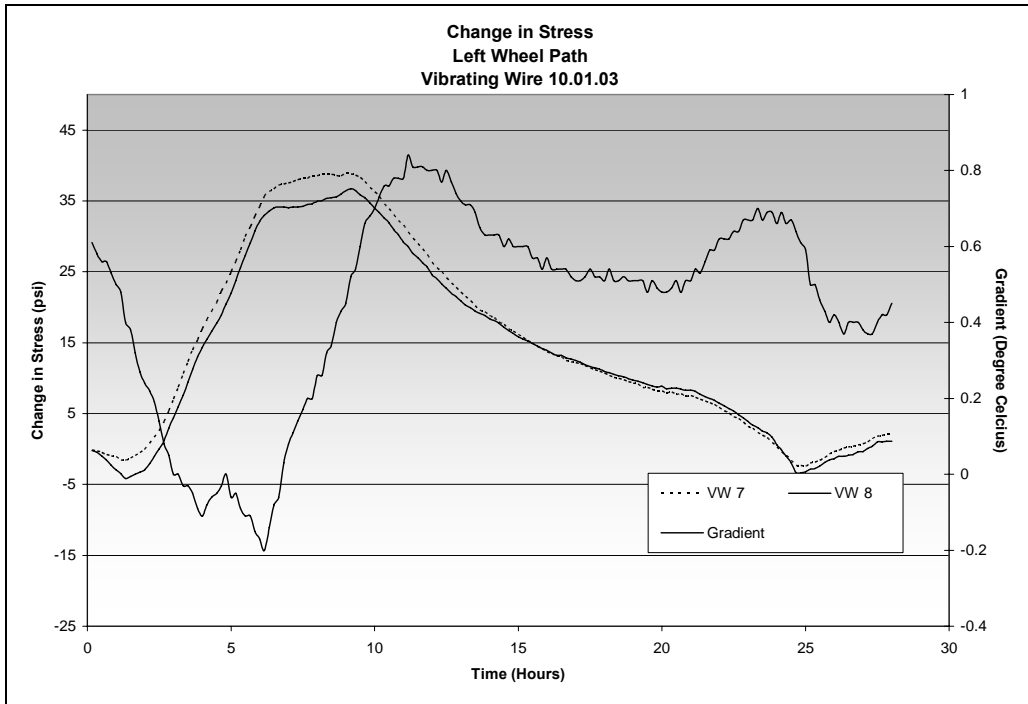


Figure D.10. Vibrating wire stress, left wheel path, October 1, 2003 (1 psi = 6.89 Pa, 5C°=9°F)

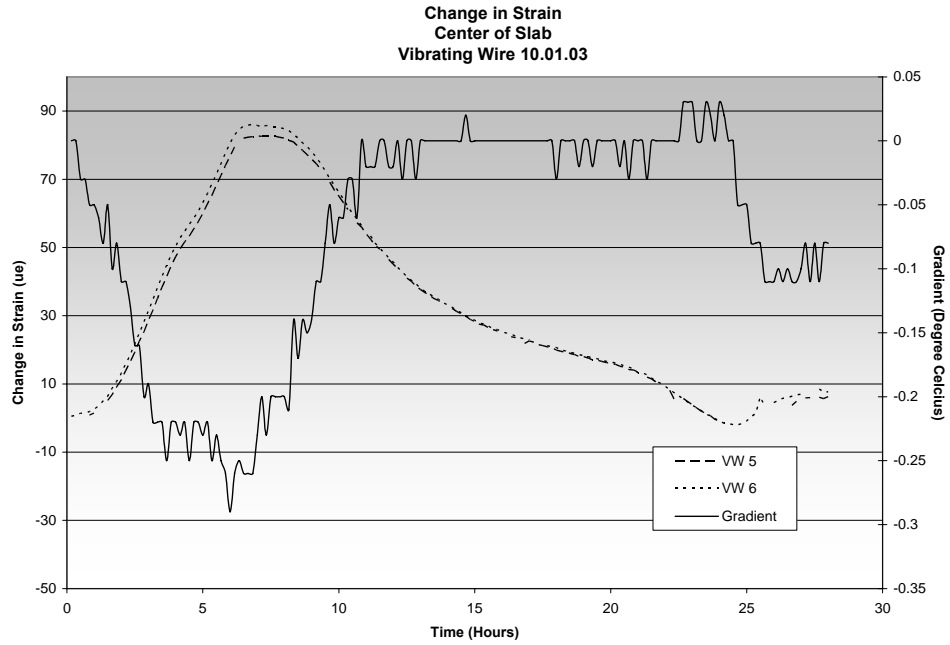


Figure D.11. Vibrating wire strain, center of slab, October 1, 2003 (5C°=9°F)

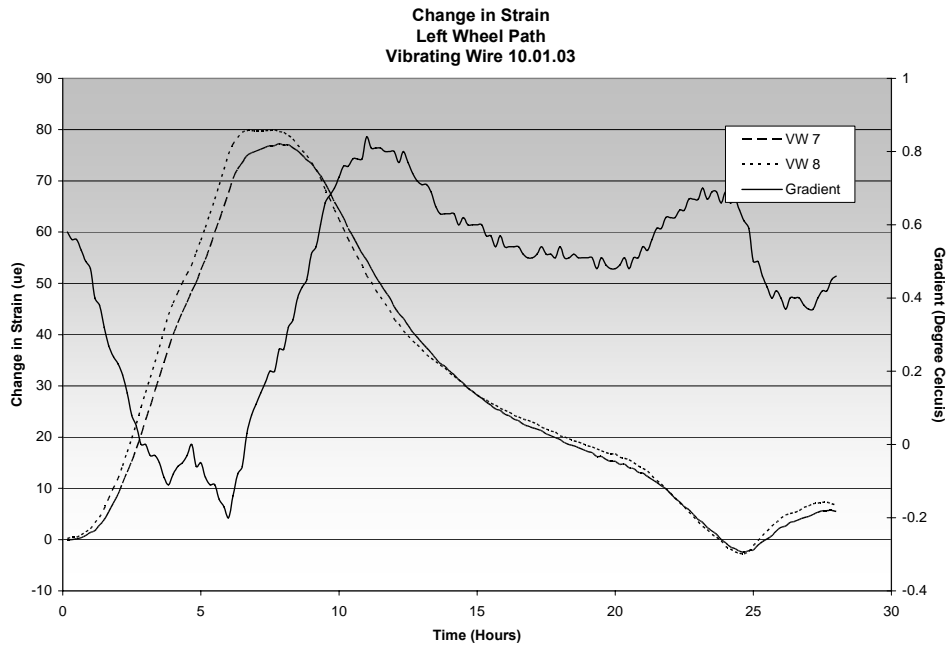


Figure D.12. Vibrating wire strain, left wheel path, October 1, 2003 (5C°=9°F)

Appendix E: I-490 West Data October 2004

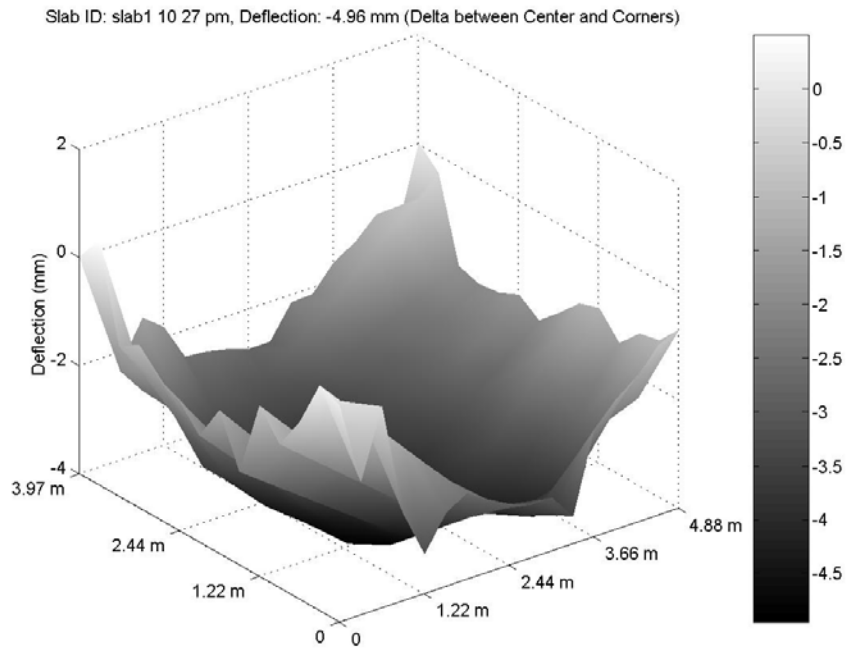


Figure E.1. Slab 1 profile at 10:30 am October 27, 2004, referenced after joints sawcut (1m=3.28 ft; 1 mm=39 mil)

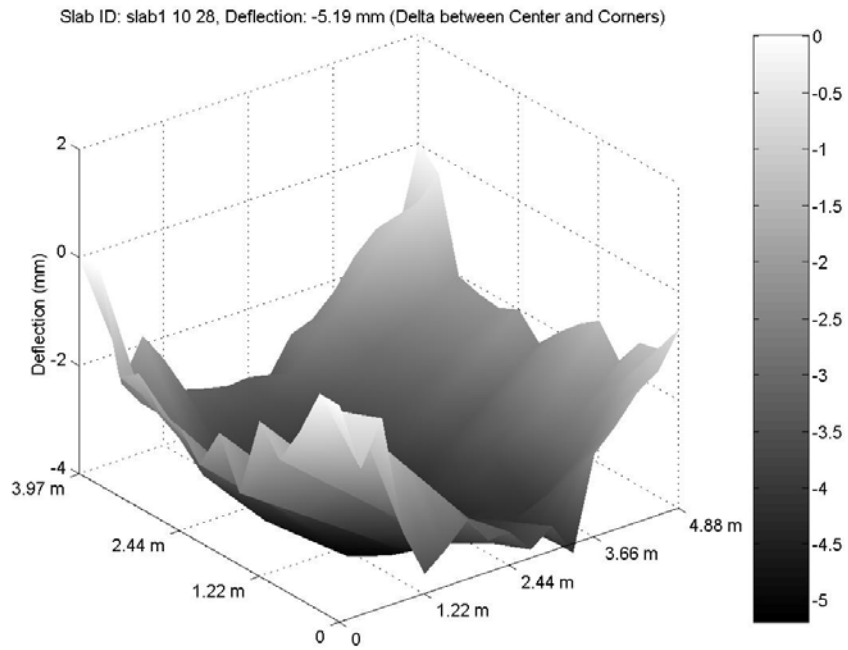


Figure E.2. Slab 1 profile at 10:30 am October 28, 2004, referenced after joints sawcut (1m=3.28 ft; 1 mm=39 mil)

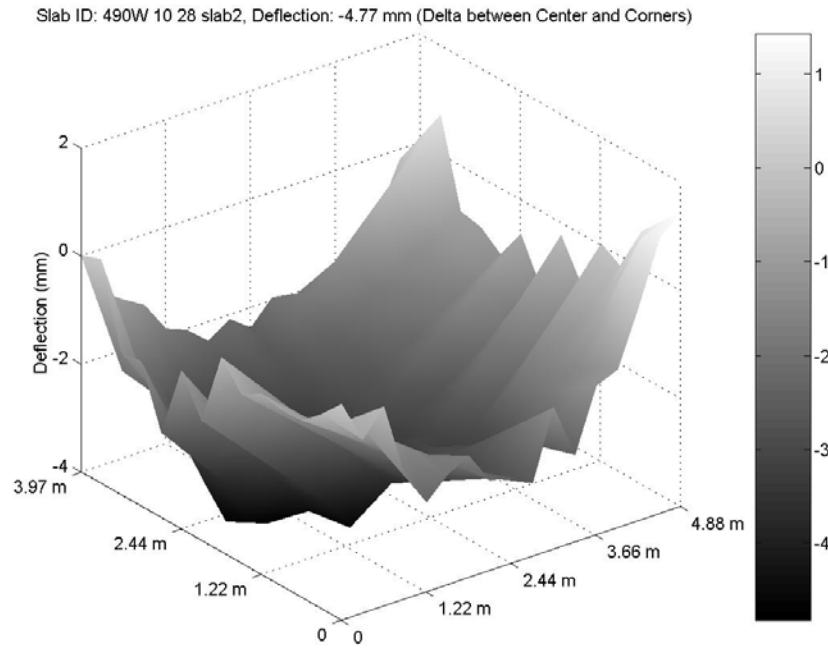


Figure E.3. Slab 2 profile at 10:30 am October 28, 2004, referenced after joints sawcut (1m=3.28 ft; 1 mm=39 mil)



ORITE • 141 Stocker Center • Athens, Ohio 45701-2979 • 740-593-2476
Fax: 740-593-0625 • orite@bobcat.ent.ohiou.edu • <http://webce.ent.ohiou.edu/orite/>